Master of Science Thesis

INTEGRATION OF BIFACIAL PV IN AGRIVOLTAIC SYSTEMS – A SYNERGISTIC DESIGN APPROACH

Submitted in partial fulfillment of the requirements for the degree of

Master of Science

in Sustainable Energy Technology (SET)

Odysseas Alexandros Katsikogiannis

Supervisor: Dr. Olindo Isabella
Daily supervisor: Dr. Hesan Ziar
Readers: Dr. Rudi Santbergen
Dr. Nico Tillie
Submission date: 11th March 2021

Table of Contents

List of Figures

ABSTRACT

Solar photovoltaic (PV) technologies offer a renewable alternative to power generation that is based on fossil fuels; however, to meet the rising demand in electricity a substantial amount of surface area is required. This will inevitably lead to the installment of these systems on agricultural land, subsequently intensifying the land-use conflict and threatening food security. To alleviate this, the use of agrophotovoltaic (APV) systems is investigated, which enable the simultaneous production of food and renewable energy. More specifically, the aim of this thesis is to determine the optimal topology for a medium-scale and stationary bifacial APV array, which is simulated under the climate of Boston, USA (42.37˚N, 71.01˚W). Irradiance modelling is performed with Radiance's raytracing algorithm in combination with the daylight coefficient approach of Daysim and the Perez All Weather sky model, which is then coupled to the crop and electrical yield models to determine the overall land productivity. The modelling approach used is robust, while offering flexible manipulation of the array's deployment configuration, which is crucial for multivariable optimization. The integration of bifacial PV offers various synergistic effects mainly due to the amplified ground irradiance necessary for crop growth. Owing to the decreased PV density and high elevation from ground, rear irradiance homogeneity and bifacial gain are enhanced. Widening of the row spacing resulted in a logarithmic increase of the incident ground irradiation, while the overall energy yield portrayed a negative exponential trend, which is attributed to the use of bifacial modules. East-west (E-W) facing and vertically installed topologies are better suited for shade intolerant species, or permanent crops since they permit additional light penetration, especially during the winter months. In contrast, south-north (S-N) facing and latitude inclined arrays lead to intense and non-homogeneous shading that is unfavorable for growth during winter or for crops that cannot acclimate to shade; nonetheless, energy yield and land equivalent ratio (LER) are significantly enhanced. Unlike previous studies where only conventional modules were examined, here the potential of a customized one is inspected to assess whether blueberries can grow effectively under shade. By integrating such a module in an E-W hinged PV topology, which is associated with the most optimal shading patterns and schedule, the agrivoltaic performance is optimized. In comparison to the reference case, the land's productivity is increased by 59% with a reduction in electrical yield by a third. Through this holistic approach that incorporates a multi-scale sensitivity analysis, it is possible to achieve a spherical understanding of the limitations and potential synergies associated with the dual use of land, ultimately encouraging the sustainability of the agricultural sector.

ACKNOWLEDGEMENTS

First and foremost, I would like to thank Dr. Hesan Ziar who showed great enthusiasm throughout the duration of the thesis. Our fruitful discussions helped me see the bigger picture and guided me through the vastness of research. Thank you Hesan, your time, effort, and trust were essential for the completion of this thesis. Next, I would like to express my sincerest gratitude to Dr. Olindo Isabella, for giving me the opportunity to conduct research in the field of photovoltaics. More importantly, his dedication during these unprecedent times inspired me to continue and finalize my work. A big thank you to the PVMD group for their stimulating feedbacks, especially Tim Stark for sharing his view factor code. I will be forever grateful to my friends, who made me laugh no matter how grumpy I was and overcome the difficulties that I experienced. Finally, special thanks to my family for their constant support, understanding, and trust that have given me the opportunity to materialize my dreams.

1

INTRODUCTION

1.1 Background & thesis motivation

According to IRENA (2020) solar PV technologies experienced a rapid expansion between 2010 to 2019 with a 14-fold increase in overall global capacity. This cumulative increase in installed power resulted in rapid cost reductions, reflected by the evolution of its learning curve. Combined with advances in solar energy conversion efficiency and significant reductions in the cost of manufacturing c-Si modules the associated levelized cost of electricity (LCOE) decreased remarkably [1]; consequently, promoting the economic competitiveness of this technology, which is already less expensive than conventional power generation in many regions [2]. Therefore, PV can provide an increasing fraction of the society's electricity demand in a renewable manner. This is essential as the global energy consumption is projected to rise by around 50% from 2018 to 2050 [3]. Naturally, to mitigate any further intensification of global climate change, this energy should be supplied by renewable sources, such as PV; however, as the solar resource is widely diffuse (depending on region) substantial land coverage is required to meet this demand. This could be partially alleviated by aggressive installation of building integrated PV (BIPV); nonetheless, the rising demand for ground mounted PV (GMPV) will inevitably lead to the establishment of these systems on agricultural land [4]. This is especially true for regions with a dense population and/or restricted land availability. As a result, the land-use conflict between energy and food production is expected to be amplified. Previous attempts in converting arable land into energy through growing biomass crops gave rise to concerns regarding food security [5-6]. Thus, it is crucial to properly address this issue to prevent the repetition of another mistake. In fact, food security is already vulnerable, due to the impact of climate change and a rising world population. To make matters worse, cropland is projected to decrease significantly due to degradation of soil and potential desertification, as well as industrial estate development, leading to a global decrease in arable land ranging between 50-650 million hectares by 2100 [7]. Therefore, it is crucial to mitigate any land-use conflict associated with the deployment of GMPV in agricultural land.

One promising solution is the use of agrivoltaics or agrophotovoltaics (APV) that allows the simultaneous cultivation of crops as well as production of renewable electricity. It has recently been gaining a lot of attention, although the concept was conceived in 1981 [8]. As of January 2020, it has been estimated that a total of 2.8 GWp of APV has been installed worldwide [9]. This cumulative capacity is expected to significantly increase, especially in Asia. For instance, South Korea has aimed for 10 GWp of APV by 2030 [10], while in China between 2015-2018 1.7 GWp of APV was installed [11]. Furthermore, China aims to expand one of its largest APV facilities of 640 MWp to 1 GWp as reported in [12]. To illustrate how their design differs from the conventional GMPV Figure 1 is included. These systems are mounted on poles to permit the operation of agricultural machinery and deployed at lower densities to enhance light penetration over the crops. In essence, the solar resource is shared

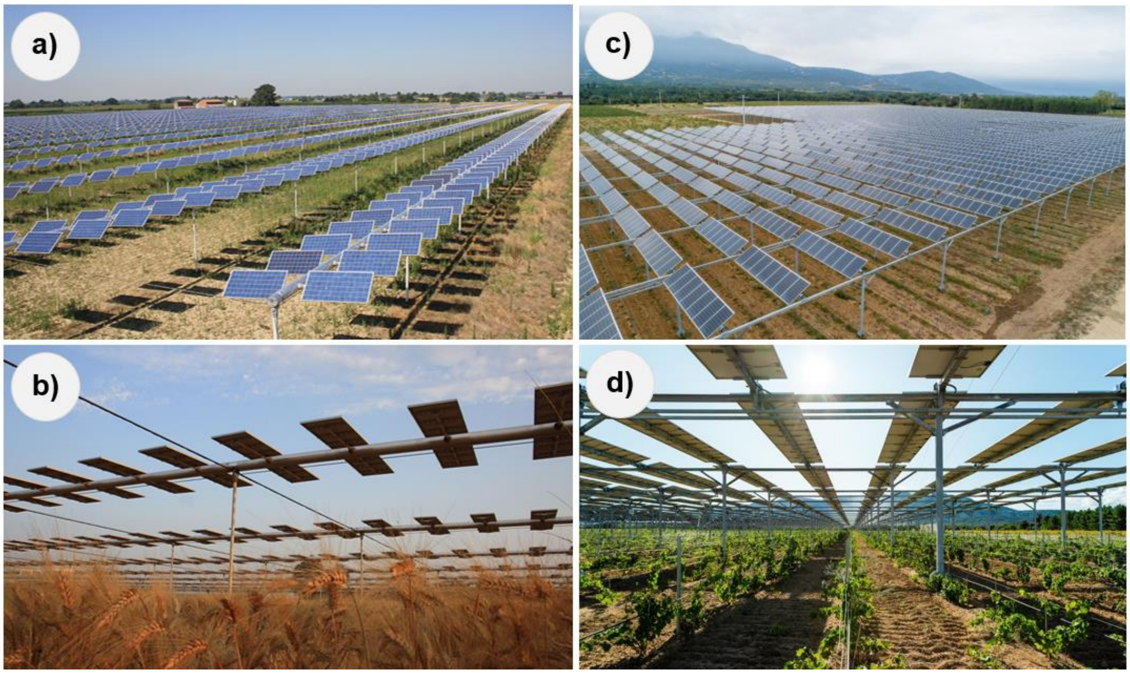

Figure 1 - Illustration of APV facilities where (a) and (b) are obtained from: www.remtec.energy and are located in Italy, while (c) and (d) display a large-scale project in France [13].

between crops and PV panels, also known as solar sharing [14]. To optimize this trade-off in light distribution, the shading ratio that is based on the array's deployment configuration must be designed according to the corresponding crop cultivated and local climatic conditions. The influence of crop selection is quite grave, as various species have different light requirements and shade tolerances, thus, ideally, they require a different shading ratio. Furthermore, the crop will determine the farming practises followed and agricultural machinery used, consequently affecting the design of the support structure (i.e. elevation from ground). Similarly, the climatic conditions will also influence the shading ratio, as the solar potential varies with region. Naturally, areas with high solar insolation are more desirable, as the shading ratio can be increased without compromising light availability for the crops below. On the other hand, northern climates which usually have intermittent or overcast sky conditions, lead to a more homogeneous distribution of irradiance and thus crop growth uniformity. In addition, there are other incentives for selecting a region, such as governmental support. In MA, USA an agricultural solar tariff unit has been in effect since April 2018 [15]; consequently, in this research the design optimization of the APV system is simulated for a system located in Boston, USA (42.36° N). Amongst other guidelines, the required parameters to obtain the APV tariff are a maximum AC rated capacity of 2 MW and a reduction in sunlight (shading rate) of 50%, as well as a minimum elevation of 8 feet for static configurations.

The aim of this thesis is to investigate the optimal deployment configuration of an APV array with an installed peak power of around 1 MW, and a total farm size of 2.7 ha (165x165 m^2) that is kept constant throughout the analysis. By formulating a design strategy for such medium-scale systems, other APV plants can also benefit, due to economies of scale [9]. As for the panel management a static configuration is adopted, since PV trackers with an anti-tracking mode (parallel to sun rays), are currently not widely available. Furthermore, it is compelling to examine the limitations of a static system, ultimately advancing all its derivatives. Logically, the PV technology selected will also influence the topology of the array. To satisfy crop specific needs, some innovative technologies have emerged. One example is the module in Figure 2 (a), where direct light is concentrated onto small cells, while the diffuse component transmits to the crops. Another option is the semi-transparent PV solution, as shown in Figure 2 (b), where the module's transparency is increased either spectrally [16], or regionally [17]. The previous involves the absorption of light that is not used for photosynthesis, since it is transparent to the spectral region of photosynthetically active radiation (PAR). Finally, bifacial PV with conventional cells and a modified cell spacing, as depicted in Figure 2 (c). The main drawback of the first two is the cost and the difficulty in mass producing them, thus being premature for medium-to-large-scale applications, at least when compared to the c-Si giant. Furthermore, additional performance testing should be achieved to ensure compatibility with in-field conditions and various crops [18-20]. On the other hand, by using conventional bifacial cells, agrivoltaic systems can benefit from the learning curve associated with bifacial modules, which applies to all PV sectors utilizing them. Since agrivoltaics are growing fast, a solution should be envisioned that is reliable, while requiring only a few adjustments to the conventional module design; consequently, in this thesis the integration of bifacial PV in agrivoltaics will be investigated along with any synergistic effects with crop cultivation.

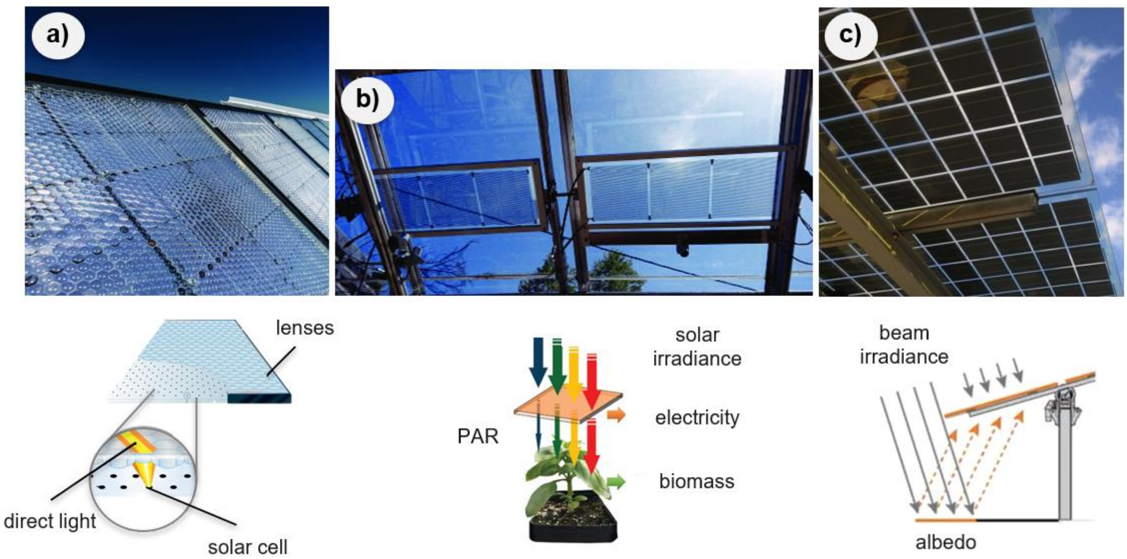

Figure 2 - State-of-the-art agrivoltaic modules: (a) concentrator PV (source: insolight.ch), (b) semi-transparent PV [16-17], (c) bifacial PV with modified cell-spacing (source: soltec.com).

1.2 Objectives & research questions

The aim of this report is to investigate the integration of bifacial PV into the agricultural sector, and to determine which topology results in the most optimal agrivoltaic performance for a certain location and crop. Naturally, by selecting the most appropriate deployment configuration, the land's productivity is maximized, thus effectively mitigating the land-use conflict in a sustainable manner. To achieve this, it is crucial to develop a robust model that can simulate irradiance on both sides of the bifacial module, as well as on the ground for a plethora of array topologies. Consequently, to obtain a comprehensive understanding of the potential benefits and limitations associated with the dual use of land, a multi-scale sensitivity analysis is necessary. Then, electrical and crop yield are derived to estimate the overall land productivity increase and the most promising topologies. Finally, a central drawback of static configurations is addressed, which is spatial light inhomogeneity on ground, through changes in the conventional module arrangement or the module itself. Essentially, to meet the objectives of this thesis the following research question must be tackled, which is broken down into sub-questions:

''What is the optimal deployment configuration of a medium-scale and static bifacial agrivoltaic array in Boston, USA?''

- Can crops be cultivated effectively in an agrivoltaic system where electricity is produced simultaneously?
    - Which factors affect the plant's growth and ultimately its crop yield, and how does the introduction of the agrivoltaic array influence those?
    - How does crop selection influence the topology design and its performance?
    - What are the potential synergies between crop cultivation and electricity production related to the integration of bifacial PV?
- Which of the parameters that characterize the deployment configuration of the PV array are most relevant in an optimization process?
    - How does the row spacing, orientation, and module arrangement influence the light intensity and distribution throughout space?
    - What are the limitations associated with the use of conventional arrangements and modules related to the performance of APV systems and can they be partially resolved by adopting modified modules?
- What are the unique features of each APV topology and the conditions under which one is adopted?
    - How does the shading pattern and sequence vary from hourly to monthly timescales for each topology?
    - How is the trade-off between electricity and crop yield addressed, and what is the overall land productivity increase of each topology?

1.4 Thesis outline

Before proceeding into the APV performance modelling, it is essential to examine what governs the productivity and growth of plants, as well as how the introduction of the array influences that. In addition, the benefits of diffuse light and crop shade tolerance are investigated to properly assess the impact on crop yield. A thorough inspection of the parameters that define the deployment configuration of a bifacial array are also included, along with the potential synergies when integrated in agrivoltaics. The literature review in Chapter 2, is concluded with the selection of the most appropriate irradiance modelling software for such systems. The methodology followed to obtain the performance of each topology is included in Chapter 3, where at first the Radiance model is developed, which is responsible for determining irradiance on both sides of the PV, and farm samples. Then, the energy yield model is disscused along the LER and other performance indicators. After the sensitivity analysis with regards to the array's deployment cofiguration is introduced, crop compatibility along with the asssociated light requirements are also examined. The results are presented and discussed in Chapter 4, which consists of the multi scale sensitivity analysis. Initially, the macro scale sensitivity with regards to conventional module arrangements is examined, with focus on the RS. Then, the limitations of conventional modules are adressed in the meso scale, followed by two generic case studies; summer and permanent crops, where various topologies are compared. The potential of utilizing a module that is modified for cultivation of blueberries along with the corresponding agrivoltaic performance finalize the chapter. The conclusion, and recommendations are described in Chapter 5, which is followed by the Appendix.

2

LITERATURE REVIEW

2.1 Plant productivity and growth

There are essentially five main factors that influence plant productivity and growth: light, carbon dioxide, and water availability, ground and ambient temperature, as well as nutrients. These factors are interconnected and any deviation from what is optimal will lead to stresses that can heavily impact plant development. In this thesis the effect of light, water and temperature will be discussed, since the introduction of the PV array is expected to impact those.

One of the primary processes related to plant productivity is the photosynthesis rate. Through photosynthesis, plants utilize the incident solar radiation to produce O_2 and glucose. Glucose is then broken down through the process of respiration, which releases chemical energy that is crucial for the plant's cellular activities. Therefore, light interception is crucial for plant growth. Leaf anatomy and its optical properties are constructed in such a way that light can be effectively absorbed and conducted to chloroplasts where photosynthesis occurs [21]. The structure of a leaf is analogous to that of a solar module, which is comprised of multiple photosynthetic cells. More specifically, due to its bifacial nature incident direct and diffuse irradiance are absorbed by the front side, while light that is reflected off the ground or scattered throughout the sky hemisphere is absorbed by the bottom side. The importance of the photosynthetic rate regarding plant growth is crucial, however the marketable value of a crop is also determined by a variety of other factors. This is especially true for fruit crops where the outcome is not just biomass.

The amount of carbon assimilated by the plant describes the increase in biomass, or dry matter, which a fundamental parameter that defines crop productivity and yield. This net carbon gain depends on the balance between the process of photosynthesis and respiration as shown in Figure 3. While photosynthesis is responsible for the carbon uptake, respiration is essentially its counterbalance, where carbon dioxide is consumed to maintain and further increase biomass. To conceptualize the plant's carbon management system, respiration is distinguished according to the use of the consumed carbon. Carbon that is used to produce energy, which results into growth and thus crop yield is termed as growth respiration. On the other hand, maintenance respiration is related to the carbon used for maintaining processes that do not influence the rate of photosynthesis, and eventually dry matter [22-23]. Although growth is the term we are mostly interested, maintenance respiration is essential for the plant's overall health.

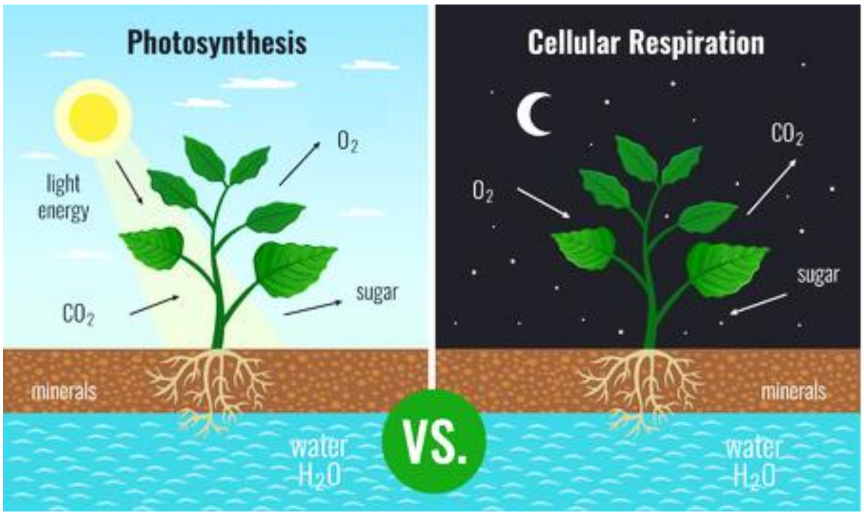

Figure 3 – Two fundamental metabolic activities of plants: photosynthesis and respiration [24].

2.1.1 Factors influencing photosynthesis

The rate of photosynthesis is influenced by a plethora of environmental factors that are interrelated. Some of them include light intensity and homogeneity, available carbon dioxide, ground and ambient temperature as well as humidity. At the same time, there are crop specific genetic factors such as plant architecture, and carbon assimilation pathway that determine photosynthesis rate across the various species [21]. These genetic factors that depend on crop selection will be examined afterwards.

To successfully photosynthesize, crops require carbon dioxide, which they obtain from the atmosphere through pores in the leaf, known as stomata as shown in Figure 4. These stomata are hydraulically operated valves that control the size of the opening according to the plant's water availability and the external climatic conditions [25]. When there is enough water, these stomata become swollen and allow the uptake of carbon dioxide for photosynthesis. However, under conditions of water stress, either due to high irradiance and temperature, or low humidity, the stomata become flaccid and obstruct the flow of carbon dioxide and ultimately the process of photosynthesis. Such a mechanism is known as

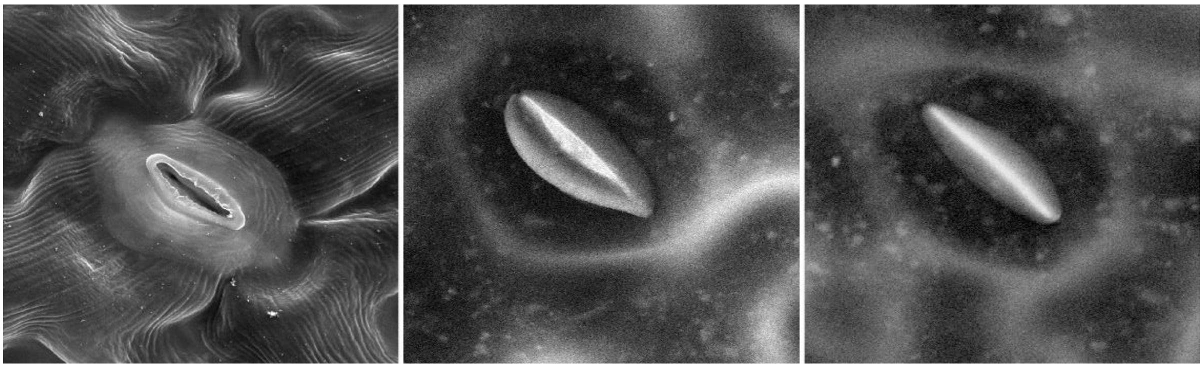

Figure 4 – Scanning electron microscopy micrographs of the stomatal complex [26]. On the left side the stoma and chloroplast are displayed. At the centre the stoma is open (flaccid), thus allowing the flow of CO_2, while on the right it is closed and swollen.

hydropassive closure, and it is the main reason why shading nets are applied over some crops during summer [27]. The available density of carbon dioxide in the atmosphere is relatively low, at least over the short term, consequently it is usually the one limiting the photosynthesis rate [21]. Although there are practices that can enrich the concentration of carbon dioxide in a controlled environment, such as in greenhouses, this is infeasible in open field conditions.

Photosynthesis occurs within a plant's cell in specialized structures called chloroplasts and similarly, to PV cells, absorptance depends on the spectral distribution of the incident light. What is useful for photosynthesis is known as photosynthetically active radiation (PAR) (μmol m^{-2} s^{-1}) and it is only a portion (400-700 nm) of the solar radiation spectrum. To visualize how it affects the plant's growth, we need to analyse the photosynthesis light response curve as shown in Figure 5. In this plot, light intensity is decoupled from the other environmental factors that influence growth rate. At low irradiance levels the development of CO_2 due to dark respiration is higher than the rate used by photosynthesis, leading to a negative net CO_2 uptake (or release). As the photon flux is increased, the photosynthetic rate increases and thus CO_2 uptake, until it is equal the amount released by dark respiration. The light intensity at which the opposing processes of respiration and photosynthesis are balanced is known as the light compensation point (LCP). Light incident on crops should be above this value to ensure growth. What follows is a linear relationship between PAR and photosynthesis rate, where photosynthesis is light limited. At sufficiently high irradiance the rate of growth saturates, and the corresponding light intensity is known as light saturation point (LSP). At this point, other factors such as CO_2 availability become the limiting factor. Furthermore, incident irradiance above the LSP cannot be utilized to further increase CO_2 uptake, rather it is converted into heat that eventually leads to hydropassive closure.

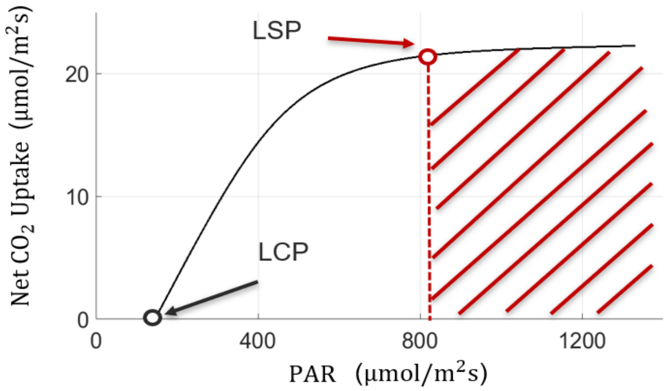

Figure 5 – Light response curve example describing the variation of photosynthesis with incident PAR. The region shown in red corresponds to light intensities that lead to saturation, while any surplus is converted into heat that can be harmful for growth.

Similar to other biological processes, photosynthesis is sensitive to the crop's temperature. As the temperature increases a higher metabolic activity is present in the leaf that reaches an optimum and then decreases. The opening and closing of the stomata follow a similar pattern [21]. The temperature response curve is divided according to the three cardinal points. These include the minimum and maximum crop temperatures that photosynthesis can occur, and an optimum one where the rate of growth is maximized. Consequently, temperature influences the balance between respiration and photosynthesis, where high values can impair latter. This is directly related to hydropassive closure, and it has been observed in certain species where their stomata undergo a midday closure, leading to a transient reduction in their photosynthetic capability [28]. Opening of the stomata occurs around mid-afternoon where the water shortage has been fulfilled through the reduction of transpiration losses. The high direct irradiance during solar noon, results in higher ambient and ground temperatures that increase the transpiration rate of the crop. This ultimately leads to water stress, which is another factor influencing photosynthesis.

The availability of water is crucial in determining crop productivity. The photosynthetic rate declines under conditions of water stress, and in severe cases it may completely stop. As previously discussed, stomatal closure imposes limitations to CO_2 uptake due to water stress. The photosynthetic needs of the plant cannot be met because the stomata cut off the supply of atmospheric CO_2 to the chloroplasts. As a result, the frequency of a stoma's opening must be considered when determining productivity and crop yield. Note that under an acute water deficit, leaf expansion is reduced, and ultimately the photosynthetic surface area. Crops can be subjected to water stress when there is a swift drop in ambient humidity or when warm and dry mass of air passes through it. Depending on the ground and ambient temperatures the rate of transpiration rises, which leads to a higher vapor pressure gradient between crop and surrounding air. Under such conditions the soil becomes increasingly dry and this has a negative impact on water absorption especially for shallow-rooted crops [21]. Control over the opening of the stomata is therefore used to balance transpirational water losses to the amount resupplied through the roots. In fact, for almost all plants studied, the movements of the stomata were found to be responsive to ambient humidity [29].

After having introduced the various environmental factors that influence the photosynthetic rate, we can now proceed to the genetic factors. At first, crops can be divided according to their carbon assimilation pathway; C3 and C4 crop species. Note that C3 and C4 refer to the corresponding pathway utilized for the dark reaction of photosynthesis. These can vary significantly in terms of their photosynthetic behaviour, as well as anatomical, biochemical, and physiological characteristics that establish what is known as C4 syndrome [30]. C4 plants originate from tropical or subtropical regions, where irradiance and temperature are considerably higher [31]. These species have adapted to such conditions, and as a result their photosynthetic rate can be up to

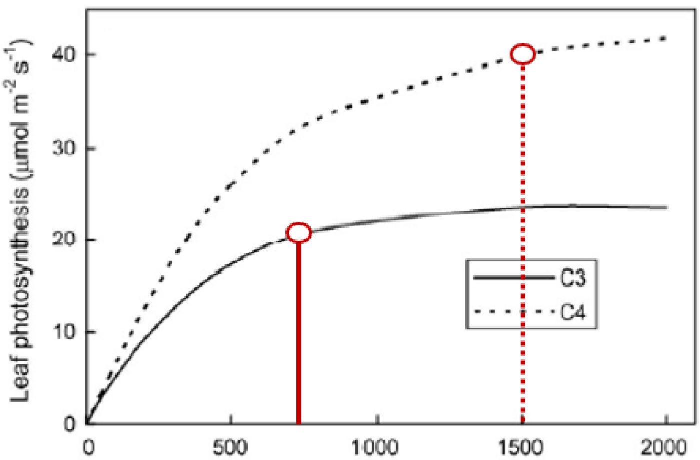

Figure 6 – Simulated light response curves for C3 and C4 species at an ambient temperature of 25°C and CO_2 of 1000 µmol m^{-2} s^{-1} [32]. The red lines approximate the LSP, although C4 species do not really saturate.

three times greater than C3. Furthermore, they can withstand drought and thus photosynthesize effectively even under water scarcity, that would lead to hydropassive closure in C3 species. To better grasp the differences in photosynthetic behaviour both species response to light is shown in Figure 6. In comparison to C3 crops, C4 have a considerably lower LCP (not shown in the plot). Furthermore, in C3 plants the supply of CO_2 is usually the limiting factor of photosynthesis, leading to an LSP of around a fourth of the total incident solar radiation. On the other hand, C4 species do not reach saturation. This, however, does not necessarily mean that C4 are more efficient at photosynthesizing. In fact, at temperatures below 30 °C, C3 plants display a higher quantum yield [21]. The opposite is true for temperature above 30 °C, since at high temperatures the solubility of CO_2 decreases, leading to decreased quantum yield for C3 species. A distinct advantage of C4 plants is their capability to better withstand water stress, and thus maintain photosynthesis without initiating hydropassive closure. This can be measured using the transpiration ratio or the inverse of it known as water use efficiency [21].

The discussion on genetic factors that influence photosynthesis is continued, with the focus on plant architecture. The amount of irradiance incident on a leaf is affected by its position on the plant canopy as well as the presence and dimensions of surrounding leaves. This effect is more pronounced in densely packed crop plantations, where partial shading from other plants can occur. Therefore, canopy structure including angle, morphology and spacing between leaves can greatly impact plant productivity. For certain crops, young leaves that develop at the top receive the full amount of sunlight, while leaves at the bottom are heavily shaded. The amount of irradiance received by the bottom can be reduced by 90%, depending on plant architecture [21]. Consequently, these leaves do not contribute to the process of photosynthesis, rather they negatively impact it through respiratory losses. Unlike solar cells; however, photosynthesis occurring at the top of the plant is not limited by shading at the bottom.

To assess crop productivity in terms of light interception, the ratio of photosynthetic leaf area to the amount of ground covered area is used, which is known as the leaf area index (LAI), a dimensionless number [21]. Light incident on the ground does not contribute to photosynthesis, therefore a high LAI is desirable. Nevertheless, planting crops at very high densities can lead to a decrease of the photosynthetic rate, due to partial shading. In general, leaves that are horizontal are better oriented to absorb light and usually have a larger surface area. At the same time, they result in additional partial shading at the bottom of the canopy. On the other hand, leaves that are erect intercept less light, and ultimately lead to lower partial shading. Therefore, different crops species in the same environment can lead to a significantly different photosynthetic behaviour.

2.1.2 Effect of diffuse light

According to the crop's architecture, a more uniform horizontal and vertical distribution of light can enhance light interception, and thus carbon gain. This is of special importance to crops with a high LAI, where middle and lower leaves receive considerably lower irradiance, and thus contribute less to the overall production. To mitigate this inhomogeneity in light distribution, the effects of diffuse light are investigated. It has been shown that by increasing the amount of light throughout the crop's canopy the photosynthetic behaviour is significantly enhanced [33]. A similar boost in productivity is observed when the fraction of diffuse light is higher, such as that found during cloudy sky conditions, or under forests [34-37]. Therefore, diffuse light can penetrate deeper into the lower leaves of the canopy [38-39]. Furthermore, research indicates that crops have developed mechanisms that can absorb diffuse light in a more efficient manner [40-41]. To amplify the fraction of diffuse light over the crops diffuse covering materials could be employed like those used in greenhouses [42-44]. The potential of these materials and their optical properties are examined in subsection 3.1.2 Optical properties.

The integration of a light diffusion film can increase plant production by 5%, thus ensuring its profitability [45]. This was verified for various crops; cucumbers with 8% increase, roses with 10%, and tomato with 8-11% [46-48]. Such benefits in plant production lead to higher yields that justify the additional cost of such a diffuse covering. As will be discussed later, light homogeneity below an APV array can be greatly reduced, due to the casted shadows. These sharp gradients of irradiance could be smoothened out using such a cover. In Figure 7 the influence of a diffuse cover on the spatial distribution of light along the horizontal

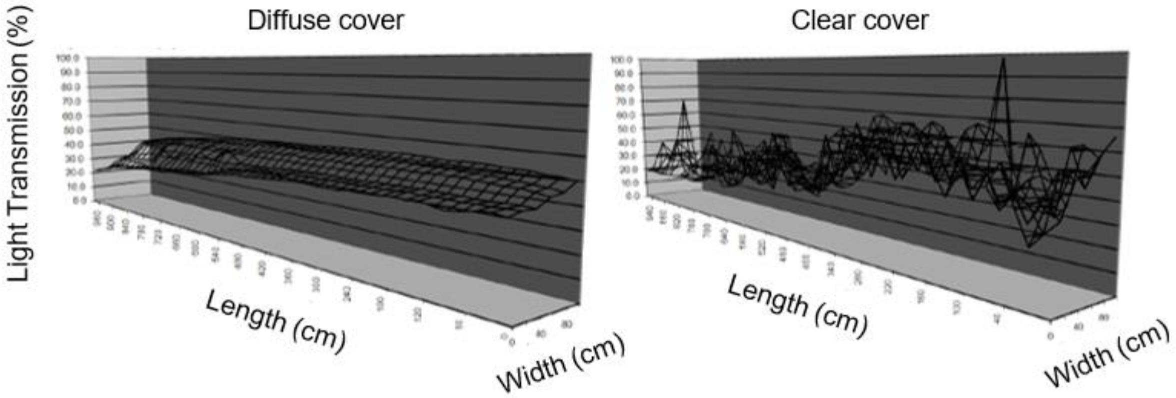

Figure 7 – Horizontal light intensity and distribution throughout ground with and without the diffuse cover [46]. The measured data are obtained for a clear day on the 11th of October 2006.

direction can be observed. Under the clear cover light transmission varies considerably, while under the diffuse it is made homogeneous. Additional benefits were observed such as increased light interception on clear days, especially in the middle layers of the canopy, leading to an enhancement of the photosynthesis rate [38, 46, 49]. This improvement in performance could also be explained by the decreased crop temperature (around half a degree) at the top of the canopy, that allows more optimal conditions for growth [46, 48]. For crops with tall canopies, the vertical light interception is reduced due to the partial shading effect. Naturally, this depends on the LAI as previously discussed. For cucumber, a crop with a high LAI, the influence of the diffuse cover on the vertical distribution of light was examined, as shown in Figure 8. The introduction of the diffuse cover resulted in an enhancement of the light interception, especially at the middle layers of the canopy [43]. Overall, a light diffusion film leads to a better spatial distribution of light over the crops, and depending on the plant's architecture, species, and the local climatic conditions the increase in photosynthetic rate and thus productivity can be substantial. Consequently, such a cover could be greatly beneficial in APV systems.

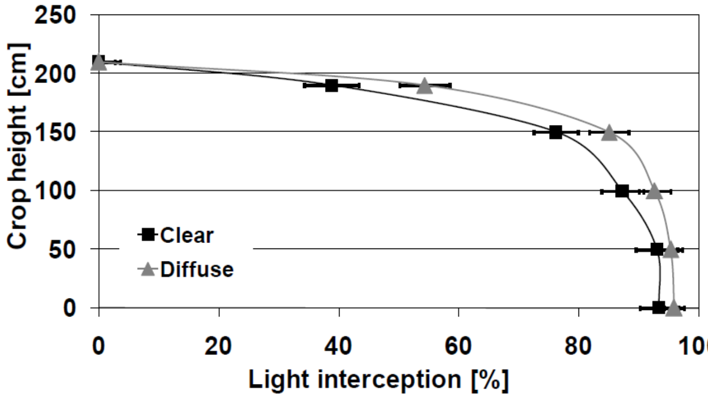

Figure 8 – Vertical light interception measured for a cucumber crop under a clear sky on the 23rd of May 2006 for two greenhouse covers [46].

2.1.3 Shade tolerance

The capability of a plant to tolerate low light intensities is known as shade tolerance. Shade tolerance is usually considered as an attribute of certain plant species, however, this compliance of plants to a certain light intensity is something that can be inherited [50-51]. Through genetic adaptation plants can modify their photosynthetic behavior according to their light environment. Plants grown under shade are not able to achieve high rates of photosynthesis even when plentiful irradiance is present. On the other hand, due to their adaptation to shade, they perform efficiently at a low irradiance. Consequently, under overcast sky conditions they are expected to outperform crops grown under high light. The latter can maintain high photosynthetic capacities when light saturation is attained, but they are incapable of photosynthesizing effectively under shade [52-53]. This adaption to external light conditions is present for both sun and shade species, and thus depends not only on the species but also on the light intensity received throughout their growth. For example, a sun specie that is shade-grown will display resemblance to a shade-plant in terms of its photosynthetic behavior [54].

Studies indicate that the rate of photosynthesis in both C3 and C4 species, is significantly affected by their light environment throughout growth [53, 55-61]. For example, the photosynthetic behavior under varying light intensities throughout a crop's growth is

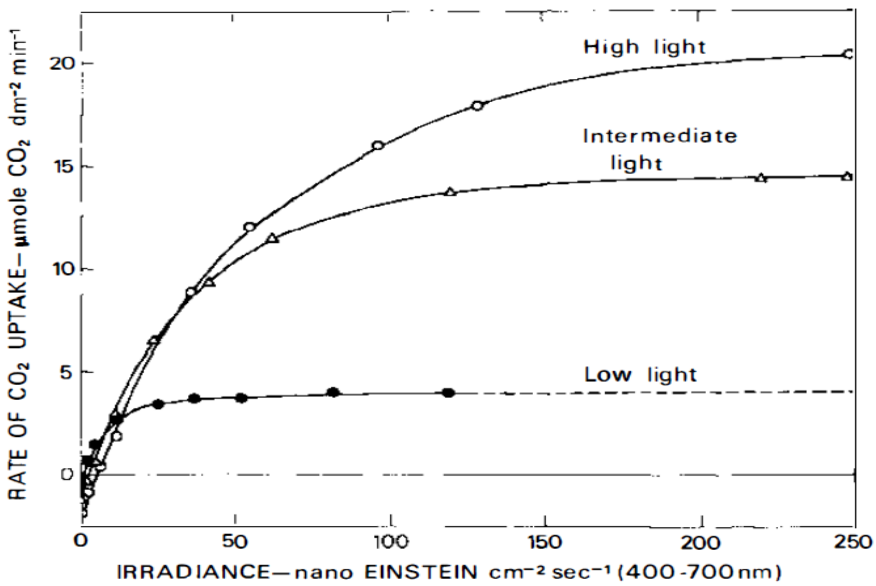

Figure 9 – Light response curves of the *A. patula* crop for varying intensities during its growth [51]; low, intermediate, and high light environment.

displayed in Figure 9. As the light intensity increases, so does the LSP and the maximum photosynthetic rate. Furthermore, at low light intensities the LCP decreases. The effect of grown light intensity on the quantum efficiency cannot be generalized. Some studies show that there are not any apparent changes in the initial slope of the curves, thus resulting in a constant quantum efficiency irrespective of growth conditions [55-56, 62-63]. Other studies claim that there is a change in the initial slope of the light response curve, that seems to portray quantum efficiency variations [58, 64]. Specifically, plants grown under shade displayed a higher efficiency, thus demonstrating adaptation to such environmental conditions.

The magnitude of light present during growth can also alter the morphology of leaves. Sun-grown leaves were found to be thicker and with a smaller surface area, while shade-grown leaves were thinner, larger, and more [55, 62, 65-72]. By increasing their surface area, leaves can intercept light more successfully. On the other hand, sun-leaves develop a higher stomatal density and thus are better equipped at dealing with elevated temperatures and high irradiance [73-75]. A thinner leaf implies a reduction in vascular tissue, which is essential for plants grown under shade, since the maintenance of the tissue is very energy intensive [76]. The capability of the leaf to absorb light is further reduced, since photosynthetic cells are replaced by non-photosynthetic tissue. One of the main functions of the vascular network is to transport water. In shade, a large network is unnecessary, because under such conditions transpiration losses are reduced. To visualize, the reduction in leaf thickness according to light intensity and crop species Figure 10 is included. The thickness of the C3 species reduced significantly more under shade in comparison to C4. Note that the change in the leaf's cross-sectional area represents a change in tissue volume. This significant reduction in vascular tissue present in C3 species allows them to perform more efficiently under shade in contrast to C4 [77-79]. Therefore, the latter have intrinsic characteristics that result in ineffective acclimation to shade.

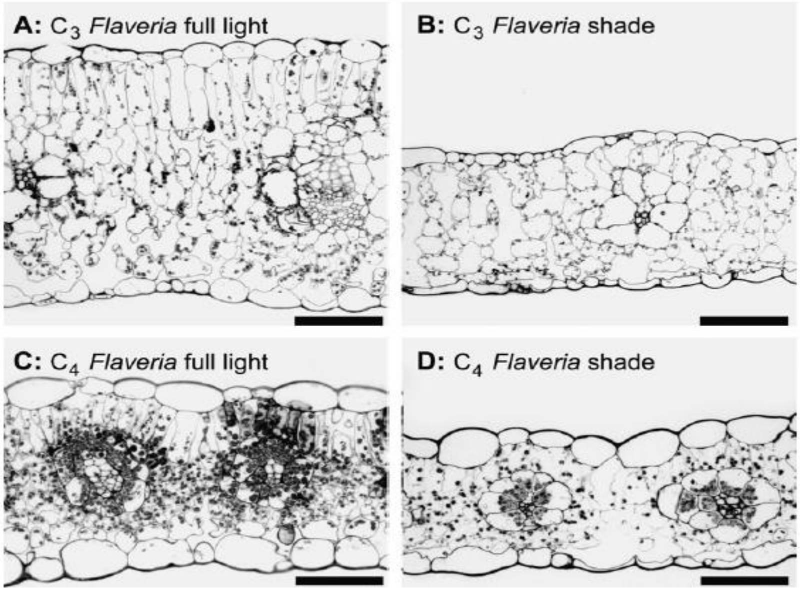

Figure 10 – Cross-sectional area of *Flaveria robusta* (C3) and *Flaveria australasica* (C4) leaves, which are grown under two light intensities; full light (500 μmol/m²/s) and under shade (100 μmol/m²/s) [76].

2.2 Crop yield

Multiple crop models exist that can determine crop yield for many species, however, they cannot be generalized to simulate the behavior of all species. They depend on crop-specific parameters that are not widely available. A simple generic crop model was recently developed that can be easily adjusted to simulate crop productivity, and yield for various species [80]. Radiation-use efficiency (RUE) is based on the process of photosynthesis and thus is fundamental to crop yield modelling. It quantifies the amount of resulted biomass according to the portion of the total incident PAR that is intercepted by the crop's leaves [81-82] Essentially, it considers both the amount of light intercepted and the crop's capability to utilize that and produce dry matter. Estimations of RUE values were examined for C3 and C4 species and it was determined that they can vary considerably. They were found to be in the range of 1.5-2.0 g MJ^{-1} and 4.0-5.8 g MJ^{-1} for C3 and C4 species respectively [83]. As previously discussed, diffuse light can enhance light interception by homogenizing light distribution over the plant's canopy. Furthermore, it was found that it has a positive impact on the RUE [84-85].

Similar to photosynthesis, biomass is influenced by a variety of environmental and crop specific genetic factors. These include daily temperature, thermal, drought, and water stresses, as well as atmospheric CO_2 concentration. In mathematical terms, the daily rate of biomass (kg/m^2 day) can be found through [80]:

$$\text{Biomass rate} = I_{daily} \cdot F_{solar} \cdot RUE \cdot f(CO_2, T, Q, \sigma) \tag{1}$$

I_{daily} (Wh/m[2] day) is the daily solar irradiation incident on a horizontal plane at crop level and F_{solar} is the fraction of the irradiation intercepted by the plant. Note that $f(CO_2, T, Q, \sigma)$ represents the influence of carbon dioxide concentration, temperature, as well as thermal and water stresses on the crop's productivity. Then the total biomass accumulated can be determined by [80]:

$$\text{Biomass}_{t+\Delta t} = \text{Biomass}_t + \text{Biomass rate}|_{\Delta t} \tag{2}$$

where Δt represents the time frame that the rate is calculated, which is usually daily. Finally, to obtain crop yield (kg/m^2) the total biomass until maturity is multiplied by the Harvest Index (HI) [86]:

$$Y_c = \text{Biomass}_{total} \cdot HI \tag{3}$$

For the sake of simplicity, HI was assumed to be independent of the environmental and crop-genetic factors.

Estimating the fraction of light intercepted by the crop is not straightforward, since it depends on the canopy's architecture; however, it can be estimated through Beer-Lambert's law [87]:

$$I = I_0 e^{-k\zeta} \tag{4}$$

where I_0 is the irradiation incident on the top of the canopy, while the light extinction coefficient is represented by k. The parameter ζ describes the cumulative LAI of the canopy along the vertical direction. Note that LAI varies along the plant's height and throughout each layer. For most agricultural systems to be productive LAI values between 3-5 are used [21]. Specifically, for canopies with horizontal leaf orientation LAI lies below 2, while for vertical oriented between 3-7. The attenuation of light is more pronounced in canopies with horizontal leaves than with vertical [88]. The effect of leaf arrangement and orientation (tilt), is accounted for through the extinction coefficient [89], which was estimated by Monsi and Saeki to be between 0.7-1.0 and 0.3-0.5 for horizontal and vertical leaves respectively [87].

Additional modifications to equation 4 are performed to represent a more realistic case. For example, in natural stands the lower leaves are oriented closer to horizontal, while in the upper layers they are more erect [89]. Since the calculated irradiation I in equation 4 is determined for a horizontal plane, the following adjustment is suggested to calculate irradiation I′ on the actual canopy plane [89]:

$$I' = \frac{I_0 k e^{-k \cdot \zeta}}{(1 - \tau_{leaf})} \tag{5}$$

, where the leaf's transmittance τ_{leaf} must also be considered [89]. By determining the amount of irradiation intercepted by the canopy and accounting for the photosynthetic response of a certain crop, photosynthesis Φ (μmol m^{-2} s^{-1}) can be calculated through [87, 89-90]:

$$\Phi = \frac{b}{ak}\ln\left(\frac{(1-\tau_{leaf}) + akI_0}{(1-\tau_{leaf}) + akI_0 e^{-k\zeta}}\right) - r\zeta \tag{6}$$

, where a and b are constants that portray the crop's photosynthetic behaviour. Along with the respiration rate r they characterize the crop's physiology, while k and ζ define the canopy's architecture. The equation describing photosynthesis was compared with experimental results for $\tau_{leaf} = 0$ and $k = 1$, and it was determined that it closely resembles actual conditions [91]. By varying k and ζ one can conceptualize how to maximize photosynthesis through leave arrangement and orientation alone. In general, a low k in combination with high ζ will result in the maximum achievable photosynthesis for a given configuration. This is verified by crops grown under full sunlight where k and ζ were found to be approximately 0.7 and 5 respectively [88]. Such values maximize the amount of intercepted irradiation by the canopy. A limitation to the use of this model arises from the assumption of overcast sky conditions [87]. However, this is partly resolved by the integration of a diffuse cover, which will be described in subsection 3.1.2 Optical properties. Note that the extent of light penetration throughout the canopy is dependent on the angle of the sun as well [92-93].

2.2.1 Influence of the PV array

In this section, the influence of the PV array on the agronomic performance of the APV farm will be examined. The introduction of the array is expected to affect not only the microclimate and thus crop productivity, but also the corresponding farming practices [4]. To allow the operation of conventional agricultural machinery, the mounting structure of the APV array must be adjusted accordingly. Essentially, the clearance between lowest PV module edge and ground must be such that large harvesters or tractors can operate at ease. A clearance of 4-5 m is assumed to be enough for most machinery [4]. A similar consideration must be made for the width between each of the support structure pillars. The expected loss in cultivation area, due to the unusable land that is occupied by the support structure was estimated to be at least 2% in [94], while another source considered 10% losses of cultivatable land [95]; consequently, this loss should be determined according to the support structure and APV design.

Various microclimatic alterations are anticipated with the integration of the PV array that can directly influence the photosynthetic rate of the canopy and ultimately its biomass production. These changes are dependent on the array's configuration, as well as crop selection. Marrou et al. (2013) concluded that only a few adaptations are required to switch from open cropping to APV, instead one should concentrate on the reduction of light intensity and selection of crops that could adapt to such conditions. Furthermore, experimental results indicate that thermal time, mean daily air temperature relative did not vary significantly in comparison to full sun conditions [96]. On the other hand, soil temperature reduced under the shade of the APV array. Because of the shading crops were cooler throughout the day, especially around solar noon, while at night the opposite occurred [96-97]. This can be observed in Figure 11, where the daily variation of a crop's temperature is plotted for a sunny

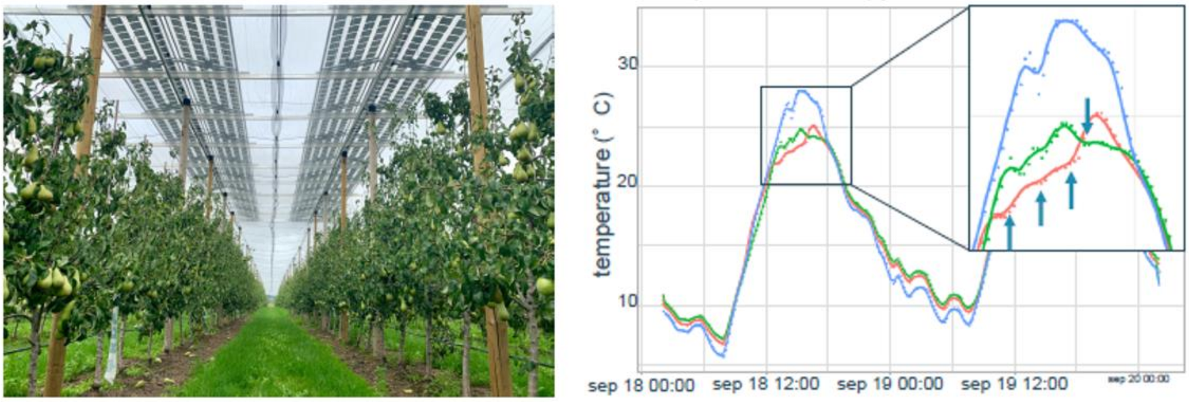

Figure 11 – Temperature variation measurements at canopy level of a pear crop [97]. In blue, one can observe the temperature fluctuation for regular farming practises, while in red and green growth is facilitated under APV.

day in September . Full sun conditions are shown in blue, while the rest represent crops grown under the shade of the PV array. The reduction is most prominent around noon when harmful direct irradiance is blocked. At night there is a slight increase, due to the obstruction of the sky by the panels, which effectively reduces radiations losses. Frost can be detrimental to plant survival, so this is of equal importance. This along with the reduced evapotranspiration rate promoted improved conditions for photosynthesis and growth [96]. Through a decrease in soil evaporation increased yields in maize were observed for non-irrigated conditions [98]. However, these findings should not be generalized since they greatly depend on the local climate as well as PV array configuration. Further research is required to assess the impact of various PV orientations and densities. Moreover, as the size of the APV farm increases, the impact on the microclimate would be greater depending on the configuration. Nonetheless, the parameters mostly affected are light intensity and homogeneity, which are the one used in this study to model crop yield.

As was discussed in subsection 2.1.3 Shade tolerance, most plants adapt to the corresponding light environment that they grow in. However, C3 plants can acclimate to shade more effectively, thus they are preferable. Crop species that are shade tolerant exhibited a series of adaptation strategies when grown underneath the PV array [99]. Shadow-grown leaves modify their morphology to be thinner and thus reduce respiration losses, while simultaneously increasing their surface area to better intercept light. Furthermore, leaf orientation was altered, while the total surface area of the canopy increased [99]. Based on these findings, it is crucial to examine whether the crop of interest can acclimate to shade well, thus being suitable for cultivation under the shade casted by the PV array.

2.2.2 Sensitivity to shading

Overall, there is a literature gap with regards to the impact of agrivoltaics on plant productivity and yield. Another path to conceptualize the effects of shading on crop growth, is to revise studies with artificial shade, such as shading nets, or those related to agroforestry

Figure 12 – A shading net experiment [100], and the corresponding irradiance intensity and distribution on ground for full sun conditions (open field), under the shade of the net, and of the APV facility (not shown). These are not simulated values nor measured, rather they are included to illustrate the differences between the shading practise followed.

experiments [4]. Nonetheless, these conditions do not accurately represent the actual shading below the PV array. In APV systems, depending on the design, the reduction of solar radiation is dynamic and non-homogeneous, while under a shading cloth it is spatially homogeneous. For illustrative purposes, the schematic in Figure 12 displays the setup of a shading net experiment along with a simplified distribution of irradiance. A thorough re-view of studies related to the interplay between shading and crop yield is already published [4]. Whether yield increases, or decreases, and by how much is determined by the local climate, crop physiology, and shading intensity. Fraunhofer ISE investigated the relation between PAR availability and crop yield for a plethora of plants and determined that crops can be divided according to their response to shading [101-102]. This sensitivity analysis is displayed in Figure 13, where three distinct responses to light can be observed. Both crop yield and PAR are expressed as a percentage of the actual values obtained under full sun (FS) conditions. In blue, the behavior of a shade tolerant crop is displayed, where yield is maximized at around 75% of FS conditions. This is because shade tolerant species cannot acclimate well to high light conditions. Furthermore, their LSP is relatively low, thus they cannot utilize FS conditions efficiently. Shade tolerant crops do not experience yield reductions if the incident PAR is above 50% of FS conditions. In yellow shade intolerant species are shown, where crop yield depends almost linearly to incident PAR. For such crops substantial yield reductions can occur. Finally, in red the behavior of many commercial crops is plotted,

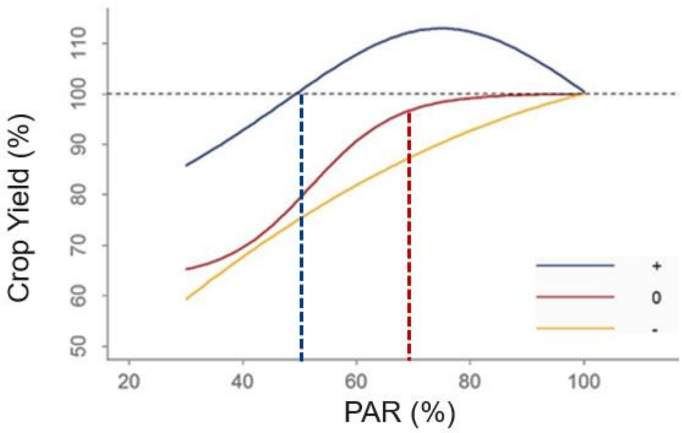

Figure 13 – Crop yield sensitivity to incident PAR and crop shade tolerance [102]. Crops are divided according to their acclimation to shade into shade tolerant (blue), shade intolerant (yellow) and in between (red). The vertical and dotted lines indicate the minimum incident PAR to ensure sufficient yield.

which is probably the most realistic response. Crop productivity is relatively unaffected for a PAR reduction up to 30%. The light requirements of crops can vary significantly, and thus careful selection of shade tolerant species is preferred to allow high PV densities to be installed, and thus maximization of land productivity.

Light intensity is undeniably the factor that influences crop yield the most, however, the time-period of shading and the crop's phenological stage during that shading period are crucial as well. The amount of light required to reach saturation varies throughout a crop's growth phase: establishment, vegetative, and reproductive. Establishment occurs through the germination of the seed, which is then followed by the vegetative stage where stems and leaves are formed until they are full-grown. In the last stage, where reproduction initiates, sensitivity to light is highest. For instance, the following PAR intensities are recommended for cucumbers, peppers, and tomatoes: 100-300 (establishment), 300-600 (vegetative), and more than 600 $\mu mol\ m^{-2}\ s^{-1}$ (reproductive) [103]. For winter wheat, the decrease in crop yield and number of grains per m^2 was attributed to the amount of PAR reduction 7 days before anthesis, and throughout grain-filling [104]. Another study on wheat found that the reduction of yield was most sensitive to the shading intensity 30 days prior to flowering [105]. For maize, flowering and early-grain filling were found to be most sensitive [106]. Specifically, during pre and early-silking a reduction of solar radiation by 50% resulted in a 12.6% decrease in yield [107]. When the same shading was applied during post-silking the reduction in yield was 21.4%. Such findings were confirmed by other studies where crop yield sensitivity to shade was highest during flowering and grain filling [108-109]. A similar dependency of crop yield to phenological stage was found in sunflowers, where the number of grains was more sensitive to shading during post-anthesis, rather than pre-anthesis [110-111]. Based on these findings, a pattern is observed for many if not all crops where yield is highly sensitive to certain growing periods. This is another important issue to consider when designing an APV array.

2.3 Synergy with bifacial PV

Through the utilization of bifacial solar cells significant reductions in PV system levelized cost of energy (LCOE) are expected in comparison to their monofacial counterpart [112]. Furthermore, bifacial modules are currently available, in comparison to state-of-the-art multi-junction modules or semi-transparent technologies that demand further laboratory research to ensure compatibility with various crops. Nonetheless, due to a lack of knowledge with regards to their design, bifacial specific benefits are not utilized appropriately. To overcome this barrier, a thorough investigation is required; a sensitivity analysis of the bifacial power output with regards to the module's orientation, elevation, ground albedo, and packing density amongst others is necessary [112-115]. In agrivoltaic systems, plentiful irradiance must be incident on the ground to ensure a marketable crop yield, which bifacial modules can better capitalize on due to their rear side absorption. To conceptualize the potential synergistic effects between crop cultivation and bifacial energy yield a thorough literature review on the influence of system deployment configuration is necessary.

At first, some parameters regarding the performance of a bifacial PV module must be introduced. Rear side power generation, and thus overall energy yield is dependent on the efficiency of the rear side, which is considered through the bifaciality factor (BF). It is defined as the ratio of rear side to front side efficiency at standard test conditions (STC):

$$BF = \frac{\eta_{STC,r}}{\eta_{STC,f}} \cdot 100\% \tag{7}$$

As a result, the rear side can convert only a fraction (BF) of what would be generated by the front side. In general, the BF can vary according to the technology used from 75% in interdigitated back contact (IBC) solar cells, to over 95% in heterojunction with intrinsic thin-layer (HIT) cells [116-121]. Consequently, through careful examination of the deployment configuration of the array, one can determine the appropriate BF that will maximize LCOE. For example, in an E-W facing and vertical bifacial array, a high BF is recommended to exploit the plentiful irradiance incident on the rear side. Logically, module configurations that permit high electrical gains from their rear side should preferably have a high BF.

In general, as bifacial modules deviate from their optimum orientation for light harvesting, the gain of the rear side increases [112]. To measure the relative energy yield gain of bifacial in comparison to monofacial the bifacial gain (BG) is used:

$$BG = \frac{Y_{e,r}}{Y_{e,f}} \cdot 100\% \tag{8}$$

For experimental or small demonstration systems the BG is expected to vary between 15 to 25%, while for PV farms values are expected to lie around 5 to 15% [114]. Consequently, for APV systems where the PV density is expected to be considerably lower, higher bifacial gains can be achieved for the same configuration [112]. Other than the packing density of the array, the orientation is also crucial in determining the BG. For example, for an optimally inclined and south facing array the overall energy yield is maximized, however BG is minimized, since the front side is prioritized. On the other hand, for an E-W facing vertically installed array BG is prioritized attaining values around 80%, while energy yield is reduced [114]. This was verified by the simulation results obtained in this thesis that are described further in subsection 4.1.2 Azimuth, tilt and row spacing. As was discussed previously, the gain of the rear-side is dependent on the BF, thus for the vertically E-W array, the BG is essentially equal to the BF, assuming both sides receive equal irradiation. Although a high BG is desirable, it does not necessarily imply that energy yield is maximized, unless highly reflective surfaces are present with latitudes close to the equator [122].

To further conceptualize what limits BG and thus overall energy yield, the non-uniformity of incident irradiance onto the rear side of the bifacial module must be analysed.

By determining irradiance G (W m^{-2}) incident per cell on the rear side, one can determine the variation in irradiance distribution through:

$$\mathrm{Non-uniformity} = \frac{G_{\mathrm{cell,r,max}} - G_{\mathrm{cell,r,min}}}{G_{\mathrm{cell,r,max}} + G_{\mathrm{cell,r,min}}} \cdot 100\% \tag{9}$$

where $G_{\mathrm{cell,r,max}}$ and $G_{\mathrm{cell,r,min}}$ are the maximum and minimum irradiance values incident onto the rear side of the bifacial cells. This non-homogeneous distribution of irradiance is a limiting factor to the performance of the module's overall rear side [123-124]. Note that rear side inhomogeneity decreases for days with a high diffuse fraction, since diffuse light results in smoothening of shadows casted on the ground [125]. Furthermore, it depends on the deployment configuration (tilt angle, elevation, etc.) as well as ground albedo, while measured values were found to lie between 7 to 35% [123-125]. Berrian et al. (2019) suggested that the overall module inhomogeneity has a bigger influence on the total power loss, since it is more sensitive to front irradiance for south and optimally inclined modules. A quadratic fit was found between the overall irradiance inhomogeneity and power loss mismatch [125]. Even though, less than 0.5% of power losses due to variation in irradiance throughout the module's cells is expected [125]. The aforementioned parameters are necessary to assess the performance of the bifacial array, under various installation configurations.

2.3.1 Deployment configuration

To conceptualize the underlying trade-offs in the design of a bifacial PV array and the potential synergies with crop cultivation, a thorough review is performed on the parameters influencing bifacial performance. The factors addressed include but are not limited to module elevation and orientation, PV array density, module transparency, size of reflective ground surface, and albedo. These factors are interrelated to a certain degree, thus complicating the optimization of bifacial systems. Note that for additional information regarding crop albedo and its spectral properties the reader is referred to the next subsection 2.3.2 Crop albedo.

As previously described, for ground mounted (GM) bifacial systems the distribution of rear irradiance is inhomogeneous. This can significantly impact rear and ultimately the overall energy yield; however, it can be alleviated by increasing the module's elevation [112, 126-128]. Note that the module's elevation is measured from its lowest edge to ground. In one study, it was determined that by raising a south facing module from 10 cm to 1 m, the standard deviation of rear side irradiance decreases from 28.4% to 2.8% for a given day at noon [126]. It was further discussed that this deviation in irradiance or inhomogeneity is time dependent. Similar results were found in another paper, where the spatial non-uniformity of irradiance equation 9 was below 2.5% for vertical clearances above 1 m [127]. However, in both papers only a single module was simulated, thus these findings do not necessarily reflect the actual irradiance inhomogeneity in a bifacial array.

Other than homogenising rear side irradiance, elevated modules benefit from an overall increase in the magnitude of rear irradiance. As the mounting height increases the view factor (VF) from PV to unshaded ground increases, thus ground reflection and rear POA irradiance are enhanced. This relationship between rear irradiance and mounting height closely resembles a logarithmic trend – at least for setups with only one module or a string – and at a sufficient height saturation of the BG is expected [115, 122, 126-128]. Specifically, for an albedo of 0.2 a clearance of around 2 m from the ground is necessary to attain 95% of the maximum irradiance [127]. A similar study investigated the influence of latitude and climate and concluded that sensitivity to elevation was higher for locations closer to the equator [128]. For northern latitudes the sun rays have a higher Angle of Incidence (AOI) and usually in such regions the diffuse fraction is also larger. Therefore, the shading effect is mitigated, which leads to a reduced sensitivity with respect to elevation. This dependency of optimum elevation to latitude was verified by another study, in addition to the influence of albedo [122]. For ground surfaces with high albedo, the optimum elevation is higher to better utilize the plentiful ground reflected irradiance [115, 122, 126, 128-129]. Consequently, energy yield is more sensitive to elevation for highly reflective ground surfaces.

This sensitivity to elevation is also dependent on the bifacial system's size as shown in Figure 14 for clear days around the summer solstice, fall equinox, and winter solstice. The energy yield and BG are determined for each of these corresponding days, system sizes, and mounting heights, for an albedo of 0.21. Three system sizes were analysed; a single module, a single row with five modules, and a multi-row (5x5) where the results are representative of the centre module. Furthermore, for each day simulated, a different tilt angle is used that corresponds to the optimum for that season. This might cause some inconsistencies, in terms of generalizing the behaviour of sensitivity to elevation, since modules that are tilted suffer less from self-shading, thus reaching saturation in yield at lower heights. Note that self-shading refers to effect where the shadow casted by the module shades the ground in its close vicinity, thus leading to a reduction in BG. Overall, the saturation height is approximately around a meter, depending on the day, and deployment configuration [115]. However, this

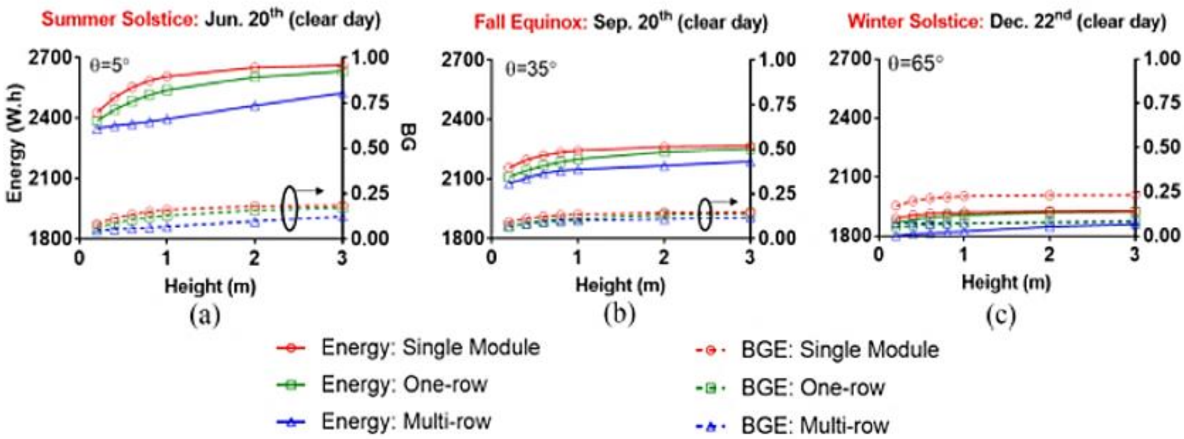

Figure 14 – Influence of elevation on daily energy yield and BG (%) for various system sizes and seasons [115]. Note that all systems are facing due south and are tilted for optimal light harvesting in the corresponding season, while they are simulated for the climate of Albuquerque, USA (35.1°N).

saturation effect is not present for bifacial arrays, instead the trend is linear as shown in Figure 14 (a), which is a direct result of the intensified ground shading due to the system's size. This behaviour is not as apparent on the other days, possible due to the increase in tilt angle, and/or increase in AOI, and/or decrease of clearness index as the analysis period is shifted towards winter. APV systems are expected to be elevated much higher than conventional GMPV systems to ensure operation of agricultural machinery, which in turn enhances the magnitude and homogeneity of rear side irradiance.

When it comes to the tilt angle sensitivity of energy yield, literature indicates that bifacial modules will outperform monofacial for the same orientation (tilt & azimuth) [112]. Initially, it was claimed that latitude inclined bifacial modules would maximize annual energy yield [130], however a more rigorous approach is required to fine tune energy yield. Yusufoglu et al. (2014) examined the influence of elevation, ground albedo, and location on the optimum tilt angle. It was concluded that higher tilt angles are optimal for GM modules, and/or high ground albedo, and/or high latitude. Modules that are elevated higher do not suffer as much from self-shading, thus the optimum tilt becomes lower. On the other hand, when albedo is high, tilted modules gain more from ground reflected irradiance in comparison to the loss of Sky View Factor (SVF) and front beam irradiance. In a later study Yusufoglu et al. (2015) considered the influence of rear irradiance homogeneity to better assess the interplay between tilt, elevation, and albedo. The results mostly agree with those reported previously, but they diverged for the case of high albedo and module elevation as shown in Figure 15 (a, b). As the albedo increases the homogeneity of rear-side irradiance decreases with a growing rate [125]; consequently, to mitigate self-shading high tilt angles are compulsory for GM bifacial modules. The discrepancy arises at high elevations and ground albedo, where a decreasing trend in optimal tilt occurs [126]. Furthermore, it is claimed that lower tilt angles enhance rear homogeneity for elevated modules, thus increasing overall energy yield. Then again, rear homogeneity is already less than 3% for modules elevated above 1 m [126-127], thus

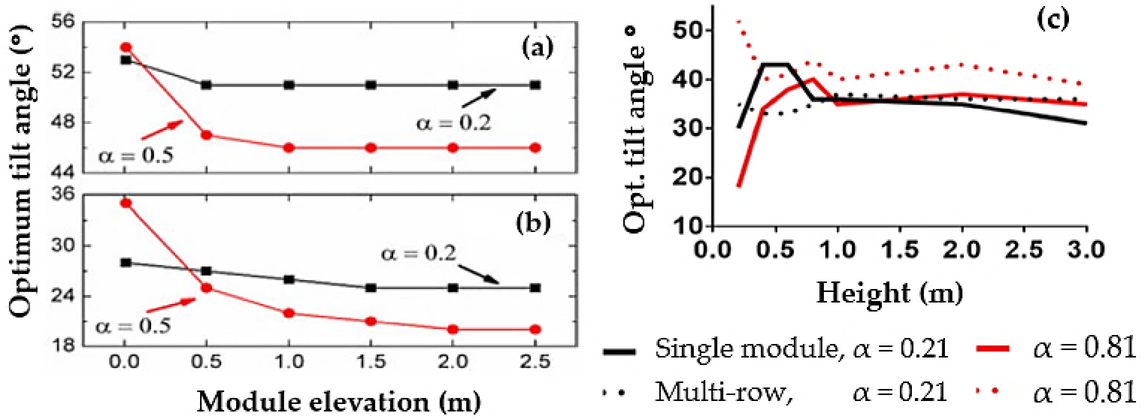

Figure 15 – Annual optimal tilt angle versus elevation for various system sizes, locations, and albedos. The simulated values are representative of a single module located in (a) Oslo, NO (60°N) and (b) Cairo, EG (30.1°N) [126]. In (c) both single and multi-row systems are analysed located in Albuquerque, USA (35.1°N) [115].

additional research into the matter might prove otherwise. Another counter argument is that for high albedo and elevation, there is abundant ground reflected irradiance, which should be exploited by further tilting the modules in comparison to a lower albedo case. This argument is supported by the sensitivity analysis performed in [115], where the PV system's optimal tilt was related to the system's size, elevation height, and ground albedo included in Figure 15 (c). For elevations above 1 m, the change in optimum tilt is almost minimized. Furthermore, the tilt that maximizes energy yield is higher for an array than a single or stringed system, where high albedos are present. For example, the optimal tilt is 36° and 40° for an array with ground albedos of 0.21 and 0.81 respectively [115]. This behaviour illustrates the additional complexity in modelling of bifacial arrays, thus justifying the need of an individual assessment per layout configuration.

Because of its capability to absorb rear side irradiance, an E-W facing vertical bifacial module is a viable option for power generation depending on the ground's albedo and site's latitude. Thus, the comparison is made between E-W vertical and S-N optimally inclined modules. For the case of a low ground albedo (0.25) a S-N module outperforms vertical E-W, generating up to 15% more energy yield [122]. On the other hand, for twice the albedo the E-W orientation can outperform the S-N by up to 15% for latitudes below 30 degrees. In higher latitudes, the optimal inclination of S-N is increased, thus the shading effect is minimized and ultimately rear inhomogeneity. However, as modules are elevated from GM to 1 m above the ground, the S-N facing array develops into the optimal orientation globally [122].

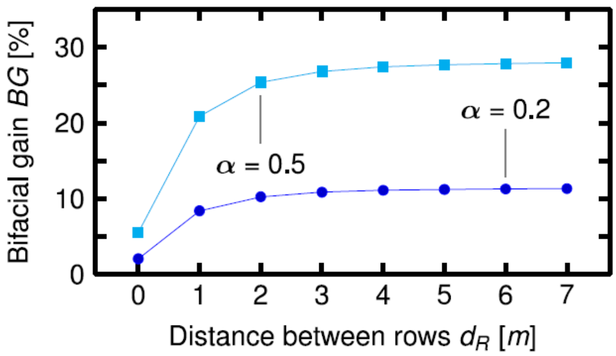

Figure 16 – Modelled bifacial gain sensitivity to row spacing for an array with two ground albedos [131].

Until now, mainly single-row bifacial systems were discussed; however, it is crucial to understand how an array will perform under conditions of increased mutual and ground shading. It is clear by now that single bifacial modules or small systems will result in significantly higher BG in comparison to large scale systems. To conceptualize the influence of the array's packing factor a bifacial system consisting of three rows with eleven modules per row was simulated under various ground albedos and row spacings as shown in Figure 16 [131]. The distance between rows was increased and the BG of the centre row was recorded. The behaviour is logarithmic, and as the row spacing (RS) is increased BG also increases, since additional ground reflected irradiance is incident on the rear side. Eventually, BG saturates depending on the ground's albedo, since more light can be absorbed when a highly reflective ground surface is employed. These findings are representative of the centre row in a small bifacial system; thus, they do not necessarily portray the actual BG of larger scale PV farms. Note that ground albedo is expected to decrease for larger systems, due to the additional shading by neighbouring rows. Another issue that must be addressed is that the BG per module varies throughout an array, depending on the PV density and orientation. Skoukry et al. (2016) investigated this variability in BG between modules in an array, consisting of five rows, with eleven modules each, set at a RS of 2.5 m. Simulation results that were validated indicate that modules at the edges of the array have a higher BG, since their view to the ground and sky is less obstructed [131]. On the other hand, modules at the centre receive the lowest rear irradiance, and thus BG. Overall, bifacial gain was found to vary between 27.7 and 31.4%. Note that in this study an albedo of 0.5 was used, while for lower albedos the variability in BG could be reduced considerably. Then again, in large-scale systems, this inhomogeneity in BG is expected to increase.

As the RS is widened, the packing factor or density of the array decreases, while the BG and rear irradiance benefit depending on the array's orientation. Consequently, the specific yield (kWh/kWp) of the bifacial system increases; however, after a certain RS is attained saturation occurs. Furthermore, the overall energy yield per area decays with wider RS after a certain optimum spacing is attained. When compared to monofacial PV, bifacial can outperform them for the same orientation and density [112, 132]. As displayed in Figure 17, bifacial systems have a different sensitivity to the packing factor or GCR compared to monofacial, depending on the albedo. For all PV densities bifacial power output is higher, and the increase saturates at high densities [132]. As the RS is increased, the PV density decreases, allowing more light to be reflected depending on the ground's albedo. This explains the difference in curvature from low to high albedo in comparison to monofacial. On the other hand, depending on the array's orientation, monofacial modules can benefit from an increased albedo. Additional parameters must be considered to properly assess the influence of GCR and deployment configuration on the energy yield of a bifacial array.

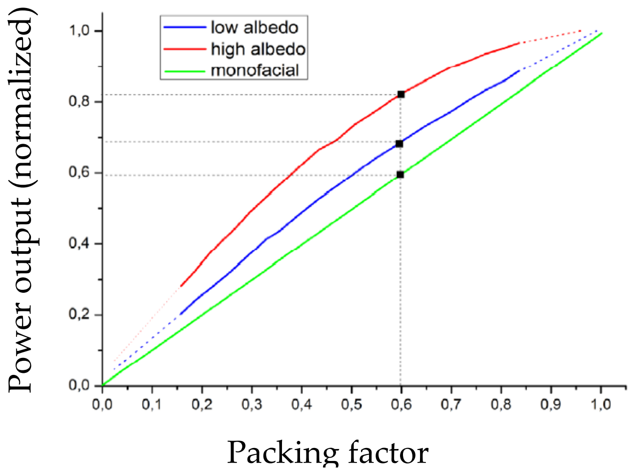

Figure 17 – Illustration of the relationship between power output and packing factor or GCR for both monofacial and bifacial (low and high albedo) [132]. The y-axis is normalized against the nominal power output of the monofacial module.

The saturation effect when large row spacings are employed was also analysed by Appelbaum (2016) for vertically installed PV. It was verified that an increase in horizontal clearance from 2.9 to 3.9 m would increase the annual incident irradiation by only 1% for south facing and optimally inclined arrays. However, for an E-W facing and vertical array the same increase in clearance would significantly affect incident irradiation by 7.9% [133]. This is a direct result of the higher sensitivity to shading when modules are placed vertically. Furthermore, as the row spacing is increased, the SVF and VF to the ground increase. Consequently, the deployment configuration of a vertical E-W facing bifacial system requires less packing to capitalize on the ground reflected and diffuse irradiance. The E-W vertical orientation was examined in-depth and a sensitivity analysis was performed for the annual energy yield per m^2 and pitch to height ratio (p/h) [134]. The parameters considered include various latitudes and clearness indices at a ground albedo of 0.5. As was discussed previously, the E-W configuration is more sensitive to RS, and while specific yield is enhanced through a wider RS, the total production per farm area reaches an optimum and then declines with increasing RS. For such configurations the trade-off between specific yield and total yield per area is intensified in comparison to S/N and optimally titled arrays. It was found that as the DNI component dominates a low pitch to height ratio would be optimum, while the opposite is true for regions where DHI dominates [134]. Furthermore, up to 30 degrees latitude a lower p/h (~0.8) is optimum, while for northern latitudes optimum p/h increases [134]. This is in accordance with the clearness index, since in high latitudes sky conditions are frequently overcast or intermittent, thus DHI dominates. To utilize diffuse light appropriately, masking should be minimized, thus RS is increased under such conditions. Overall, APV systems are expected to be employed at wider RS to allow sufficient light for crop growth, thus increasing the specific yield of bifacial PV.

In an attempt to increase rear side homogeneity and magnitude the influence of module transparency is investigated. Deline et al. (2017) examined this relationship and concluded that for close to GM configurations rear irradiance is increased by around 10%; however, for higher elevations rear irradiance is slightly impacted by the module's transparency [127] as shown in Figure 18. In another paper, the influence of cell spacing on the panel's electrical efficiency was explored and found out that there is a nonlinear response between efficiency and cell packing factor [135]. As the packing factor decreases, transparency increases, and thus more irradiance is incident on the ground (reflector in this case). Rear irradiance increases and consequently module efficiency as well. However, according to the reflector's efficiency (albedo, orientation), module efficiency saturates at high packing factors. [135]. At high PV cell densities, there is additional shading on the reflective surface, thus saturating the overall module efficiency increase. Furthermore, as transparency increases,

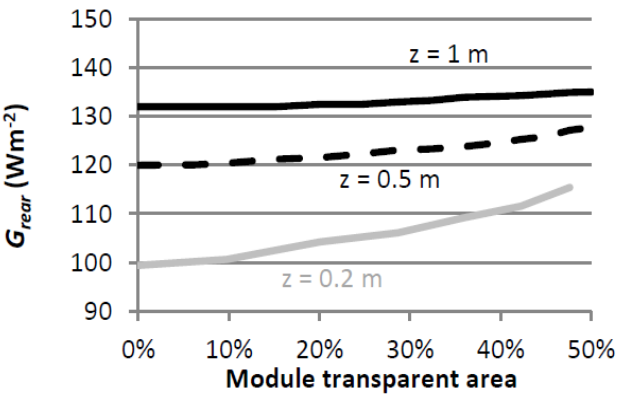

Figure 18 – Modelled rear irradiance as a function of module transparency [127]. The results are representative of a single module, that is facing due south, tilted at 37°, with an albedo of 0.2.

specific yield is enhanced, while overall yield per area is reduced. Therefore, another trade-off arises between specific and total yield.

One more benefit of increasing bifacial transparency, is a reduction in the module's operating temperature [136]. In general, due to the glass material and exposed rear surface, absorption of infrared light and operating temperature are reduced in comparison to a monofacial module [137-138]. Module temperature is expected to be further reduced when transparency increases, due to improved heat dissipation [136]. This in turn boosts the open-circuit voltage, and thus the module's electrical performance. In the context of APV, increasing the module's transparency can be a viable solution for light demanding crops, especially when ground irradiance is saturated through widening of the RS. The potential of varying the cell's spacing and the underlying trade-offs are examined further in section 4.5 Cell sensitivity – micro scale.

2.3.2 Crop albedo

The influence of albedo on the energy yield of bifacial systems is already discussed, along with its relation to the array's configuration. In APV systems however, the ground albedo will be crop-specific, and consequently vary with season [139]. Furthermore, Ziar et al. (2019) concluded that albedo can also vary according to optical and morphological properties of the surface and surroundings, as well as time, location, climate, and PV configuration. By clustering all these parameters in a comprehensive model, the ground albedo of a complex environment was accurately determined [140]. The PV modules cast shadows on the ground, thus leading to a reduction of the overall albedo, since shaded patches reflect only diffuse light. The weather conditions can impact the contribution of DHI and DNI components, and in turn the amount reflected by the ground [141]. Furthermore, it is reported that the position of the Sun on the hemisphere can also influence albedo, thus verifying latitude dependency as well [142]. These parameters are entangled through time, and according to the Sun's position, the geometry of the shadows casted by the PV modules will vary. However, in comparison to conventional GMPV arrays, an APV system's power output will also be crop specific, based on the optical properties and the canopy's architecture. Equation 6 in section 2.2 Crop yield describes the amount of solar irradiation intercepted by a plant, which relies on its LAI, as well as leaf arrangement and orientation [89]. Furthermore, depending on the crop's height, additional shading can occur, thus obstructing a portion of the reflected irradiation. On top of that, the planting density of the crop can significantly impact ground albedo since a portion of the ground will be covered by the crop dependent albedo. Overall, bifacial modules heavily rely on ground albedo [143-144], thus complicating their integration and modelling in agrivoltaic systems. Finally, additional implications arise by considering the spectral distribution of incident irradiation and its influence on the spectrally responsive albedo.

It has been established that the spectral distribution of reflected irradiation varies according to daily and seasonal shifts, as well as location [145-146]. To account for these changes, in addition to the crop's reflectance per wavelength and angular distribution, the spectral response of the PV technology used is also required. In general, plant leaves show a similar behaviour in terms of their spectral reflectance characteristics; reflectance is minimized for ultraviolet, blue, and red wavelengths, with a small peak in green, and then gets maximized in near infrared [147]. Naturally, there are differences in the magnitude of reflectance amongst species according to their optical properties, which are defined by important pigments such as chlorophylls and carotenoids [147]. On the other hand, c-Si solar cell absorbs most efficiently between 450 and 1050 nm, with a peak at around 900 nm [148], thus mostly benefiting from the near-infrared crop reflectance. Nonetheless, the spectral and anisotropic characteristics of albedo are beyond the scope of this report, while the interested reader is referred to [149] for a more in-depth analysis. Reflectance of thirty plant species for some wavelengths are included in [150], and two more in [151]. For a more detailed spectral distribution bean, avocado, sorghum, and pigweed are depicted in [152], potato, alfalfa, canola, and oat hay in [153], corn and soya bean in [154], while cotton, wheat, and rye in [155-157] respectively. Reflectance values for wavelengths in the infrared region vary depending on the crop. For instance, 63% in lettuce and 87% in beans [150]. Additionally, up to 700 nm reflectance values lie below 20% for most crops, except for lettuce. To estimate the actual ground albedo, the crop's reflectance and morphology – LAI, extinction coefficient, canopy height – as well as planting density must be factored. As previously discussed, the albedo of vegetation depends on season, and commercial crops are no exception. For example, during their early growth stages leaves and branches have not been properly developed to allow considerable contribution to the overall albedo. Finally, fruits can also impact albedo, as shown in [158], where reflectance values varied from 60-80% in the infrared region for apple, orange, nectarine, and pear. This results in additional complications in deriving the actual albedo, since fruits develop at a much later stage and occupy only a portion of the total plantation. For crops with high light requirements the potential of reflective mulches could be investigated to effectively increase ground albedo [159-160], and thus benefit both crops and bifacial PV simultaneously.

2.4 Simulation software

In this section a literature study is performed on the simulation techniques used for modelling irradiance in bifacial modules as well as for the ground. The purpose is not to exhaust all the potential options, rather to compare between techniques and determine the one that is most robust for agrivoltaic applications. To achieve the objectives of this thesis, the modelling approach must be flexible in terms of its capability to address various PV deployment configurations as well as detailed features of the design, such as module and cell spacing modifications.

2.4.1 Irradiance modelling

In terms of modelling front side irradiance of bifacial modules, optical models developed for monofacial modules can be utilized with minimal adjustments [161]. However, due to the plethora of parameters that rear irradiance is sensitive to, modelling of the rear side can complicate the derivation of the overall energy yield. In other words, an individual assessment is required for each deployment configurations. A thorough analysis of simulation tools MoBiDiG, BIGEYE V3, and PVsyst was achieved in [162], while to assess their performance the output was compared to measured data. MoBiDiG was developed at ISC Konstantz [163] and incorporates a quasi 3D VF concept to determine ground reflected irradiance, while BIGEYE V3 at ECN.TNO [164] uses a fully 3D VF approach. They both utilize the Perez model for the contribution of diffuse irradiance. On the other hand, PVsyst [165] simplifies the analysis to a 2D VF model that assumes long rows, as they usually occur in large PV farms. The simulation results are representative of the central module in an array of 3x3 modules, elevated by 0.75 m, with a ground albedo of 0.51. To determine the influence of the insolation conditions three days were selected, with different skies; clear sky, intermittent, and overcast. For all tools analysed, the results obtained for the front irradiance closely resemble the measured data, with some deviation for horizontal or vertical installations [162]. A similar behaviour was observed for the rear irradiance, however with an increasing deviation reaching a maximum of 10% under overcast conditions for a vertical orientation. Other than being sensitive to the module's orientation, the error was also sensitive to sky conditions; a lower deviation with increasing share of direct irradiance was observed [162]. Nonetheless, since energy yield is primarily affected by days with clear sky conditions and by the contribution of the front side, the overall deviation decays in an annual scale. Therefore, results from the simulation tools coincide with the measured data.

A similar study investigated the potential of ray tracing (RT) for the determination of rear irradiance [166], using bifacial_radiance, an open-source tool developed by NREL [167]. It is based on an open-source backward ray tracer known as Radiance [168]. Here a distinction is made between forward and backward ray tracing, where in the latter rays are traced from the surface of interest to the source, while in the previous they are traced from source to the surface. Naturally, for rear irradiance determination backward RT is more efficient, as less rays are traced without compromising on accuracy. The results were obtained for an hourly time-step and then compared to MoBiDiG and subsequently validated by measurement data. For a mean measured albedo of 0.5, both RT and the VF approach displayed an agreement with the experimental values of irradiance apart from some inconsistencies during noon [166]. In addition, the sensitivity of deviation to climatic conditions discussed in [162], was also observed in [166]. By accumulating hourly data to daily to monthly, the deviation between simulated and measured data decays. Overall, both RT and the VF approach can model rear irradiance of bifacial modules with an accuracy varying between +-0.5% to +-2% [166]. For both articles discussed the modules are close to GM, with an elevation of 0.75 m in [162] and

0.15 m in [166]; consequently, the performance of the aforementioned tools for highly elevated modules must be examined.

To allow the operation of agricultural machinery APV arrays are usually mounted 4 to 5 m above the ground, thus it is essential to examine the potential discrepancies in modelling of such bifacial systems. A comparison between three simulation tools is achieved in [169] to determine which modelling approach offers the least deviation to measured values of a large bifacial plant in La Silla, Chile [170]. Specifically, three distinct approaches were used to model irradiance; PVsyst and MoBiDiG that utilize VF for both front and rear, and a hybrid approach that consists of MoBiDiG VF for front and bifacial_radiance RT for rear side irradiance. By utilizing a hybrid approach, and thus applying VF for the front side, the overall computational time is reduced considerably. The results are representative of a bifacial array with unlimited rows and columns, a GCR of 33% and an albedo of 0.28. As expected, front irradiance remains almost constant with increasing elevation from ground [169]; however, rear-side irradiance considerably increases with elevation as shown in Figure 19. The VF approach leads to an underestimation of the rear side irradiance for elevations above a certain threshold [169]. Results accumulated for a four-month period verify this behaviour in BG, which are displayed in Figure 19. Overall, the MoBiDiG Hybrid approach represents the experimental values with the highest accuracy. Consequently, RT instead of the VF approach should be utilized to determine the contribution of the rear side in bifacial PV.

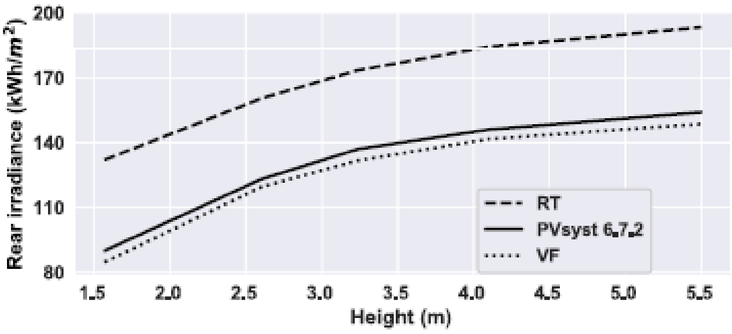

Model. approach	Bifacial gain
Measured	10.4 – 12.4%
MoBiDiG Hybrid	9.3%
PVsyst	6.8%
MoBiDiG VF	6.5%

Figure 19 – Comparison in rear irradiance values obtained through different optical models [169]; RT approach with bifacial_radiance, VF with MoBiDiG, and VF with PVsyst. The table on the right includes the measured (La Silla) and simulated bifacial gain of the array for a four-month period based on the modelling approach used [169].

The increased reliability in determining rear irradiance through RT was also verified by [171], where the simulation results of two approaches: PVsyst (VF), and Fraunhofer ISE (RT) based on Radiance [172] were compared to measured data for two systems. System 1 consists of a single string of eight bifacial modules, elevated at 1.5 m from the ground with albedo of 0.55, tilted at 37°, and facing southwest, while system 2 consists of a larger bifacial array, elevated at 6.6 m with albedo of 0.2, tilted at 20°, and also facing southwest. The mean biased error (MBE) between simulated and measured values is summarized in Table 1. Although for the determination of the front irradiance both approaches yield similar results, the MBE of rear irradiance is considerably reduced when simulated using RT [171]. As a result,

Table 1 – View factor and ray tracing modelling approach performance for agrivoltaic systems [171]. The values in percentage represent the MBE with respect to the measured values for both front and rear side irradiance.

	Model. approach	System 1	System 2
Front Irr.	PVsyst (VF)	4.6%	4.9%
	Fraunh. ISE (RT)	6.3%	2.9%
Rear Irr.	PVsyst (VF)	-21.5%	-23.2%
	Fraunh. ISE (RT)	-3.9%	-3.5%

based on the literature findings of [169, 171], RT will be utilized for irradiance modelling of the bifacial agrivoltaic array.

Multiple research institutes and companies have employed the use of RT for the evaluation of bifacial performance as shown in Table 2. Électricité de France (EDF) developed their own RT approach, and by considering rear irradiance inhomogeneity, they evaluated the impact of the module's frame and support structure on the overall distribution and magnitude of irradiance [173]. Overall, the error in estimating the energy yield for a 3-month period in a site located in Paris, was less than 1%. EDF's RT and Fraunhofer ISE RT approach based on Radiance, were validated experimentally for a variety of climates, deployment configurations, sizes, as well as tracking systems [172]. The average total error in deriving energy yield and POA irradiance lies between 3-7%. The RT simulation tool developed by Fraunhofer ISE was also compared to PVsyst VF, for two distinct systems [171], whose results are summarized in Table 1. Another pre-described study [169] indicated that NREL's bifacial_radiance tool based on Radiance can effectively estimate BG of a large-scale bifacial array for a 4-month period. Researchers in [174] compared the performance of a VF cell-level approach to Radiance, in addition to COMSOL, a forward ray tracer that uses the simplified isotropic sky diffuse model. For the determination of front irradiance, Radiance resulted in 5% lower values in comparison to the other two approaches, while for the rear, it led to an overestimation. Consequently, RT is an accurate optical modelling approach that can be integrated in comprehensive energy yield models to ultimately derive the performance of a bifacial array.

2.4.2 Raytracing with Radiance

Many RT tools are based on Radiance which utilizes backward RT, thus offering increased computational efficiency for the derivation of rear-side irradiance. This is especially true for complex environments, or deployment configurations, since some of the rays emitted by the source do not reach the rear side, thus not contributing to energy yield. The accuracy of RT over the VF approach for modelling of agrivoltaic arrays that are highly elevated is already described. However, there are additional benefits such as the capability to model complex geometries [168] – influence of frame, support structure, SVF obstruction – and detailed design features (module and cell spacing) that are not easily addressed through the VF approach [172-174]. An increasing amount of studies have explored the use of Radiance RT software for the derivation of bifacial rear irradiance, thus proving its modelling robustness for various system sizes, deployment configurations, and climates as described in Table 2.

Table 2 – Literature review of studies related to the use of ray tracing for irradiance modelling of bifacial PV systems. Information regarding PV topology, albedo, and analysis time-period are also included.

Literature Description	Deployment Configuration	Other factors
bifacial_radiance RT, MoBiDiG VF, PVsyst VF, experimental values [169]	Unlimited rows & columns, GCR = 33%, $h_{hub} = 2.1m$, varying tilt	$\alpha_{Gr} = 0.28$, hourly to annual data
Fraunhofer ISE RT, PVsyst VF, experimental values [171]	1) String of 8 modules, $h_M = 1.5m$, $\theta_M = 37°$, $A_M = 217°$ 2) bifacial array, GCR = 40%, $h_M = 6.6m$, $\theta_M = 20°$, $A_M = 234°$	1) $\alpha_{Gr} = 0.20$, 2) $\alpha_{Gr} = 0.55$, hourly to annual data
Fraunhofer ISE RT, EDF RT, experimental values [172]	1) single module, varying tilt 2) small-scale array, $\theta_M = 30°$ 3) small-scale E-W HSAT tracking 4) large-scale array, $\theta_M = 12°$	1,2) $\alpha_{Gr} = 0.25, 0.30$ 3,4) $\alpha_{Gr} = 0.30, 0.32$ various time scales and climates
EDF RT, experimental values [173]	small-scale array, GCR = 50%, $\theta_M = 30°$	$\alpha_{Gr} = 0.30$, three-month period
Cell-level VF, Radiance RT, COMSOL RT [174]	2x4 modules, $h_M = 1m$, $\theta_M = 40°$,	$\alpha_{Gr} = 0.20$, hourly data
Radiance RT, experimental values [175]	single, varying tilt	mirror, daily data
Radiance RT, experimental values [114]	single, varying tilt	$\alpha_{Gr} = 0.64$, hourly to annual data
Radiance RT, experimental values [127]	single, varying BF, $h_M = 1m$, $\theta_M = 37°$	$R_{Gr} = 0.21, 0.81$, hourly data
Radiance RT, experimental values [115]	4x16 modules, varying tilt, $h_M = 1m$	$\alpha_{Gr} = 0.21$, daily data

Note: unless otherwise, all modules face due south and are ground mounted (<1 m elevation)

Additional pre-described studies indicate that Radiance can accurately determine the magnitude [114] and distribution of rear irradiance [115, 127]. An increase in deviation occurs for high tilt angles, nonetheless the overall accuracy is not jeopardized [114]. Furthermore, uncertainty in estimating Pmpp was found to lie within 1-2% [127]. For an array modelled in [115] the root mean square deviation (RMSD) of front and rear irradiance of the centre module in each row was found to vary between 4.6-6.8% and 4.3-16.4%, respectively. It was further noted that the deviation increases for the rows that are closer to south. The simulation period was a day in September, with clear sky conditions. Finally, a thorough validation of the results obtained through Radiance was examined in [175], where a root mean square error (RMSE) of 40% was obtained for the simulation of IV curves, under a clear sky. Based on these literature findings the modelling approach used to derive POA irradiance of the bifacial agrivoltaic array will be based on Radiance that has been extensively validated under various PV topologies and climates.

Radiance is a physically-based rendering and illuminance mapping software, which recursively solves the rendering equation for most conditions, through the use of backward raytracing [168]. In specific, it describes the transport of light that includes specular, diffuse, and directional-diffuse reflection, as well as transmission for a given geometry and environment. The RT algorithm of Radiance simulates the propagation of electromagnetic waves as rays that travel in straight lines, while their paths and interactions are described through refraction and reflection at each boundary. Such models are known as ray optics, where the wavelength of light is considerably smaller than the minimum geometric detail. Radiance does not consider effect of diffraction, interference, or polarization effects [168], that can be modelled with wave optics, where light propagation is treated as a wave phenomenon. For a more rigorous optical model of PV performance, the reader is referred to [176] which describes GenPro4, developed at TU Delft.

To model energy transfer flowing through a point in a specified direction, Kajiya's rendering equation [177] is recursively solved by the RT algorithm in Radiance [168]. However, it would be impractical to estimate the solution of this equation using uniform stochastic sampling, for example Monte Carlo, due to the heavy computational burden in computing the contribution of the Sun. To optimize between speed and accuracy, the simulation combines deterministic and stochastic ray-tracing techniques [178]. To achieve fast convergence, it is essential to separately compute certain parts of the integral in [177] deterministically. For a point on a surface, when the sample ray reaches the sun unobstructed, then for that point a deterministic approach is followed to derive the total solar contribution. Direct and specular components are thus computed on a per-pixel basis for the whole scene, while hemispherical sampling is less frequent [168]. Random sample rays are then sent throughout the hemisphere, thus estimating the integral of the light transport equation, where stochastic sampling is super-imposed on the deterministic source. To assess the contribution of diffuse irradiance at any point in the scene, this sampling process is iterated for multiple reflections throughout the modelling environment.

Radiance simulates irradiance distribution under one sky condition at a time, while the Radiance-based daylighting simulation tool, Daysim [179], can perform dynamic simulations for multiple sky conditions. It combines the algorithms found in Radiance, along with a validated daylight coefficient approach, as well as the Perez all weather sky model [180] to speed up the simulation without a significant loss of accuracy [181]. Daylight simulations determine irradiance distribution, as a result of daylight, through predicting daylight factors (ratio of incident to available horizontal illuminance). To determine diffuse daylight coefficients the celestial hemisphere is completely discretized into 145 continuous and rectangular sky patches [182] while for the ground, 3 ground patches are selected according to [179]. The luminances of the diffuse sky patches are based on the Perez all weather model [180] according to the corresponding date, time, DNI and DHI. The daylight coefficients of the ground segments are modelled based on *gendaylit* program of Radiance [183]. On the other hand, to model the contribution of direct light the selection of sun positions is site dependent, and for example, for latitudes above 70˚, they vary from 61 to 65 positions [183]. Each sun position is represented by a direct daylight coefficient, which describes the solar contribution. In order to faithfully represent the actual contribution of the sun for a given point on a surface, the method of interpolation is coupled to a shadow testing procedure [183], where sample rays determine whether a point receives direct light (DNI), or whether it is under shadow (only DHI). Subsequently, the irradiance that a point receives is interpolated based on those sun positions that are incident on that point without being obstructed.

For overcast sky conditions, the simulated results based on Daysim coincide with those measured experimentally, while for clear sky conditions deviation between the two increases [183]. The performance of Daysim was compared to the measured data of internal illuminances in an office room that utilizes a dynamic venetian blind system, for more than 10,000 sky conditions. The daylight coefficient approach in combination to the Perez all weather model, resulted in a relative error (MBE & RMSE) of less than 2% [183], and it was attributed almost equally to both the Radiance algorithm and Perez model. The use of Daysim was also validated in a later study [184], and it was verified that deviation is dependent on solar insolation conditions as well as scene complexity; values almost coincide for overcast conditions, while for clear sky error lies between 5-10%, and for intermittent it mostly lies within 10-15%. The deviation for partly cloudy sky conditions is mainly attributed to the limitations of the Perez model [183]. Overall, although the results obtained through Daysim are not as reliable as those from “classical Radiance” for clear or intermittent skies, its computational requirements are considerably reduced. Since the objective of this thesis is to simulate the effect of various PV topologies, it is deemed as a more practical modelling approach of irradiance, considering the time limitation.

3

METHODOLOGY

To optimize the deployment configuration of the APV array, various topologies will be analyzed, and their performance in terms of electricity and crop yield will be assessed. Consequently, the modelling approach used must be robust, yet flexible enough to allow manipulation of the design and efficient optimization.

To perform simulations in Radiance, a CAD model describing the surrounding scene must be inserted. Rhinoceros, also known as Rhino, is a 3D geometrical modelling tool that can create and visualize complex geometries. In fact, to model the agrivoltaic array any CAD software will suffice; however, by using Rhino's plug-in, Grasshopper, it is possible to attain precise parametric control over the installation configuration of the APV array. Grasshopper utilizes a visual programming language, where the user manipulates certain components (logic elements) graphically, instead of textually such as in C# [185]. Therefore, such a graphical interface allows the designer or engineer to focus on the "why" rather than the "how". Although the surrounding environment of an agrivoltaic array is expected to be simple, due to the open-field conditions, the sensitivity analysis of yield to PV deployment configuration can be quite cumbersome without the use of a parametric model. In other words, through the combination of sliders, mathematical expressions, and scripting (Python based), the most influential parameters regarding the design of an agrivoltaic array can be defined and subsequently adjusted to perform the sensitivity analysis.

To couple the geometric modelling performed in Grasshopper/Rhinoceros, with the irradiance modelling of Radiance/Daysim, another plug-in of Rhinoceros will be used, DIVA. It stands for Design Iterate Validate Adapt, and it is an environmental analysis tool [186] that can perform daylight analysis simulations based on Radiance/Daysim, for a given modelling scenario. Furthermore, due to the rapid visualization of daylight availability, a plethora of design parameters can be tested without the need of manually exporting a series of software [187]. Finally, by using DIVA, the user can easily select between a static irradiance simulation for a single sky condition at a certain time instant (Radiance), or a dynamic simulation for any chosen time period according to the given climatic conditions of the selected site (Daysim).

To gain a better understanding of the modelling framework and how each tool is integrated in the overall workflow the reader is referred to Figure 20. The workflow is divided into three main stages: geometric, irradiance, and yield modelling. In the first stage, the CAD model is generated, which includes the APV array, as well as farm sample. The deployment configuration of the array can be characterized by a series of parameters depending on the design's complexity such as tilt and azimuth angle, row and column spacing, mounting

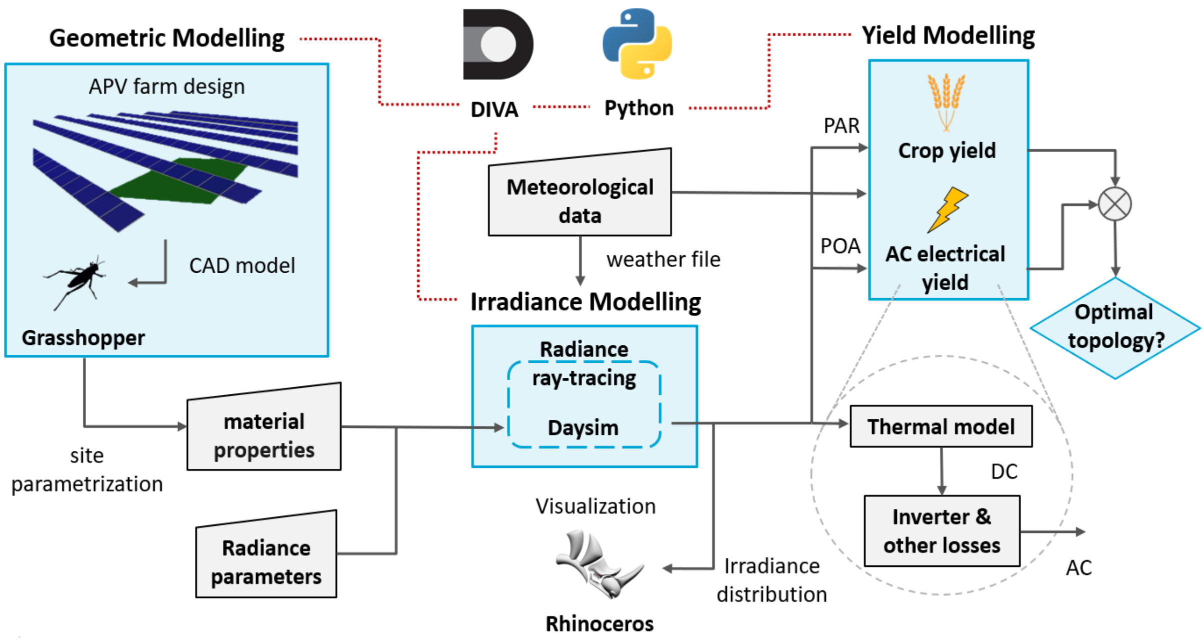

Figure 20 - APV system modelling framework consisting of three stages; geometric, irradiance, and yield modelling. The rigid lines display the flow of data, while the dotted and red lines couple the various stages through the DIVA and Python plug-ins. On the bottom right the AC electrical yield model is shown deconstructed. The overall process is iterated for several topologies to perform the sensitivity analysis and select the most optimal scenarios.

height, module and cell arrangement, as well as cell spacing. On the other hand, the geometry of the farm sample is quite simple, since the impact of crop architecture is not considered. However, its size must be carefully selected, since it can significantly influence the overall ground reflected irradiance, and thus performance of the agrivoltaic array, depending on the array's topology. By using Grasshopper, the plethora of parameters that characterize the APV array's deployment configuration can be quantitatively defined, and subsequently adjusted with ease. Although it is not explored in this thesis, there are means to geometrically simulate the architecture of various crops in Grasshopper, which could offer great insight. For example, through the development of a 3D RT model various crop architectures, planting orientations and densities could be examined with regards to the crop's overall growth rate [189]. After the site of interest is parameterized, and the CAD model is generated, material properties are then assigned to each geometry. This includes reflectance, transmittance, and surface roughness, as will be discussed in more detail in subsection 3.1.2 Optical Properties.

The second phase incorporates the use of Radiance's RT algorithm, along with the daylight coefficient approach of Daysim and the Perez all weather model to determine irradiance or irradiation for the surfaces of interest; in specific, ground, as well as front and rear bifacial PV (POA irradiance). It is possible through one of the components available in DIVA to perform an illuminance distribution of the visible spectrum of light in specific, thus being able to quantify the amount of PAR incident on the ground. Since the core of irradiance modelling is based on Radiance, all the methods used – solar spectrum or visible, hourly to monthly to annual time-step – necessitate the same geometry, material, weather file, and radiance parameters [183]. The weather file consisting of solar irradiance potential for a given site, is in the form of an epw file, which can be easily obtained from the EnergyPlus database. With all the inputs included, the simulation is initiated, and then results of irradiance and its distribution across the surfaces of interest are observed in Rhino's viewport. The POA irradiance incident on the bifacial array along with the PAR availability of the ground, will be used as inputs for the total yield of the APV farm.

The third phase utilizes the results obtained through Radiance, along with additional environmental parameters such as ground and ambient temperature, wind speed, as well as humidity. Note that although the electrical yield model accounts for the effect of temperature and wind speed, the crop yield model does not as it is assumed that the introduction of the array does not heavily impact those parameters. Irradiances or irradiation values are then utilized by the crop and AC electrical yield models to determine the overall performance of the APV system. The PV yield is comprised of the conversion of POA irradiance to DC power according to the operating temperature, efficiency, and bifaciality of the modules, which is further reduced due to inverter, soiling, current mismatch, and resistive losses. Scripting with Python can be easily integrated into the Grasshopper-Radiance model as a block component, thus automating the flow of calculations. This procedure is repeated for various PV topologies, and orientations, and the yield results are compared to assess the system's performance. Through this process a sensitivity analysis is performed, thus information required to assess the optimal topology are obtained. This trial and error process could be handled by an evolutionary computing tool, such as Galapagos that is integrated in Grasshopper. However, due to the complexity of the scene, the size of the APV sample used, and number of topologies, such an option was not possible. By performing the simulations manually, vital information regarding the sensitivity analysis is obtained that can be used to assess regions of higher importance.

3.1 Development of the Radiance model

3.1.1 Geometric modelling

The aim of the geometric model is to interrelate all the parameters that establish the APV topology. It is deconstructed into various levels, from cell, to module, to array level. Starting from the "micro" scale, cell shape, dimensions, spacing, and number of cells are all parametrically defined, and are shown in Figure 21 (a). It is essential to have flexibility over their adjustment to later perform the cell arrangement and spacing sensitivity. The conventional values are obtained from the data sheet in [190] for a PERC mono-c-Si bifacial module. Then, the front and rear cover (glass or translucent material), as well as the aluminium frame are defined according to their corresponding sizes, and in relation to the overall solar cell active area. This concludes the geometric modelling of a single bifacial

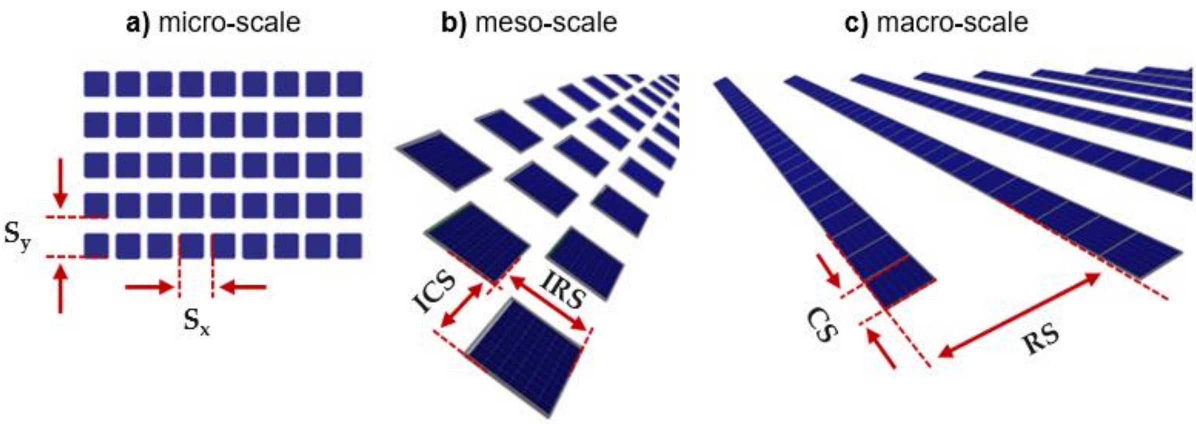

Figure 21 – Geometric modelling of the PV array, which is decomposed into three levels: micro, meso, and macro-scale. After the cell's dimensions and layout are established a single module can be simulated. By parametrically the module arrangement a string can be obtained, and after some additional parameters a whole array.

module. By varying the inter-column-spacing (ICS) and inter-row-spacing (IRS), or through additional rows per row (RPR), it is possible to examine various module arrangements. This sensitivity analysis is part of the "meso" scale, as shown in Figure 21 (b), where a checkerboard Carrangement with three rows per row is displayed. The pattern of modules can then be converted into an array, by considering the column and row spacing. For the conventional module arrangement, displayed in Figure 21 (c), the column spacing (CS) is equal to the module's width, which depends on the module's orientation (landscape, portrait). Finally, the array is elevated and oriented, according to its mounting height, tilt and azimuth angle. Specifically, for the hinged E-W configuration, a row consists of two inter-rows with the same tilt, one facing east and the other west. The hinged E-W, vertical E-W, and south facing with optimal tilt arrays are the main APV topologies examined in this thesis, as displayed in Figure 22. This concludes the cell-module-array 3D parametrization procedure, and the CAD model used to set the environment in Radiance.

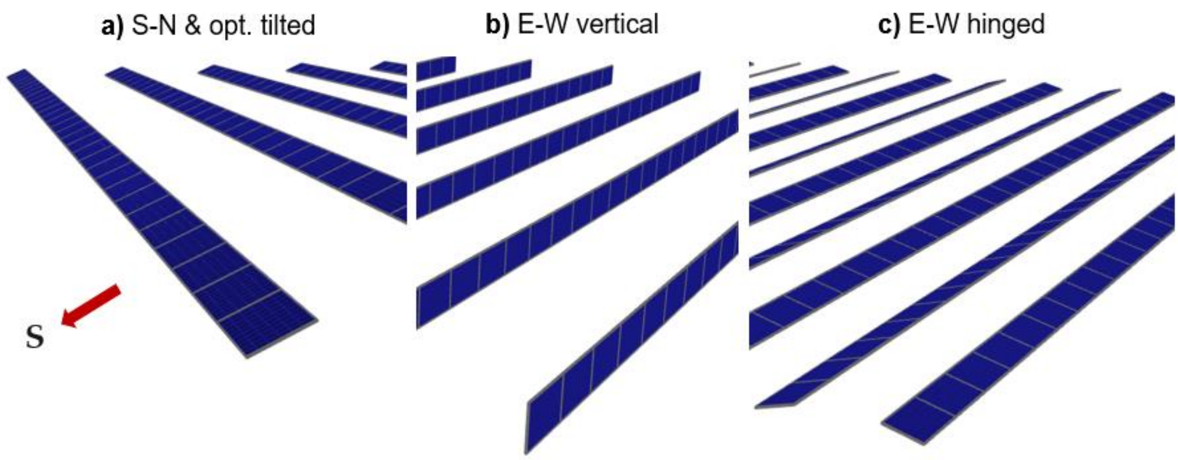

Figure 22 – Illustration of the main topologies simulated in this thesis: a) south-north facing and optimally inclined (for light harvesting) b) east-west facing and vertically inclined c) east-west facing and tilted aka E-W hinged.

3.1.2 Optical properties

To model the magnitude and distribution of irradiance throughout the scene, it is essential to accurately model the optical properties of all the geometries present. Radiance is well equipped to model the optical behavior of various materials; diffuse, specular, glazing [191]. Each material type requires a different set of inputs, for example *plastic*, and *metal* are characterized by the diffuse reflectance, while *metal* type also necessitate the spectral component of reflection. On the other hand, *glass* materials are described by their thin surface and direct (normal) transmittance. Cover materials that convert direct light into diffuse, also known as translucent materials, *trans*, require a series of parameters to be properly defined, which are not widely available.

In Radiance translucent materials are simulated as ideal diffuse light transmitters with a fixed specular transmittance component. The fraction of light that is transmitted diffusely is defined as the haze factor HF, which depends on the microstructure of the material and presence of pigments. Covers with a high HF result in additional scattering, thus homogenizing the vertical and horizontal distribution of light, as was discussed in subsection 2.1.2 Effect of diffuse light. The amount of scattering is proportional to the cover's optical properties; surface morphology, spectral and diffuse reflectance, absorptance, as well as spectral and diffuse transmittance as shown in Figure 23. In addition, diffuse reflectance and transmittance are characterized by their angular distribution, which is modelled as Lambertian. Note that the actual scatter angle of diffuse greenhouse cover materials is quite narrow in comparison to Lambertian [43].

The integration of a PV array along with the support structure can result in sharp irradiance gradients throughout the agrivoltaic array. Such non-homogeneous distribution is greatly mitigated by utilizing a diffuse cover, while the amount of scattering or HF, should be selected according to the crop grown and local climate [42, 191]. The greatest benefit is to be gained under clear sky conditions, and thus the potential is higher for locations closer to the equator. Furthermore, the HF should be selected according to the crop's architecture, where a dense canopy necessitates a lower HF [191].

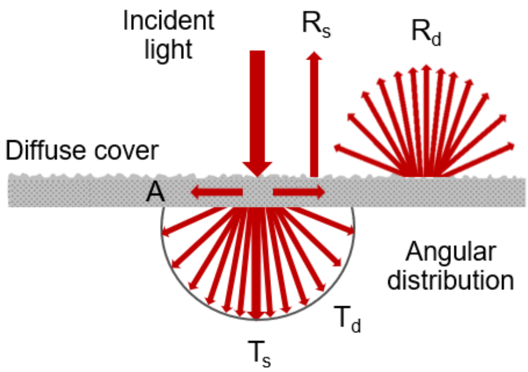

Figure 23 – Optical properties that define the translucent cover's performance.

To model the translucent cover in Radiance, the material description is based on the calculation of certain formulas that will be presented here. The *trans* model approximates the incident angle dependency of transmission as constant, based on the perpendicular transmittance. For a more rigorous model that accounts for the AOI the reader is referred to

[181], where goniophotometer data and integrating sphere measurements were combined to accurately estimate the optical behavior of the translucent material. The Radiance description of *trans* type materials is dictated by seven coefficients (A_1 to A_7) which can be determined from the following relations [168, 192]:

$$A_7 = T_s/(T_d + T_s)$$
$$A_6 = (T_d + T_s)/(T_d + T_s + R_d)$$
$$A_5 = S_r$$
$$A_4 = R_s$$
$$A_3 = R_{d,red}/(T_d + T_s)$$
$$A_2 = R_{d,green}/(T_d + T_s)$$
$$A_1 = R_{d,blue}/(T_d + T_s)$$

Table 3 – List of optical properties for the prismatic glass (SG80); some were given, others were estimated, and the absorptance was assumed negligible.

Perpendicular light transmittance	$T_\perp$	95.2% [43]
Hemispherical light transmittance	T_{hem}	84.3% [43]
Absorptance	A	0
Specular reflectance	R_s	3% [192]
Surface roughness	S_r	5% [193]
Haze factor	HF	78% [43]

, where $R_{d,red}$, $R_{d,green}$, and $R_{d,blue}$ are the diffuse reflectance in the red, green, and blue wavelength regions. The translucent material examined, whose properties are shown in Table 3, is a prismatic glass (SG80) with high diffusion that has been studied in the University of Wageningen for greenhouse applications [43]. To assess the overall transmission in the cover, it has been claimed that the hemispherical component is better suited, since incident light is rarely perpendicular in relation to the cover's surface [42]. This was verified by another study [181], where the use of the hemispherical light transmission component led to a significant decrease in the RMSE and MBE of internal irradiance due to daylight in a room with a large translucent window. By applying conservation of energy on the thin translucent cover (assuming negligible absorption), it is possible to approximate the overall reflectance to:

$$A + T + R = 1 \Rightarrow R = 1 - T_{hem} \tag{10}$$

In general, the specular reflectance component of translucent materials is expected to be below 7% [192], thus a value of 4% is anticipated for coated glasses. Next, the diffuse reflectance component can be calculated, which is assumed to be constant across the RGB wavelengths. Surface roughness values lie below 20% [193], thus a value of 5% is expected to be practical for the cover of interest. Finally, to derive the specular component of transmission, the HF is used [194], which is the ratio of diffuse to the overall transmittance or hemispherical transmittance for this case. The optical parameters necessary to model the translucent materials are obtained, thus coefficients A1 to A7 can be determined. The results are shown in Table 4 along with the other geometries that make up the scene.

To accurately estimate the overall ground reflectance, one must consider the optical properties of the crop grown. In fact, the energy yield of bifacial PV is highly dependent on the ground's albedo, which depends on a plethora of parameters ranging from climatic conditions, PV configuration, season, as well as spectral distribution. Although in Radiance we have control over the reflectance of various materials, we cannot simply set a ground albedo. Instead, the software estimates the albedo, based on the climatic conditions, shading casted by the APV array, and optical properties of the surrounding materials. Seasonal effects are currently not considered, but they could be accounted for through adjusting the ground’s reflectance according to the crop’s growth stage. In essence, the derivation of the annual energy yield would be divided according to growth stage, where during the early stage ground reflectance is dominated by the optical properties of the soil, while from crop development to harvest it is greatly influenced by the presence of the crop, and it is thus species dependent.

Table 4 – Summary of the optical properties of each geometry that defines the simulated scene.

Geometry	Optical properties	Radiance material description
Ground surface	20% diffuse reflectance approximated [195-197]	plastic[1] 0.25 0.25 0.10 0 0
PV module	10% diffuse reflectance [198-202]	plastic[1] 0.1 0.1 0.1 0 0
Frame	30% diffuse reflectance, assumed 40% spectral reflectance [201-204]	metal[1] 0.3 0.3 0.3 0.4 0
Glass cover	88% normal transmittance [199,205]	glazing[2] 0.88 0.88 0.88
Translucent cover (SG80)	84.3% hemispherical transmittance, 78% haze factor [43]	trans 1 1 1 0.04 0.05 0.869 0.22

[1] material type, R, G, B diffuse reflectance, specular reflectance, surface roughness

[2] material type, R, G, B specular transmittance

Furthermore, soil spectral distribution and magnitude varies according to humidity, soil organic matter, iron oxide composition, and texture [195-196], which complicates the analysis even further. Soil spectral reflectance was found to vary between 5-35% [195-197] ranging from visible to near-infrared wavelengths. On the other, for various crops and vegetation in general, reflectance is relatively low in the visible range (5-15%), while it is considerably higher in the near-infrared as was examined in subsection 2.3.2 Crop albedo. To simulate the spectral distribution of optical properties, Radiance approximates the overall behavior through three wavelength regions in the visible range; 400-500 nm (blue), 500-600 nm (green), and 600-700 nm (red). However, c-Si results in an effective absorber of light in the red and near-infrared wavelengths, where crop reflectance is also maximized. Consequently, the influence of the near-infrared region is superimposed onto the red wavelength region.

The typical absorptance of encapsulated c-Si PV cells was found to be higher than 90% [198-199], thus by neglecting transmission, the overall reflectance can be estimated to be around 10%. Such values of reflectance are commonly used in other literature [200-201], as well as some lower values, 2.5-4.6%, that were measured in [202]. Note that reflection occurring from the PV cell's surface is expected to be semi-specular; however, this is not considered, due to the low overall reflectance. The aluminum frame used in the datasheet of [190], is a clear anodized aluminum, and expected values of reflectance are in the range of 65-85% [201-204]. The front and rear cover of bifacial PV is usually made of glass; however, the influence of a translucent cover that can convert direct into diffuse light is also investigated. For the glass cover, the transmittance is approximated based on the spectral behavior of soda-lime-silica-low-iron glass, with values of transmittance around 92% [199, 205]. However, transmittance can decrease considerably because of soiling and aging, thus 88% is more realistic as was included by default in DIVA for single glazing windows.

3.1.3 Sampling size

After the APV topologies are parametrically defined and material properties are assigned to each geometry, sampling is initiated. There are three surfaces of interest where irradiance/irradiation must be calculated: front and rear side of bifacial PV array, as well as ground surface. Conventional monoculture farms occupy large areas, thus agrivoltaic systems are also expected to be quite large (at least when they've matured). It is not computationally feasible to model such large systems, therefore only a sample of the actual farm and APV array is modelled. The aim of this subsection is to provide justification for the selection of each sample, and whether it can faithfully represent the actual system.

Farm sample

The main consideration when selecting the size of the farm sample, is to ensure that it is representative of the actual light distribution present in an APV farm. Assuming that the APV farm is large enough, the distribution of irradiance at its centre is not expected to vary considerably , unlike the border regions. Depending on the deployment configuration of the array, and most importantly its mounting height, light penetration can occur during winter months, where solar elevation is low. The horizontal distance covered by light penetrating below the array, is defined as the penetration depth, which mostly depends on module and sun elevation. These border effects lead to sharp irradiance gradients, which can significantly impact the overall magnitude and distribution of light in an agrivoltaic farm. However, as the size of the APV farm increases, the border effect is minimized relative to the central farm area, which now occupies most of the land. Nonetheless, border effects in the east, south, and west sides should be further examined in future research, along with ways to mitigate them.

The APV farm modelled is meant to represent the central patch of a large system, thus the size and orientation of the farm sample is not of great importance, since irradiation gradients repeat over the length and width of the sample. Furthermore, as the size of the sample modelled increases, a higher computational burden is expected as well as loss of accuracy. Because of the imposed constraint (by DIVA) on the maximum number of grind cells per surface simulated, it is essential to reduce the farm's size. By modelling a smaller farm sample, 10x20 m^2 (WxL), the mesh can be finer without computational exhaustion.

APV array sample

At this point, a distinction is made between the APV array sample, whose aim is to faithfully represent the actual shading conditions in a large agrivoltaic array, and the PV modelling sample, which defines the surfaces where front and rear irradiance is calculated. As a result, the sample of the APV array is chosen according to the shadow length casted in December 21st, for Boston, MA, USA. Since the penetration depth depends on the array's topology, the size of the sample is not constant. For arrays that are elevated higher, shadows are elongated further, thus necessitating a larger array to minimize border effects. Light penetration is more pronounced in the east and west sides since the sun's elevation is lower in the morning/afternoon. However, during winter, light can also penetrate from the south, as shown in Figure 24. Furthermore, the north side of the array is also extended to mimic the SVF reduction and masking present in medium-to-large-scale systems. Note that any further

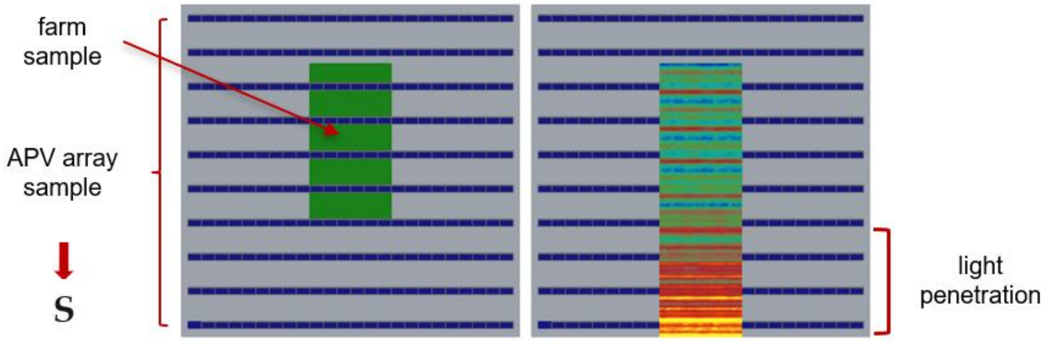

Figure 24 – Illustration of light penetration and border effect for a south facing and latitude inclined APV array (top view). Notice the size of the farm sample, which is significantly smaller than the surface occupied by the APV array, thus alleviating border effects.

increase of the APV array sample does not significantly impact irradiance on ground or PV, however it prolongs the simulation time.

PV modelling sample

It is computationally infeasible to determine the irradiance of front and rear side for the whole APV array sample considering that various configurations and topologies will be examined. Consequently, irradiance will be calculated only for a portion of that sample, which consists of the maximum number of rows that can be fit in the farm sample with one module per row as displayed in Figure 25. By minimizing the PV modelling sample, the ground shading and masking conditions at the centre of a medium-to-large-scale bifacial array are effectively mimicked. Naturally, the PV sample will then depend on the RS employed, where for a wide RS fewer rows will be simulated. Note that both samples are interlinked, since modelling of medium-scale PV arrays necessitates an even bigger number of surrounding modules to ensure adequate shading conditions. The PV modelling sample shown in Figure 25 consists

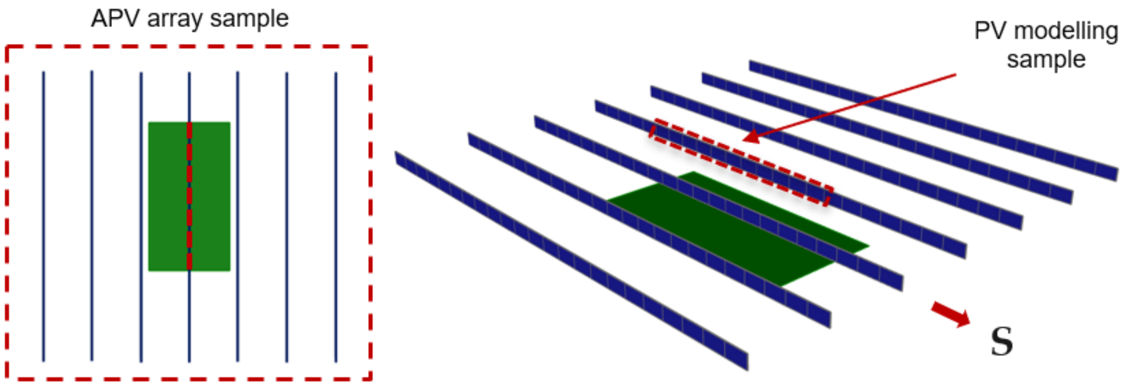

Figure 25 – Example of the PV modelling sample for a vertical and E-W oriented bifacial array, where the left plot depicts the top view.

of eleven rows of modules with one module per row. Since the array is facing E-W, one could argue that the sample consists of one row with eleven modules. It is a matter of perspective, and for the E-W orientation the latter is adopted.

The sizing of both samples is justified by another study [169], where the decline in bifacial gain was examined for increasing number of modules (single row). The bifacial gain was calculated for the central module, while the row was tilted at 30°, and elevated 2 m above ground, with an albedo of 0.51. A saturation in the decrease of BG occurred for a row of 5 modules. In Figure 25 the number of additional modules per row that the APV sample has in comparison to the PV modelling sample is 11, thus satisfying the aforementioned condition. Researchers in [169] also investigated the effect of additional rows with 5 modules per row. The decrease in BG saturated for 5 rows in front and behind the central row [169], thus leading to a total of 11 rows. The number of rows to attain saturation is mostly dependent on the elevation and the row spacing itself. For instance, in Figure 25 the row spacing employed is 6 m with a vertical clearance of 5 m above the ground. Nonetheless, shadows casted by rows that are further east or west than the ones displayed, do not reach the vicinity of ground near the PV modelling sample. In other words, by increasing the APV array sample, the ground reflected irradiance close to the PV modelling sample does not reduce any further, thus leading to a converged BG.

View field extension

For bifacial arrays, the size of the ground impacts the overall energy yield considerably, depending on topology. Thus, a sensitivity analysis between the view field extension (ground surface increase) and the change in VF from ground to PV, displayed in Figure 26. Naturally, each array topology and configuration will result in a different view field extension. The aim is to select the dimensions of the ground patch (farm sample and view field extension) in such a way that any further increase of its area does not impact the overall energy yield. Therefore, it is essential to determine the topology that requires the largest ground patch to attain saturation in BG. Starting with the width extension the vertical and E-W facing PV modelling

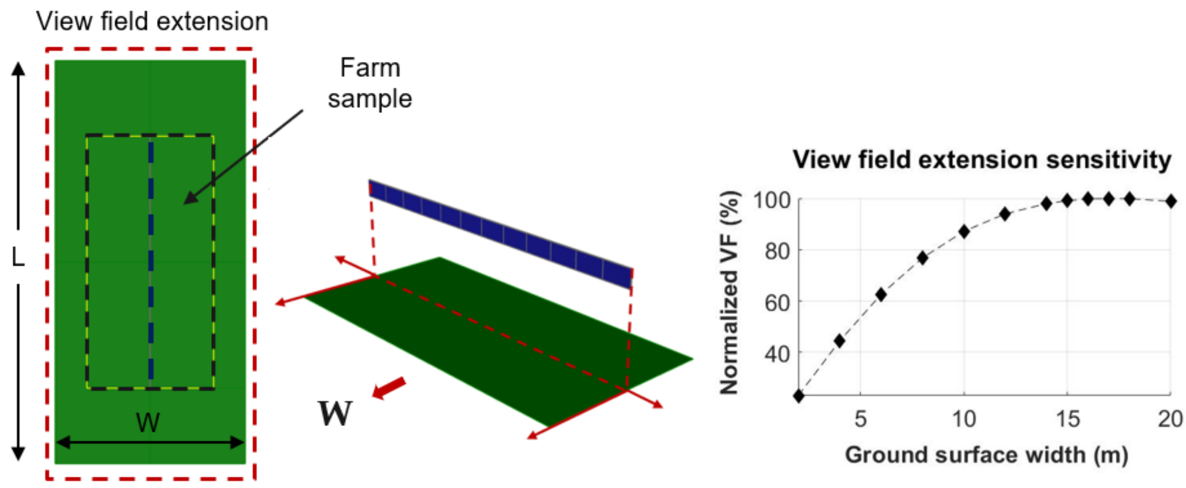

Figure 26 - View field extension for a vertical E-W facing string with 12 modules. At first the top view of the environment and then the ground extension are displayed. Followed by the VF from ground to PV sensitivity to ground surface area along the E-W direction.

sample is used, since it is the one that is most sensitive to ground reflection. As the patch is extended from below the modules towards the west direction, the $VF_{Gr \rightarrow PV}$ increases with a decreasing rate, attaining saturation at 17 m of total ground width. Any additional extension of the view field decreases the VF, since the long distance between the two surfaces overcomes any benefit obtained from the larger ground area. Moreover, computational cost is increased, thus a width of 15 m is selected, which results in 99% of the maximum $VF_{Gr \rightarrow PV}$ possible.

In a similar manner the view field extension along the south-north direction is also examined. However, for this case, the topology is switched to a south facing and latitude inclined array, since it is more sensitive to ground reflected irradiance along the length of the ground patch. As expected, the north side should be more extended than the south, because the rear bifacial side benefits more from ground reflection. On the other hand, by extending the ground patch further towards the north side and applying this view field extension on other topologies such as the vertical E-W, the north side of the PV modelling sample would perform better than the south. To deal with this discrepancy, the ground patch is elongated equally along the north-south direction with a total length increase of 12 m. Overall, the farm sample along with the view field extension occupy an area of 15x32 m^2 (width by length).

The influence of reflective surface area on the energy yield of a single module was examined in another study [126], where a saturation in gain was observed with increasing ground area. The module was tilted at 25°, and elevated 0.5 m above ground with an albedo of 0.2. A realistic ground patch to attain close to maximum energy yield was calculated to be 69 times larger than the module area [126], while for the vertical E-W configuration studied here the ground patch is approximately 28 times larger than the PV modelling sample. Once again, due to the plethora of topologies analysed, a smaller ground area is sampled to optimize between accuracy and simulation speed. In another paper [206], a sensitivity analysis was performed with regards to view field extension and energy yield for an array consisting of 4x18 modules, tilted at 30°, and elevated 0.5 m above ground with reflectivity of 40%. It was concluded that a 50% increase in length was necessary to attain saturation in yield [206]. Thus, the field extension along the north-south gradient should be at least 50% longer than the PV modelling row. In specific, for the case analysed here the extension is 59% longer, thus satisfying the condition.

3.1.4 Sky model

After each geometry has been assigned with its corresponding optical properties, the sky model must be set. This can be in the form of an .epw file which contains hourly weather data for a selected site, or to generate a standard sky based on CIE (overcast and clear sky), or the Matsuura intermediate sky model. The latter is based on *gensky*, a sky model generator program, which produces the sky irradiance distribution of a certain location and sky condition [207]. This approach is mainly used to test the performance of the APV array in specified conditions, such as a worst-case scenario. For example, to simulate the magnitude of irradiance on the ground under a CIE overcast sky model, during the months of winter where solar availability is limited. Alternatively, one can utilize a weather file, which represents what the site experiences and consists of DNI and DHI measurements that are then fed into the Perez All-Weather model [180]. For this approach the *gendaylit* sky model generator is used. Mardaljevic (2000) examined the accuracy of each sky modelling approach, and determined that for both sky and internal illuminances, the Perez All-Weather and CIE Overcast performed best, followed by the Matsuura Intermediate, while the CIE Clear sky model performed the worst.

Most of the simulations performed involve the use of Daysim, which is based on Perez All-Weather model along with the corresponding weather file. After the time series of DNI and DHI measurements are inserted (Boston, MA), the daylight coefficients – 148 diffuse, 63 direct, and three ground – are calculated for the samples of interest (PV modelling, and farm sample). The sky luminance of each patch is then related to the daylight coefficients in accordance with the Perez sky model [180]. This is iterated throughout the simulation period per time-step (hourly). Finally, the daylight coefficients and sky luminances are coupled to recreate the illuminance profile.

3.1.5 Radiance parameters

Before initializing the ray tracing algorithm, the Radiance parameters that govern it must be defined. The same set of parameters can be applied to both the classical Radiance approach as well as Daysim, which result in comparable accuracies for various geometries and sky conditions [183]. Selecting the appropriate Radiance parameters is not straightforward, since they greatly depend on the complexity of the scene, the corresponding material properties, and climatic conditions. There is a wide plethora of rendering parameters that describe simulation accuracy, while only a few of them are introduced here. For additional information the reader is referred to [178, 207-210].

Ambient bounces (-ab)

It describes the number of diffuse inter-reflections that can occur before a ray is terminated. The minimum value that can be set is 0, where only DNI can be traced on unobstructed surfaces. By setting -ab to 1, the inter-reflection calculation is initiated [207], and hemispherical sampling (DHI) is possible. This is displayed in Figure 27 (a), where the red patch receives both DNI and DHI for -ab 1. On the other hand, shaded patches receive only DHI, thus necessitating a minimum of 1 bounce to assess illumination. The analysis becomes more involved for the derivation of rear PV side irradiance, shown in red, in Figure 27 (b). At -ab 1, only direct light reflected from the ground is considered, while with 2 bounces several other routes are analysed. For example, diffuse light reflected off the ground or from surrounding modules. In other words, for -ab 2, surfaces that are not directly visible to sun or sky are illumined (rear PV). Additional complexity arises when simulating the influence of the front

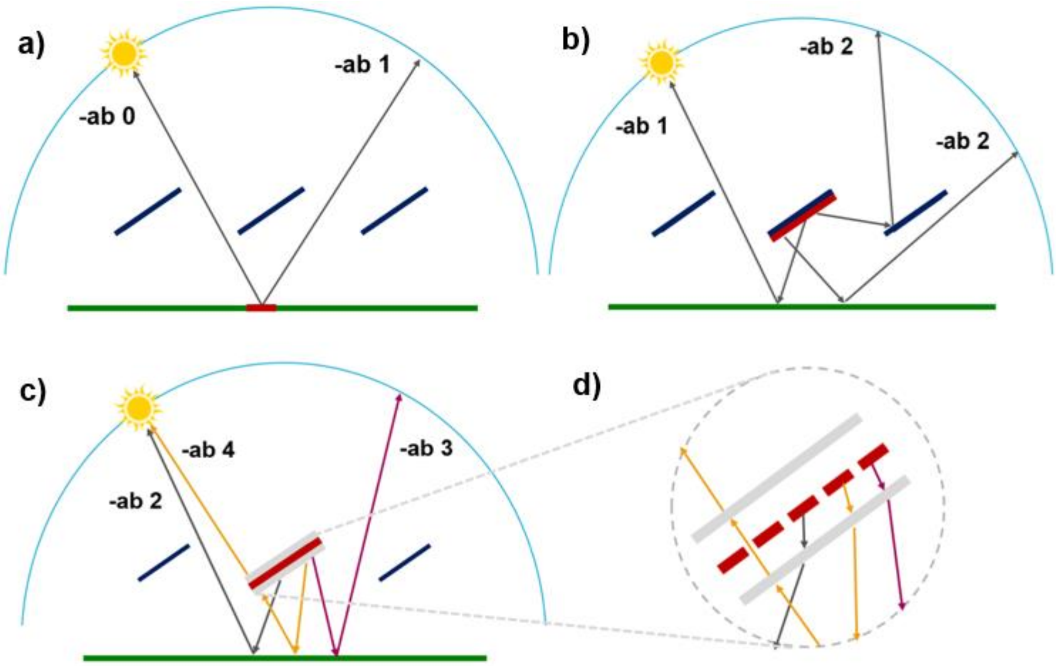

Figure 27 - Necessary -ab (or inter-reflections) to account for the various irradiance components on different surfaces: a) ground surface, b) rear PV cover, c) & d) rear PV cell. In (d) the inter-reflections occurring between the two covers are shown in more detail.

and rear glass cover, Figure 27 (c). In essence, an extra bounce is required each time a ray transmits through a glazing or translucent surface, therefore requiring a minimum of 3 bounces to consider the contribution of ground reflected DNI and DHI, as shown in grey and purple respectively. At -ab 4, as displayed in Figure 27 (d), it is possible to trace rays that transmit though both covers, subsequently reflected off the ground, and finally transmitted back to the rear PV side. Note that this contribution greatly depends on the overall transmittance of the cover, as well as module transparency, which is influenced by the cell spacing employed.

Ambient division (-ad)

This parameter defines the number of hemispherical sampling rays that are sent out in search of the indirect source. A high value results in smoother irradiance gradients. This can be seen in Figure 28, where the spatial distribution of light in a simple room is examined for various -ad values. In addition to smoother shading, the error associated to the Monte Carlo calculation of diffuse light is mitigated [178]. To determine the number of rays, -ad is multiplied by the number of pixels. For complicated scenes, such as the structure of an atrium a relatively large -ad, 1024, should be used [210].

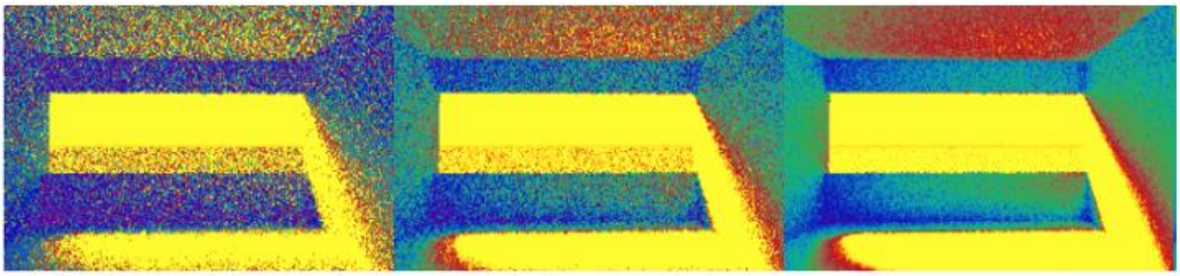

a) -ad 500 time: 4.48s **b) -ad = 2,000 time: 12.61s** **c) -ad = 10,000 time: 57.44s**

Figure 28 - Sensitivity of light distribution throughout space to -ad parameter for a simple room with a south-facing window [211].

Ambient samples (-as)

Ambient samples or super-samples designate the number of additional rays sent out to sample regions in the hemisphere with high variance [209]. Thus, this parameter applies only to those ambient divisions where large deviations can occur. It is usually set to around half or a quarter of the -ad value [210]. A high value results in extra sampling rays towards those high variance regions, where sharp irradiance gradients are present, thus reducing the "patchiness" effect.

Ambient accuracy (-aa)

The ambient accuracy approximates the error from indirect illuminance interpolation [178]. When it is set to zero, the interpolation between pixels will be switched off. Radiance assumes that the magnitude of diffuse light does not significantly change throughout a scene, thus it estimates irradiance values between sampled pixels. Every point that has been sampled for ambient light represents the centre of a sphere of influence, where pixels that lie within its radius are not sampled rather, they are interpolated.

Ambient resolution (-ar)

The resolution signifies the maximum density of interpolated ambient values in each sphere of influence, thus giving the necessary criteria to refine. Along with the -aa parameter they define the minimum ambient value spacing or radius (sphere of influence) [210]:

$$R_{min} = \frac{d_{max} \cdot aa}{ar} \quad (11)$$

, where d_{max} represents the maximum scene dimension, which is around 37 m for the APV array sample. For pixels that lie within this radius, their values are interpolated, rather than sampled, thus greatly reducing computational effort. As will be examined in section 4.5 Cell sensitivity – micro scale, it is compelling to perform a sensitivity analysis on the module's transparency to assess its influence on the ground's light availability. One way to achieve this is through modifying the cell spacing, which should be compared to the value obtained from equation 11. To simulate light penetration through the bifacial module, -aa and -ar are selected according to trial and error with the aim to comprise between speed and accuracy.

Although it is possible to use one single set of rendering parameters for all the various surfaces and topologies simulated, the "quality" setting, and consequently computational time would have to be high. For example, rear side irradiance determination requires additional bounces than the front side. Furthermore, the overall energy yield of a south facing array that is latitude inclined is mainly affected by irradiance incident on the front side. Consequently, coarser settings can be used to obtain reasonable results, which is not the case for an E-W vertical bifacial array that greatly depends on the irradiance reflected by the surroundings.

Table 5 – Summary of the Radiance parameters used to simulate irradiance on each surface of interest: ground, as well as front and rear PV sides. The same set of parameters are used for all topologies modelled unless otherwise mentioned.

Amb. bounces[1]	Amb. division	Amb. sampling	Amb. accuracy[2]	Amb. resolution
4	1024	256	0.25	256

[1] -ab 4 for ground and front PV side, while -ab 5 for rear side (4, 5, 5 for E-W vertical)

[2] -aa 0.1 for the cell spacing sensitivity

3.2 PV energy yield modelling

In this section, the procedure of converting POA irradiance to annual AC electrical yield will be discussed. Initially, by considering the module's operating temperature and the underlying environmental factors, as well as soiling conditions the corresponding DC power can be determined. Then, for the conversion to AC electrical yield, inverter and other losses must also be examined. Note that the optimization and comparison between each deployment configuration is based on annual POA results obtained through Daysim. Although Daysim performs the annual derivation of irradiance according to an hourly time-step, the hourly data was not available, thus the overall energy yield modelling is quite simplified. To accurately assess the influence of each topology on the PV module's performance a more rigorous model should be developed that is based on electrical, fluid dynamic, and orientation dependent inverter models.

It is assumed that all modules in the array operate at the same efficiency, however, depending on the size of array, and its deployment configuration the efficiency can vary considerably due to the inhomogeneous distribution of irradiance throughout space. Furthermore, since the obtained results of irradiance are for the whole year (annual irradiation), an accurate determination of the module's conversion efficiency is not possible. Consequently, efficiency is determined for two days per month; one that represents sunny and one for overcast conditions. This is performed for every month to obtain a better representation of the module's actual efficiency variation throughout the year. Then, the average of the monthly results is used to obtain an estimate of the overall efficiency.

There is a great number of losses associated with the conversion of solar energy into AC electricity. These sources of inefficiency can be divided into geometrical, optical, PV conversion, and PV system related. The geometrical losses are due to the array's deployment configuration; tilt and orientation (azimuth), row spacing, elevation, as well as module dimensions. For instance, tilt and orientation determine the SVF and VF to ground that dictate the POA irradiation incident on both sides of the bifacial PV cover. The row spacing will determine the density of the PV array, and whether mutual shading or masking will occur. Along with the mounting height they can significantly impact light availability on the ground, and thus the magnitude and distribution of reflected irradiation. Optical losses arise from the morphology and material properties of the front and rear cover surfaces, in addition to the PV module's reflectance. Both geometrical and optical losses are considered by default through Radiance, while its output, POA irradiation on both sides of the PV module, is further utilized to model DC and AC electrical yield as shown in Figure 29. Note that the dependency of optical properties (cover transmittance, cell reflectance) to incident angle (AOI), is not

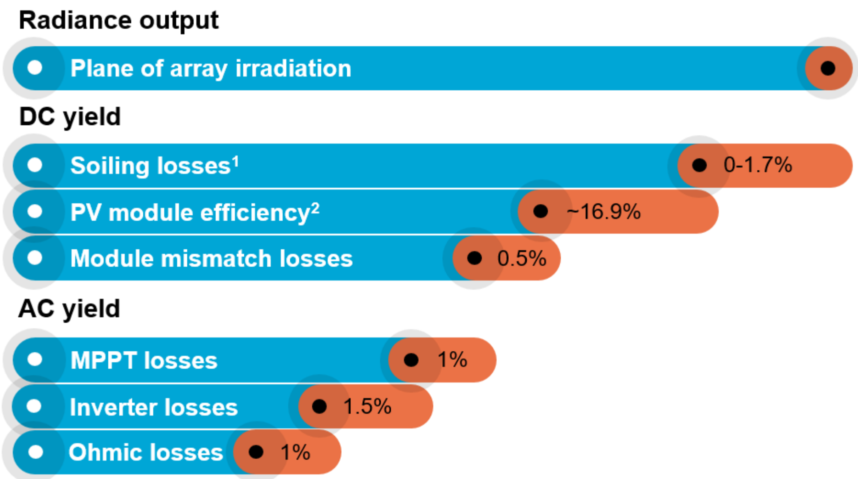

Figure 29 – Loss analysis related to the conversion of solar energy to AC electrical yield. Note: the reduction illustrated is not drawn to scale.

[1] vary according to PV topology; they are assumed as 1.7%, 1.5%, and 0% for E-W hinged, south facing and optimally inclined, and E-W vertical respectively.

[2] vary according to PV topology with increasing order of efficiency: south facing and optimally inclined, E-W hinged, E-W vertical

considered, rather it is approximated as a constant value. Soiling losses are due to dust deposition that occurs on the front PV cover, and contribute to the overall optical losses, since they reduce the transmittance of the cover. With soiling included, the actual POA irradiation incident on the PV module can calculated appropriately.

The biggest source of loss is due to the PV cell's efficiency, which varies depending on environmental conditions; light intensity of incident light, ambient temperature, and wind speed. Those are accounted for through changes in maximum power point MPP power. The module's operating temperature is determined through the SNL model. Note that each PV topology analyzed operates at a slightly different cell efficiency, due to changes in POA irradiation, which subsequently affect the module's operating temperature. To determine the actual power output per module, mismatch losses due to non-homogeneous irradiance distribution across its cell's must also be considered. With this, the conversion from solar energy to DC yield is concluded. For the conversion to AC electrical yield, MPPT algorithm losses, and those related to the operation of the inverter must be calculated. Finally, by including DC and AC cabling ohmic losses as one, the overall loss intrinsic to the PV system components can be identified. In the following subsections, these losses will be further examined, and their values will be justified.

3.2.1 DC electrical yield

Soiling losses

Soiling of PV modules can be detrimental to their overall performance, depending on the deployment configuration [212-213], climate, as well as local environmental conditions [214]. Furthermore, researches in [215] proposed an empirical equation to assess the impact of soiling throughout the day, with highest losses during morning/afternoon. A thorough review of various research articles related to soiling of PV modules is described in [216]. However, there is a literature gap – at least up to the author's knowledge – on the actual soiling conditions in an APV farm, which are expected to be influenced by agricultural activities during certain periods (tillage, harvesting). Naturally, such studies would necessitate an experimental setup to measure the dust deposition rate. Nonetheless, soiling could be greatly mitigated by integrating PV cleaning with an irrigation system [217]. They suggested the installation of a sprinkler to clean the module, while the run-off water could be used directly for the crops beneath.

Since the energy yield of the APV array is based on annual results of incident irradiance, a constant single value of soiling losses is applied. A three-month test consisting of a single PV panel with a tilt of 30° located close to Boston, MA, USA was performed in [218] to investigate the influence of soiling in an industrial area. It was concluded that dust deposition during that period resulted in an average reduction of incident solar radiation by 1%. Although this value could reasonably estimate soiling for latitude inclined modules, it cannot be applied to other orientations. For instance, in [212] the effect of dust deposition for various tilts was investigated and for a three-month period in Mesa, AZ, USA it was determined that losses decrease for higher tilt angles, while modules that were horizontal had the highest losses. Another study [213] examined the potential mitigation of soiling when bifacial modules are vertically installed, and experimental data indicated that soiling losses are insignificant. To meet the objectives of this thesis, three main APV topologies will be simulated and according to literature the soiling losses are approximated. For the vertical E-W soiling losses are assumed to be zero, while for the hinged E-W, and optimally inclined south facing orientations the relation between tilt and soiling is based on the trend found in [212]. These values along with the influence of other parameters on the overall PV system efficiency were summarized in Figure 29.

Irradiance-dependence

After the optical losses due to soiling are quantified, it is essential to consider the actual irradiance conditions incident on the module, and the subsequent impact on its electrical performance; short circuit current I_{sc}, open circuit voltage V_{oc}, and maximum power point P_{mpp}. This is achieved through the following series of equations:

$$I_{sc}(25°C, G_{POA}) = I_{sc}(STC)\frac{G_{POA}}{G_{STC}} \tag{12}$$

$$V_{oc}(25°C, G_{POA}) = V_{oc}(STC) + n_s\frac{nk_BT}{q}\ln\left(\frac{G_{POA}}{G_{STC}}\right)_{|T=25°C} \tag{13}$$

$$P_{mpp}(25°C, G_{POA}) = FF \cdot V_{oc}(25°C, G_{POA}) \cdot I_{sc}(25°C, G_{POA}) \tag{14}$$

, where n_s is the number of cells in series, and n is the ideality factor (assumed as one). These values along with the module's STC characteristics are summarized in Table 9 included in the Appendix, which are derived from the data sheet in [190]. Next, it is possible to calculate the influence of incident irradiance on efficiency:

$$\eta(25°C, G_{POA}) = \frac{P_{mpp}(25°C, G_{POA})}{G_{AOI} \cdot A_{m,act}} \tag{15}$$

, where $A_{m,act}$ is the active surface area of the module. To account for the effect of temperature on efficiency, a thermal model must be integrated to determine the module's operating temperature.

Temperature-dependence

The NOCT model is one of the most widely known and practical thermal models that can calculate the operating temperature of a PV module. It is based on the nominal operating cell temperature (NOCT) measured under the specific climatic conditions; solar irradiance of 800 W/m^2, ambient temperate of 20 °C, and wind speed of 1 m/s [219], which is usually provided by the manufacturer. The linear relation between T_m and G_{POA} proposed by the NOCT model was compared to experimental data in [220], which reported that they are in good agreement. Nonetheless, a high deviation is expected for agrivoltaic systems, especially those located in areas with high wind speeds, since the effect of convective cooling is not considered. Additional deviation in module operating temperature is anticipated, due to the unique mounting configuration of an APV array, or the potential cooling caused by the microclimate below where crops are grown. In future studies, a fluid dynamic and heat transfer model should be developed for APV systems in specific that can account for all these changes, thus assessing potential synergies between crop cultivation and PV electricity production.

To partially solve these inconsistencies, the thermal model used by US Sandia Laboratories (SNL) [221] is adopted, which considers wind-induced convection. The performance of the SNL model was compared to NOCT in [222] for a roof system with various mounting configurations and it was determined that the NOCT model overestimates energy production. This is verified by other studies [223-224], where both NOCT and SNL overestimate the module's operating temperature for a tropical climate; however, the SNL model had a tendency towards more accurate results. Furthermore, researches in [224] concluded that the associated RMSE in the calculation of temperature was lowest with the SNL approach even compared to other models that account for the influence of wind (i.e Faiman [225]).

The SNL model is a simple empirically based thermal model, which has proven its flexibility in characterizing various deployment configurations with an estimated module operating temperature accuracy of around ±5°C [221]. This in turn results in less than 3% deviation on the module's power output. The following equation can be used to estimate the modules operating temperature, T_m, based on the SNL model [221]:

$$T_m = T_{amb} + G_{POA} \cdot e^{(a+b \cdot w)} \tag{16}$$

, where the coefficients (a, b) are empirically determined and characterize the module's construction and materials used, as well as mounting configuration. The latter has units of (s/m) and describes the drop of temperature with increasing wind speed. On the other hand, coefficient "a" is dimensionless and it establishes the maximum temperature that can be attained in the absence of wind and in combination with high irradiance. From the coefficients available in [221], those that are most relevant to bifacial agrivoltaic systems are the open rack mounting, with module type glass/cell/glass. For this case in specific, the coefficients "a" and "b" where estimated to be -3.47 and -0.0594 respectively. The environmental parameters, wind speed "w" (m/s), ambient temperature T_{amb} (°C), and incident irradiance G_{POA} (W/m^2) are determined for two days per month – one with clear and the other with overcast sky conditions – to approximate the annual behavior. The module's operating temperature is then estimated as the average of the 24 values obtained for the whole year. Note that the wind speed is obtained for a standard height of 10 m.

By considering the influence of light intensity as well as temperature, it is possible to define the actual P_{mpp} as [226]:

$$P_{mpp}(T_m, G_{POA}) = P_{mpp}(25°C, G_{POA})[1 + \kappa_P(T_M - 25°C)] \quad (17)$$

, where κ_P is the temperature coefficient of the P_{mpp} (%/K) obtained from [190]. Now it is possible to determine the final module efficiency:

$$\eta(T_m, G_{POA}) = \frac{P_{mpp}(T_m, G_{POA})}{G_{POA} \cdot A_{m,act}} \quad (18)$$

Module mismatch

Before proceeding into the losses associated with the conversion from DC to AC electricity, it is necessary to consider the mismatch losses due to non-uniform irradiance distribution throughout the PV module, or system. Since in agrivoltaic applications modules are elevated higher, the irradiance distribution throughout the module is homogenized considerably, thus alleviating module mismatch losses as discussed in section 2.3 Synergy with bifacial PV. This is in accordance with the findings in [227], where the reduction of power due to mismatch was minimized with increasing clearance from ground. These results were simulated for a low-tilt bifacial array, with various climates and locations considered. It was concluded that losses in power output for highly elevated modules are expected to be below 0.5% [227], which was also verified by [125]. Note that rear irradiance distribution is greatly impacted by the module's frame – at least for vertical oriented – and the design of the support structure. These, however, are not considered here.

Furthermore, as it was analysed in [125], the module's tilt can affect rear side homogeneity, where vertically inclined usually offers the lowest inhomogeneity depending on climatic conditions. Either way, these variations will probably diminish for the agrivoltaic array simulated, since the mounting height is typically above 4 m. In addition to irradiance inhomogeneity between cells, modules throughout an array also result in different BG as described by [131]. This is especially true when comparing the BG of modules in the corner to those at the centre of the array, with values of 27.7% to 31.4% respectively. Modules at the end sides of the array have their view to sky and ground unobstructed, unlike those residing at the centre. For agrivoltaic arrays, where lower PV densities are present, these mismatch losses between modules are then expected to be reduced. This was also verified through the simulations performed for this thesis, where rear irradiance slightly varied throughout a string of modules. Nevertheless, mismatch losses due to variation of rear side irradiance throughout the array are not separately considered, because the PV array modelled is relatively small. Moreover, microinverters and optimizers at the module-scale could be utilized instead of string-level MPPT to further reduced these mismatch losses [112].

3.2.2 AC electrical yield

After the DC yield is obtained, the losses associated with the conversion to AC electrical yield are discussed. Initially, the MMPT algorithm, and then the operation of the inverter itself – conversion from DC to AC – result in a certain loss of energy. Regarding the MPPT algorithm, the amount of energy lost depends on the tracking algorithm employed, and the climatic conditions (fluctuations in cloud cover can greatly affect efficiency). It is assumed that the overall annual efficiency decreases due to the MPPT tracking algorithm by around 1% [228]. Similarly, the operation of the inverter is also dependent on the irradiance incident on the PV modules, and thus the subjected environmental conditions. This is direct result of the inverter's dependency on DC input power and voltage. When irradiance on modules is plentiful, the DC power is close to rated, thus allowing efficient use of the inverter; however, as light availability decreases, depending on the inverter's sizing and characteristics, efficiency can drop sharply. On the other hand, if the DC power produced is higher than the rated power of the inverter, this surplus cannot be utilized. Consequently, it is crucial to optimize the trade-off between inefficient conversion at low irradiance (oversized inverter), and energy surplus cut-off at high irradiance (undersized).

Since the DC power output of the array varies depending on the climatic conditions, inverter efficiency will naturally follow a similar trend. A simple method to account for these variations is through adopting the weighted efficiency European model, which is based on empirical formulas for climates with low insolation [229]. Inverter efficiency is then calculated as a sum of efficiency values at each corresponding % of nominal inverter power, represented as $\eta_{\_\%}$:

$$\eta_{Euro} = 0.03\eta_{5\%} + 0.06\eta_{10\%} + 0.13\eta_{20\%} + 0.10\eta_{30\%} + 0.48\eta_{50\%} + 0.20\eta_{100\%} \quad (19)$$

By having distinct coefficients for each DC input power level, the contribution of inverter efficiency per power level is accounted for more appropriately than a single value of peak efficiency. The EU efficiency for three-phase solar inverters, which are necessary for large-scale systems, is around 98.5%, as shown in [230]. Nonetheless, this value underestimates the losses associated to the operation of the inverter, since more rigorous models that account for switching and semi-conductor losses have resulted in more than 5% reduction of efficiency [231]. In addition, the sizing approach is greatly influenced by the corresponding PV topology, where those that are oriented non-optimally would require an under-sided inverter [232], since the DC power production would be reduced. Because of the number of PV topologies analyzed in this thesis and the optimization process which scans through various deployment configurations, it would be quite complex to select and size the inverter properly. Consequently, a single annual value is used to approximate the losses for all topologies.

Finally, by considering the ohmic losses due to DC and AC cabling, it is possible to obtain the AC electrical yield. Thermal dissipation in cabling of a PV array usually lies between 0.5-1.5% [233], while the value adopted is 1%. By considering all the previously mentioned losses, the overall efficiency of converting annual solar irradiation to electrical AC yield can be calculated for each respective PV topology.

3.3 Performance indicators & optimization

To successfully perform any optimization process it is necessary to identify the most influential parameters and the desired outcome. Once again, the goal is to maximize energy yield, while maintaining or even boosting crop yield. However, by solely considering these two the agrivoltaic performance cannot be properly assessed, rather a merit should be used that quantifies the benefit in comparison to the refence case, which is standalone electricity and crop production. Therefore, it is crucial to examine the land productivity increase offered by an agrivoltaic system that cultivates crops and produces electricity simultaneously. Electricity and crop yield, and consequently land productivity, are proportional to the amount of irradiance incident on the front and rear side of the bifacial modules, as well as on the ground. As previously discussed, the POA irradiance of bifacial modules depends on a plethora of parameters; array deployment configuration, climatic conditions, as well as surrounding environment. In this thesis, emphasis is given primarily to the deployment configuration of the array. To assess the influence of each parameter that characterizes the deployment configuration, a sensitivity analysis is performed. In essence, each parameter is isolated to properly evaluate its impact on the light availability throughout space in the agrivoltaic system. The information provided by the sensitivity analysis is then utilized to make informed decisions regarding the selection of the most optimal agrivoltaic topology.

3.3.1 Land productivity

To measure the land productivity increase for the simultaneous production of crops and electricity the land equivalent ratio (LER) is adopted, which has been previously utilized to assess the potential of mixed cropping systems [234-235]. Through the LER, a comparison can be made between a monoculture and mixed cropping approach. Dupraz et al. (2011) proposed the use of the LER to quantify the benefits of integrating crop and electricity production, and since then it has been widely adopted in studies concerning agrivoltaics [95, 98, 236]. It was defined as a sum of two ratios; electrical AC APV yield to that of a conventional monofacial GMPV array, as well as the corresponding crop APV yield to that of a monoculture [95]:

$$\mathrm{LER} = \left(\mathrm{Y_{e,APV}}/\mathrm{Y_{e,ref}}\right) + \left(\mathrm{Y_{c,APV}}/\mathrm{Y_{c,ref}}\right) \tag{20}$$

The LER is a dimensionless number, and values above unity imply that the examined APV system results in an increase of the land's productivity. For mixed cropping or agroforestry systems LER usually lies below 1.5 [234-235], while for agrivoltaic systems LER varies considerably based on the deployment configuration, panel management and type of crop grown, with values reported as high as two [98]. To determine the land productivity increase it is necessary to quantify the amount of crop and electricity yield obtained from the APV

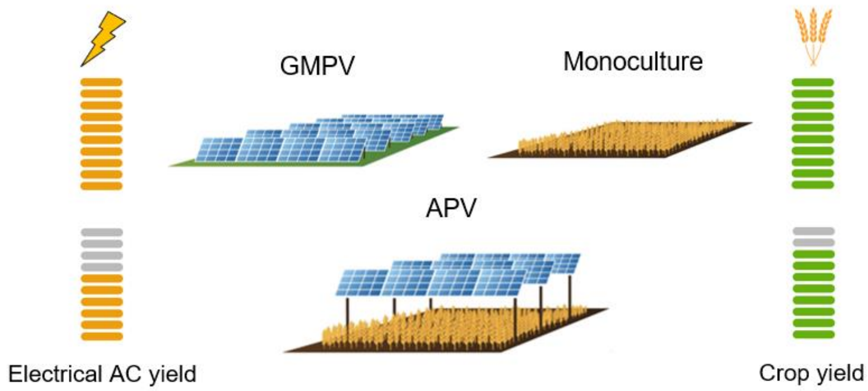

Figure 30 – The APV concept which permits the simultaneous production of crops and electricity. These systems are usually employed at lower PV densities to ensure enough growth for crops; thus, they are associated with significantly lower electrical yields and considerably decreased crop yields. Nonetheless, this behaviour can greatly vary based on the PV deployment configuration, crop specie cultivated, and local climate.

system, as well as the reference cases.

The procedure followed for the derivation of the APV's electrical yield is already discussed, thus what remains is to assess the reference case (GMPV). Naturally, the design of the reference case should also be optimized, to ensure that the comparison is accurate and representative of the actual performance, thus resulting in a realistic LER. There are multiple optimization objective functions that can be considered; total kWh/m^2 (total yield per area), and kWh/kWp (specific yield). When optimizing for the total yield per land area covered systems with dense arrays will dominate; however, the initial capital cost greatly increases. Furthermore, the array might be susceptible to shading during the winter months, leading to power losses. On the other hand, if the optimum is based solely on specific yield the result is a cost-effective design. At the same time, monofacial arrays do not suffer as much from high PV densities as bifacial arrays; consequently, the optimal design is closer to the one that maximizes total production and land productivity. The parameters that characterize the deployment configuration of the reference GMPV array are summarized in

Table 6. The RS of the array is selected according to the shadow length casted in December, thus significantly reducing mutual shading. In large-scale PV farms high PV densities are expected, which results in some mutual shading between rows; however, in this thesis, the influence of partial shading on PV is not considered. Therefore, the RS employed in the refence case is slightly

Table 6 – Deployment configuration parameters for the GMPV reference case, along with number of modules and electrical yield performance.

Elevation	Tilt	Azimuth	Row spacing	# modules	AC yield [1]	Specific yield
50 cm	18°	180°	270 cm	9900	3020 kWh/m^2	1130 kWh/kWp

[1] This is the total AC electrical yield estimated for the whole 2.7 ha of land based on the results

corresponding to the sample simulated.

wider than conventional. Furthermore, the tilt angle deviates from the one that maximizes light harvesting to reduce the length of shadows, thereby allowing denser PV configurations to be installed.

Next, the ratio of APV to monoculture crop yield must be determined to obtain the LER. The derivation of crop yield greatly depends on the crop selection, thus varying across species. Furthermore, the amount of biomass produced has a complicated dependence on microclimatic factors as was described in section 2.2 Crop yield. It is beyond the scope of this thesis to formulate a rigorous crop yield model that accounts for all these variables. Instead, to determine LER, the ratio of crop yields is estimated according to the reduction of light intensity and homogeneity, since the introduction of the APV array is expected to significantly affect those. This justification was discussed in detail in subsection 2.2.1 Influence of the PV array. The biomass rate, and in turn crop yield are expected to linearly depend on the amount of incident light intensity, where the slope of the line is dictated by the crop's genetic characteristics and the subjected environmental conditions as described in equation 1 (Biomass). Since the comparison between APV and monoculture crop yield is made for the same species, and in the same location, these parameters can be omitted without greatly jeopardizing the validity of the crop yield modelling. Dupraz et al. (2011) examined the potential of growing winter wheat under the shade of agrivoltaics, and concluded that both biomass (dry matter) and crop yield had a good correlation to a linear fit for a wide range of incident PAR intensities and various PV densities. This is in agreement with the trend observed in Figure 13 for shade-intolerant crops. Furthermore, the linear relationship between crop yield and light intensity, was verified for a mixed cropping system consisting of maize and cabbage, two shade-intolerant species [237]. On the other hand, crops that are not shade-intolerant do not necessarily portray a linear trend, while the crop yield of shade-tolerant species, in specific, may be portrayed with a negative parabola. Due to lack of data with regards to this behaviour, the crop species examined in this thesis are modelled with a linear fit instead. To distinguish between different shade-tolerances the parameter m is introduced that defines the crop's response to shade as suggested in [238]. Then the ratio of crop yields can be estimated through:

$$\frac{Y_{c,APV}}{Y_{c,ref}} = c\left[m\frac{I_{Gr,APV}}{I_{Gr,FS}} + (1-m)\right] \tag{21}$$

, where m varies from 0 to 1, with low values indicating a shade-tolerant crop. The parameter c represents the decrease in yield, due to loss of cultivatable land that is occupied by pillars. It depends on the design of the support structure, and it is assumed as 0.95 [4, 94] for most topologies apart from the E-W hinged. For the latter, blueberries are grown, and it is assumed that they are harvested manually; consequently, the region between pillars that would not be accessible with agricultural machinery can now be utilized, thereby increasing the area of cultivation. The assumed value for the c parameter is 0.98 based abides by the minimum loss reported in [94]. The total amount of irradiation incident on the ground under the shade of the APV array $I_{Gr,APV}$ and under full sun (FS) conditions $I_{Gr,FS}$ (open field) must be simulated for the corresponding growing period. As will be further analysed in section 4.3 Generic case study, two growing periods are examined: summer crops (March to October) and permanent crops (annual). However, the crop yield ratio obtained through equation 21 can deviate from reality, since fundamental processes and potential synergies due to the introduction of the PV array are not integrated in the model [238].

3.3.2 Ground irradiance homogeneity

As previously discussed, the spatial homogeneity of irradiance on the ground is considerably influenced by the presence of the array. In essence, regions which are shaded during solar noon – especially in summer months – will receive considerably lower annual ground irradiation values. Consequently, certain crops will receive plentiful sunlight, while others will be heavily shaded. This can lead to non-homogeneous growth throughout the farm, which could jeopardize the overall marketable yield depending on the species grown and climatic conditions. In an APV system, the main source of irradiance inhomogeneity is the shade casted by the PV array, thus the deployment configuration is the main parameter influencing irradiance distribution. For a south facing array, fluctuations in ground irradiance are expected with a frequency that is dependent on the row spacing along the N-S direction, while for an E-W facing array the fluctuations occur along the E-W direction. Naturally, the magnitude of inhomogeneity also depends on PV topology; therefore, ground irradiance inhomogeneity is a "property" of the PV array. For this reason, it is necessary to use a merit that can quantify this variation in light intensity throughout the farm sample simulated for various deployment configurations and array topologies.

The statistical measure used to assess the homogeneity of incident light is the coefficient of variation CV, which is a dimensionless number that quantifies the magnitude of variability in relation to the mean [239]. It has been widely applied in many research areas including engineering [240]. The sample CV is defined as the ratio of sample standard deviation σ to sample mean μ:

$$\mathrm{CV} = {}^{\sigma}/_{\mu} \tag{22}$$

At this point it is important to consider the size of the farm sample simulated, as was determined in subsection 3.1.3 Sampling size. Ground irradiation is calculated for that surface only, which is represented as a mesh of rectangular grid cells with a spacing of 21 cm. A smaller value would be desirable; however, this is the constraint imposed by DIVA based on the maximum number of grid cells. Note that for the case of blueberries, which will be discussed further in subsection 3.4.2 Blueberry case study, a wide row spacing is employed. Consequently, only a portion of the farm sample is simulated, since the remaining surface consists of ground. This allows the use of a finer mesh, and a grid spacing of 10 cm is adopted.

In general, a larger sampling size results in a more reliable estimation of the "true" standard deviation (whole APV farm). However, shading conditions at the centre of a large-scale system are not expected to vary considerably, since light penetration below the array cannot reach. Therefore, at least for the central patch, there is no benefit to be gained from increasing the farm sample, since the irradiation distribution is constant along one direction and periodic in the other. To account for the influence of border effects, additional farm samples would be required. Furthermore, a confidence interval could be calculated, but that would require the actual standard deviation, which is not known. In fact, there is no standard with regards to ground irradiance homogeneity in APV systems, at least up the author's knowledge.

3.3.3 Sensitivity analysis

To obtain a thorough understanding of the agrivoltaic system's performance, which is based on its deployment configuration, it is essential to perform a sensitivity analysis with regards to the availability of irradiation throughout the array, and subsequently the influence on LER. A multi-level analysis is required to investigate the underlying trade-offs in the design of APV systems, which is divided into array, module, and cell sensitivity as shown in Figure 31.

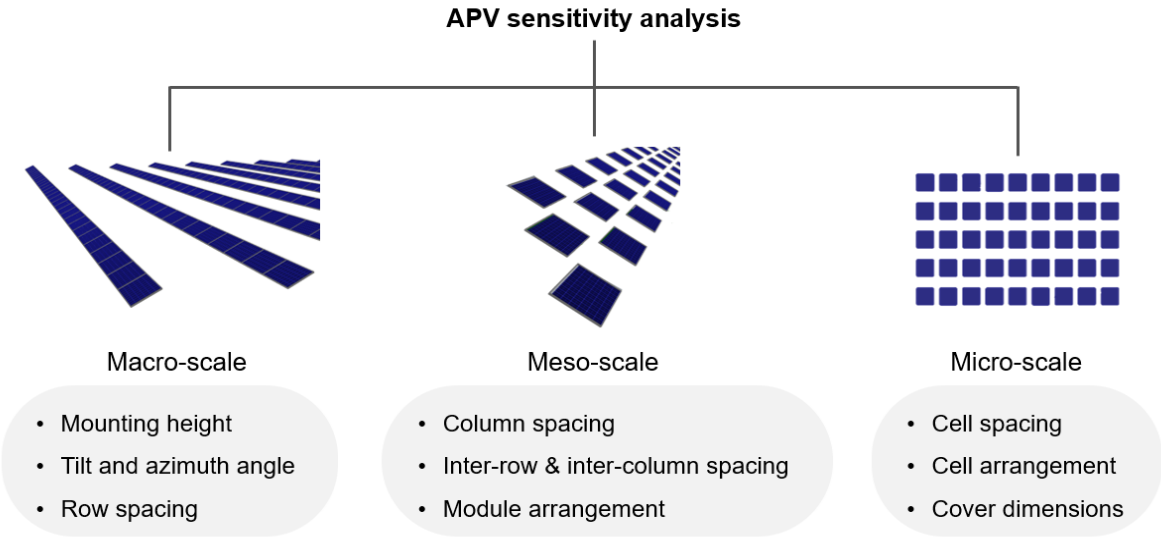

Figure 31 – A holistic approach for evaluating the performance of APV systems that is deconstructed into array, module, and finally PV cell sensitivity. At first the main parameters characterizing the deployment configuration of the PV array are addressed, then by modifying the arrangement of modules and the module itself it is possible to fine-tune the APV design.

Starting from the array, which represents the macro-scale, the main parameters that characterize the deployment configuration are examined. The aim of this sensitivity is to inspect the limitations of conventional PV topologies, as well as explore modified ones (E-W vertical and E-W hinged), and to assess the optimal for a certain climate and crop. Due to the dual function of agrivoltaic systems, additional module arrangements are explored. This is part of the module sensitivity (meso-scale), where complex configurations are analysed to push the limits in light intensity and distribution that are imposed by conventional module arrangements. Finally, by zooming into the micro-scale the parameters that characterize the cell layout are investigated. This is of special importance, since conventional modules lead to intense shading patterns that are non-homogeneous. Furthermore, APV systems that cultivate certain crops restrict the array's row spacing to be equal to the crop's, thus ensuring their alignment and permitting appropriate shading during solar noon. In such cases, the modification in cell layout can be used instead to optimize for ground irradiance. In other words, the transparency of the module can be set according to the crop's light requirements, thus allowing photosynthesis to occur even under the shade casted by the PV module. Through this holistic approach that incorporates a multi-level sensitivity analysis, it is possible to achieve a spherical understanding of the limitations and potential synergies associated with the dual use of land.

Macro-scale sensitivity

Due to the plethora of parameters investigated and the heavy computational requirements of simulations performed in Radiance, it is essential to reduce the range of the sensitivity analysis. Each PV topology is expected to operate efficiently for a certain combination of deployment configuration parameters, which will become clearer through the following discussion. To allow the operation of agricultural machinery below the array, the lowest edge elevation from the ground is set to 5 m for most simulations, as shown in Figure 32 (a). However, the E-W vertical topology occupies considerably less space due to its orientation, thus lower elevations are examined as well. Furthermore, for the E-W hinged in specific, the cultivation of blueberries is explored, which do not necessitate the use of large machinery, thus the mounting height can be greatly reduced. The next parameter is the RS, which is of great importance, if not the greatest, when it comes to light availability below the array. Consequently, a large range is examined, with the lowest RS indicating the minimum distance required to mitigate partial shading effects, while the maximum RS is approximately four times larger to ensure that saturation of ground irradiation is achieved. Note that the minimum RS for the E-W vertical topology is slightly higher than the south facing and optimally inclined, since the vertical tilt results in longer shadows.

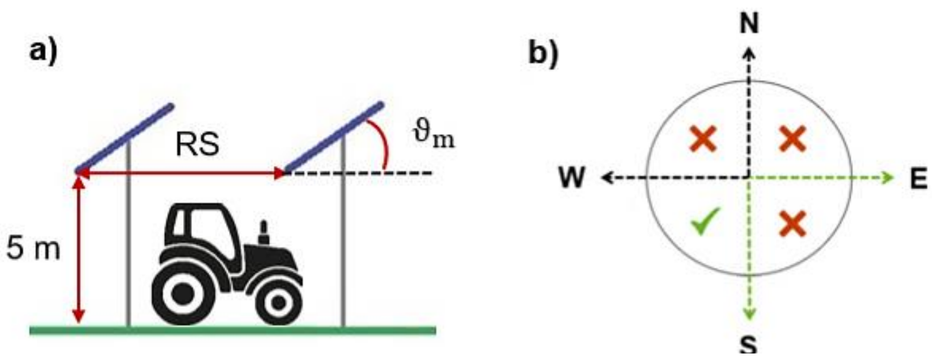

Figure 32 – The drawing in (a) depicts the minimum elevation of the array, which is based on the maximum height of the agricultural machinery used. The diagram in (b) divides the azimuthal range of the PV array into four quadrants to determine which is the most promising for the sensitivity analysis.

Following, the parameters that identify the array's orientation are examined, tilt and azimuth angle. The azimuth range can be reduced considerably, since modules (located in the northern hemisphere) that are facing due north cannot properly utilize DNI; consequently, north-west and north-east azimuths are omitted from the analysis as shown in Figure 32 (b) in red. For an array that is oriented E-W the front side of the module should be facing east, since the BF is not 100%, thus allowing optimal light harvesting during the early hours of the day where ambient temperature is reduced. Ultimately this leads to enhanced efficiency and increased annual energy yield. Based on the above, one might be tempted to orient the array south-east; however, the deployment configuration of APV systems is mainly dictated by the crop's light requirements. The shade casted during morning can be detrimental for growth, while shading during afternoon is beneficial since high temperatures and harmful irradiance are present. Ultimately, by setting the array to face south-west crops photosynthesize effectively throughout the day, with an increased light intensity in the morning and beneficial shading in the afternoon, thus increasing the accumulated biomass. As a result, the range of azimuths simulated includes due east and south (indicated by the green and dotted lines), and south-west as displayed in Figure 32 (b) with green. Similarly, the tilt angle can be reduced based on the topology analysed. South facing arrays are usually inclined for optimal light harvesting, consequently large tilt angles are not recommended, and the range used for the sensitivity analysis is between 0-60˚. On the other hand, for the E-W vertical topology, tilt angles ranging between 50-90˚ were simulated. To permit more control over the microclimate beneath the array, lower tilt angles were also examined. This concludes the discussion on the macro-scale sensitivity related to conventional module arrangements.

Meso-scale sensitivity

Ground availability is impacted the most by the array's RS, which is verified by the results obtained in this thesis discussed in subsections 4.1.2 Azimuth, tilt and row spacing and 4.1.3 Row spacing in-depth. However, it is intriguing to analyse the influence of the array's CS, which can effectively increase light availability on crops especially when a saturation is obtained through widening of the RS. Consequently, the CS is varied from being equal to the module's width (conventional string of modules), to three times the width in order to examine the potential saturating behaviour. Once an additional row-per-row RPR is included, while the CS and inter-column-spacing ICS are set to twice the module's width the resulting module arrangement is termed as checkerboard. An illustration of the checkerboard arrangement with three RPR is shown in Figure 21 (b), along with the parameters that characterize it. The influence of the inter-row-spacing IRS is also investigated; however, it is limited by the increasing bending stresses that occur on the support structure, due to the longer moment arm. This effect is amplified when more than two rows are installed per mounting structure, and for this reason the maximum width per row – distance from lowest module edge at the start of the row to the upper edge of the last inter-row – is chosen as 3.5 m. In addition, various module sizes and subsequently arrangements are examined. Conventional bifacial modules are quite large for agrivoltaic applications, since they result in extended shadows that can cover multiple plants simultaneously. It is thus compelling to decrease the module's size and place multiple modules per PV panel that are spaced apart. Through such a modification, it is possible to mitigate shading of entire crops, which can significantly increase the rate of photosynthesis for the entire crop canopy. Note that the 3.5 m constraint for the width of each row applies here as well.

Micro-scale sensitivity

So far, the sensitivity with regards to conventional modules is discussed. Although the possibility of modifying the module's size was introduced, the design is not significantly different, thus it is still termed as a conventional module. On the other hand, by considering the impact of cell spacing and arrangement it is possible to overcome the limitations related to conventional modules, and ultimately optimize the performance of the APV array. Note that bifacial modules usually have a transparency of 7%, while for the micro-scale sensitivity analysis higher values are investigated, up to 73%. In general, high transparencies are not recommended, since a large amount of cover material would be needed in comparison to the overall active surface area. Nonetheless, they can provide useful information by investigating potential saturation effects, similarly, to those obtained through widening of the array's RS. Through varying the cell's layout, an appropriate APV module can be designed that can effectively cultivate blueberries in the climate of Boston, MA, USA. In future studies, other crop specific modules could be designed to appropriately address the light requirements of the crop cultivated. This concludes the introduction to the sensitivity analysis, where a plethora of parameters are examined, due to the parameterized design that accelerates APV performance fine-tuning.

3.4 Crop selection

To optimize the deployment configuration of the array, it is essential to know the type of crop cultivated. In fact, the optimal APV topology will heavily depend on crop selection; consequently, an open-field agricultural system can be converted into APV, while a conventional PV array cannot. There might be some shade-tolerant crops (i.e. mushrooms), that could be grown with minimal adjustments; however, by promoting the cultivation of a variety of crops the global acceptance of APV systems is expected to be enhanced. The light requirements of crops can differ considerably across the species, due to their unique genetic factors that influence their morphology and carbon assimilation pathway. Owing to the introduction of the agrivoltaic array shade intensity and inhomogeneity are increased, which inevitably lead to the use of shade tolerant crops. This is a direct result of their shade acclimation and lower LSP. In addition, crop value and area potential should be considered as well to properly assess suitability with APV [241]. For instance, berries, lettuce, and tomatoes have a low area potential, yet they are deemed more appropriate for APV than wheat and corn that have a large area potential. Furthermore, high value crops necessitate protection from harmful weather conditions such as hail, heavy rainfall, frost, and drought. Depending on the array's deployment configuration, crops can be sheltered at least partially, and if necessary, hail nets can be easily incorporated. Such synergies are more pronounced for crops that require a support structure, thus partly justifying its cost. Finally, by cultivating crops that do not necessitate large machinery, support structure costs can be significantly reduced, thus promoting the economic feasibility of the APV system [4]. Ultimately, crop selection is based on wide variety of factors including light requirements and shade tolerance, value and area potential, as well as need for a support structure or protection, which result in complementary synergistic effects.

3.4.1 Generic case study

At first, the design of the APV system is based on a generic case where a minimum daily irradiation threshold is applied instead of selecting a crop. Naturally, this method ignores crop specific parameters that can greatly influence the deployment configuration of the array; however, it can provide insight with regards to the trade-off between light availability above and below the APV array. For example, to ensure enough growth tomatoes require a minimum of 2.6 MJ/m^2/day of solar irradiation as indicated by [242-243]. On the other hand, researchers in [20, 244] claimed that 5 MJ/m^2/day result in optimal growth of most horticultural crops, while in [245-247] 6 MJ/m^2/day was used instead. Consequently, for the generic case study the latter is used as a constraint for daily ground irradiation availability, since any further reduction can significantly affect the quantity and quality of the harvested product in terms of colour, size as well as nutritional value [243]. Crops are expected to be planted in lines, parallel to the strips of the PV array, and to simplify the analysis it is assumed that they fully cover the farm sample simulated. Thus, the irradiation incident on the ground, obtained through Radiance, is directly applied to the crop yield ratio and the calculation of the LER.

3.4.2 Blueberry case study

To fine-tune the design of the APV system and optimize the cell-layout it is crucial to know the crop's light requirement. As previously discussed, shade-tolerance and crop value are desirable traits for species cultivated in such applications. One crop that satisfies these requirements is the 'bluecrop' highbush blueberry, Vaccinium corymbosum, which grows naturally in deciduous forests. The net CO_2 assimilation rate, or the rate of photosynthesis, was inspected in [248] using a growth chamber for photosynthesis measurements and the incident light intensity (PAR or PPFD) was varied using light emitting diodes (LEDs). The results are shown in Figure 33 (a), while for this study irrigated conditions are assumed. The light intensity resulting in the maximum rate of photosynthesis or LSP is around 800 μmol m^{-2} s^{-1}, while considering the whole spectrum of light it is equivalent to 380 Wm^{-2}. Because of the

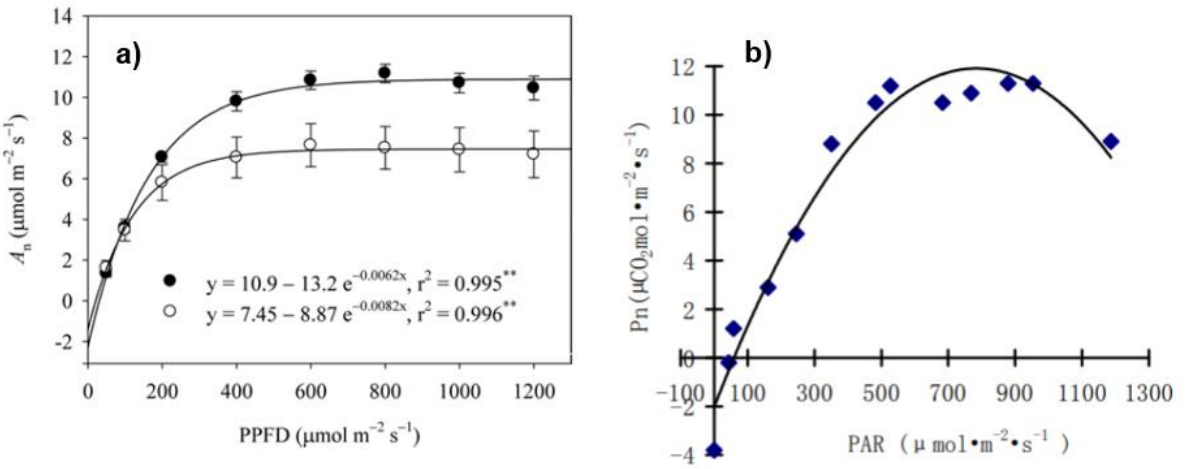

Figure 33 – Light response curves for 'bluecrop' highbush blueberry: a) measured under artificial light in a greenhouse [248] b) measured under open field conditions [249]. Note that in graph (a) both irrigated (black circles) and non-irrigated conditions (white circles) are displayed.

logarithmic trend, lower light levels can still provide an adequate photosynthesis rate, simultaneously allowing high PV densities to be installed, which ultimately increases the LER. In other words, the range where growth is highly productive (>80% of max rate) lies above 290 μmol m^{-2} s^{-1} or 145 Wm^{-2}. However, values considerably higher than 380 Wm^{-2} can significantly reduce the rate of photosynthesis, potentially due to hydropassive closure. For this reason, Figure 33 (b) is included, to highlight the adverse effects of temperature on crop growth, under open field conditions as was examined in [249]. The differences between the two figures, mainly arise due to the distinct growth conditions, as well as local climate. Either way, crop cultivation under APV closely resembles open field conditions, thus it is crucial to set a maximum PAR intensity where any higher values would be detrimental to crop growth.

To determine the optimal shading ratio, Retamales et al. (2008) performed experiments with various coloured shading nets in Miraflores, Chile. It was concluded that although a 50% shading rate did not affect yield in the first season, it can significantly reduce yields in the following years. On the other hand, for smaller shading rates (35%), crop yield was enhanced by 26-91% in relation to the control treatment (no shading), through mitigating stressful environmental conditions present at midday [250]. Furthermore, under shade, canopy length and leaf size increased, while fruit weight remain unchanged. These finding were verified by [251], where acclimation to shade was examined in detail for the climate of Seoul, Korea. Blueberries can adapt to low light conditions by altering their morphology, increasing leaf length and size, yet reducing leaf thickness; thus, they effectively minimize respiration losses. However, as the intensity of light reduced, number of flowers, fruit number per bud, and fruit yield were significantly reduced [251]. In summary, for optimal plant productivity shading rates above 40% should be avoided. Lobos et al. (2013) also investigated the influence of incident PAR on blueberry productivity through an experiment conducted in Gobles, MI, USA. Their results indicate that shade levels between 40-60% of incident PAR do not significantly affect yield and fruit quality; however, they are responsible for harvest delays. Nonetheless, this delay could increase the product's marketable value since fruit prices are usually highest towards the end of harvesting [253]. Overall, depending on the climatic conditions and shading rate, the yield of blueberries can increase, or remain relatively unaffected. The results presented by Lobos et al. (2013) are the most relevant as they were investigated in a similar climate to that of Boston, USA; however, note that Boston is relatively sunnier.

Unlike the general case study, for blueberries a considerable spacing is applied between crop rows that must be defined before proceeding into the design and optimization of the array. The most common crop row spacing (CRS) employed, which is adopted here, is around 3 m [254]. This CRS has been claimed to mitigate light competition between closely spaced rows, while maximizing the overall crop yield of the farm. For blueberries, in specific, dense crop plantations can significantly reduce light penetration within the plant's canopy as reported by [255]. Due to the increased CRS, the farm sample simulated is reduced to the portion that is occupied by the crop. Thus, the farm sample for this case consists of three parallel strips offset at 3 m, with a width of 1.4 m each (assumed crop width).

4

Results & Analysis

4.1 Array sensitivity – macro scale

4.1.1 Mounting height

As it was previously discussed, the APV sample simulated is selected in such a way that light penetration below the array cannot reach the farm sample. Consequently, by further elevating modules ground irradiation is not expected to be influenced considerably. This can be verified by the plot in Figure 34, where the lowest edge height is varied to assess the impact on the average ground irradiation throughout the farm sample. Overall, the relationship between the two is approximated as linear, while the increase in annual irradiation is 3.4% when the array is raised from 2 to 7 m. These results are representative of a south and latitude inclined topology; and a similar trend was observed for the E-W topology as well. Additional benefits are expected from elevating modules, such as cooling due to increased wind speeds and free convection, as well as reduced dust deposition rates. Either way, to minimize support structure costs the lowest edge height is selected according to the maximum height of agricultural machinery used. For most crops, this is around 4-5 m, and thus 5 m is selected for the following simulations, with some exceptions in E-W orientated arrays that will be clarified later. Note that the array's size (APV sample) for this sensitivity analysis is based on what is necessary to mitigate border effects for an elevation of 7 m. As the mounting height increases, the length of shadows increases proportionally, thus necessitating larger array sizes.

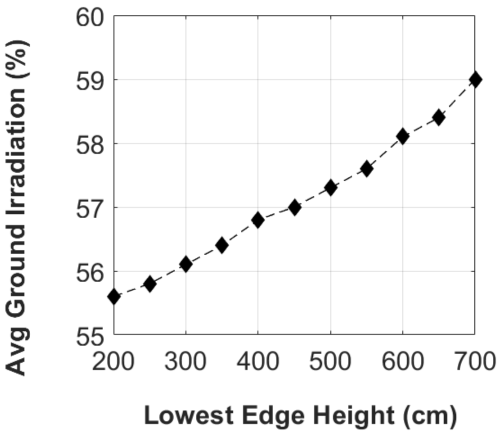

Figure 34 – Annual, average ground irradiation incident on the farm sample simulated for various PV array elevation heights. Ground irradiation is expressed as a percentage of what would be available under FS conditions.

4.1.2 Azimuth, tilt and row spacing

After the mounting height has been set, a multi-dimensional sensitivity analysis for the array's azimuth and tilt angle, as well as row spacing can be performed. These parameters are analysed separately for S-N and E-W topologies, and their influence on the distribution of light throughout the APV system is examined. Starting with the S-N, the sensitivity of the annual average ground irradiation to deployment configuration is depicted in Figure 35 for the farm sample simulated. The main parameter that influences ground irradiation is the array's RS, where wider spacings reduce shading on the ground considerably. In specific, when the RS is doubled, ground irradiation increases from 58.1% to 79.6% for an array tilted at 35° (optimally inclined) and facing due south. In general, tilting modules results in longer shadows, and consequently direct shading (no DNI) over a larger ground area. As expected, shading is maximized at around 30-35° tilt, depending on the RS. Tilt angles that deviate from this range enhance light availability below the array, with shorter shadows for lower tilts, and reduced shading at noon for higher tilts. The sensitivity to the azimuth angle is relatively higher, where a south-west facing array receives additional ground irradiation. However, the sensitivity to orientation greatly decreases for a wide RS due to the reduced number of rows, and thus ground shading. Naturally, varying the orientation of a dense array will significantly impact ground irradiation in comparison to an array with a large RS. For instance, at a RS of 240 cm, when the array is tilted from 10° to 35° while facing due south, ground irradiation reduces by 2.2%, while for twice the RS the same tilt adjustment results in a reduction of 1.3%. Similarly, by modifying the array's azimuth from 180° to 205°, with a tilt of 35°, irradiation increases by 3.9%, while for twice the RS it is enhanced by 1.5%. This is reasonable since a lower RS results in an increased GCR and proportional intensification of ground shading depending on orientation.

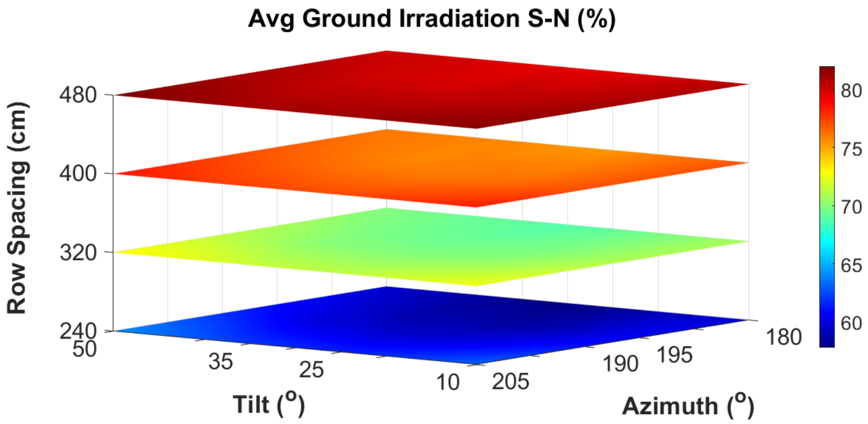

Figure 35 – Annual, average ground irradiation sensitivity to tilt and azimuth angle, as well as row spacing for south-north facing topologies. The colour bar on the right displays the intensity of ground irradiation expressed as a percentage of full sun conditions.

The analysis is continued for the annual POA irradiation on both sides of the bifacial PV module as shown in Figure 36. The influence of the RS is quite straightforward, since a wider RS results in additional POA irradiation for any combination of tilt and azimuth angles; however, the amount gained is highly dependent on orientation with the tilt angle being dominant. When the RS is doubled, a south facing array that is tilted by 10° receives a boost of 3.1%, while for a tilt of 50° the corresponding boost in POA irradiation is 5.6%. As the RS is

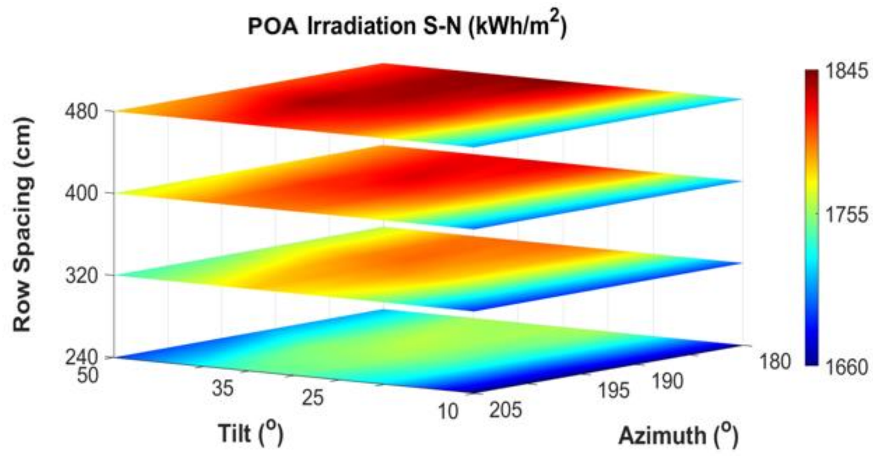

Figure 36 – Annual, average plane of array irradiation sensitivity to tilt and azimuth angle, as well as row spacing for south-north facing topologies. The colour bar on the right displays the intensity of irradiation incident on both sides of the PV module in kWh/m^2, with a bifaciality factor of 90% as described in [190].

increased ground reflected irradiance is enhanced, which subsequently increases BG depending on the array's tilt angle, with higher tilts resulting in enhanced gains. Furthermore, for highly tilted modules, increasing the RS mitigates any partial shading that occurs between rows, thus allowing the front side to benefit considerably as well. In general, horizontally placed modules – at least for northern latitudes like Boston's – are associated with low specific yields, due to the large AOI between sun and PV. As the tilt angle is increased, up to 30-35° depending on the RS, POA irradiation reaches a maximum, and then declines for higher tilts due to the increasing AOI. These findings agree with those reported previously, where ground irradiation is minimized for optimally inclined modules. In essence, due to the relatively low ground albedo, the optimal tilt is mainly dictated by the absorption of the front side, similar to monofacial modules. Furthermore, for a wider RS, the optimal tilt angle is slightly increased, due to the abundant ground reflected irradiance. This effect is expected to be more pronounced for highly reflective ground surfaces. Regarding the azimuth angle, south orientated arrays are associated with the highest POA irradiation, while any deviation, in this case south-west, results in a decay. Interestingly, arrays with a large RS that are facing south-west promote higher tilt angles. This could be explained by the additional ground reflected irradiance under such configurations, and the need to reduce the AOI for an array that is diverging from south, since the sun's elevation is lower. In contrast to the findings regarding ground, POA irradiation is more sensitive to orientation for a wide RS. A dense array is accompanied by intense ground shading that deteriorates BG; consequently, modifications in the array's orientation do not influence POA irradiation considerably. Contrary, as the RS is increased, the sensitivity to orientation is amplified, due to the plentiful ground reflected irradiance. For instance, an array that is facing due south, with a RS of 240 cm, gains 5.6% in POA irradiation when the tilt is adjusted from 10° to 30°, while for double the RS the same modification in tilt results in an enhancement of 7.4%. A similar behaviour is observed for the azimuth angle, where the decrease in POA irradiation is only 0.7% in comparison to 1.3% for double the RS. Note that the change in azimuth is from 180° to 205°, while the tilt angle is constant at 35°.

The same procedure is followed for an E-W facing array, nonetheless the sensitivity analysis portrays a different behaviour for some parameters. Initially, the average ground irradiation is examined, as represented in Figure 37, which is considerably higher than the one available under a S-N facing array. This is logical, since the main incentive for adopting such orientations is to enhance light availability on the ground. However, in comparison to the S-N orientation, the gain of ground irradiation with wider RS is lesser. Specifically, for a RS of 270 cm a vertical and E-W facing array permits 75.9% of irradiation, while for double the RS ground irradiation increases to 88.6%; consequently, for such topologies, light availability throughout the farm sample is less sensitive to RS. Indeed, as the array's configuration converges to what is conventional – south facing and optimally inclined – the gain in ground irradiation with increasing RS is amplified. For instance, an array with a tilt of 50° and azimuth of 245° allows a gain in ground irradiation from 70.1% to 85.9% when the RS is doubled. Either way, vertically installations maximize ground irradiation, which is true for all RS and azimuth angles simulated. Any reduction in tilt diminishes ground irradiation depending on the azimuth angle. This decrease in irradiation is maximized as modules deviate from E-W and face south-west instead, which is further amplified for dense arrays. For example, at a RS of 270 cm with an azimuth of 90° (E-W), when the tilt angle is changed from 90° to 50° ground irradiation decreases from 75.9% to 74.5%, while for an azimuth of 245° (south-west facing) the same tilt variation results in a reduction from 76.1% to 70.1%. On the contrary, for twice the RS, the same set of adjustments result in reductions of 88.6% to 87.7% and 89% to 85.9% respectively. The additional decrease in ground irradiance for dense arrays is justified by the higher number of modules, which are accompanied by intensified ground

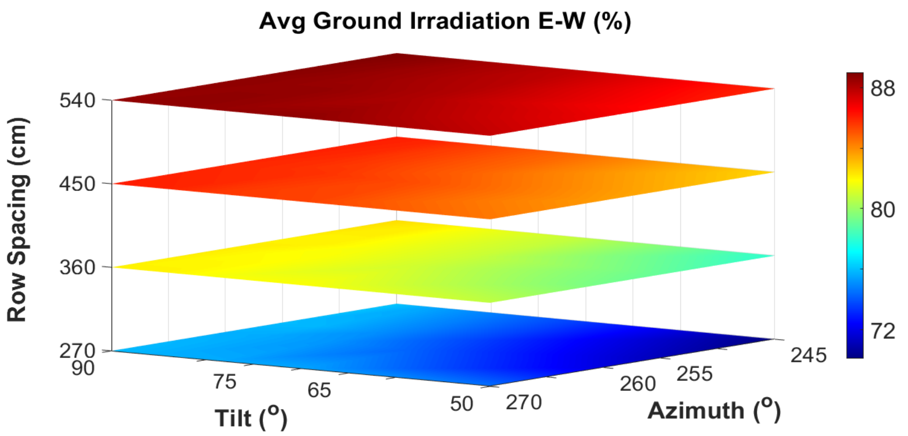

Figure 37 - Annual, average ground irradiation sensitivity to tilt and azimuth angle, as well as row spacing for east-west facing topologies. The colour bar on the right displays the intensity of ground irradiation expressed as a percentage of full sun conditions.

shading. As a result, it can be concluded that for all topologies simulated, ground irradiation sensitivity to orientation is considerably higher for dense arrays.

Finally, the sensitivity analysis of POA irradiation to deployment configuration can be examined for the E-W facing and vertically inclined topology as shown in Figure 38. Initially, the influence of the RS is investigated, which is of crucial importance for such topologies. In fact, a vertically installed and E-W facing array gains 9% in POA irradiation when the RS is doubled (270-540cm), while an array that is tilted by 50° and has an azimuth of 245° receives a boost of only 5.1%. Vertically installed arrays, especially those that face E-W, heavily rely on ground reflected irradiance; consequently, they scale better with RS, even more so when high albedos are present. As the RS is increased, partial shading as well as masking between rows is effectively minimized. Even though vertical E-W topologies benefit more from widening of the RS, the overall POA irradiation is considerably lower than that of S-N and optimally inclined array for the same RS; therefore, a wider RS is required to obtain comparable results, at least for relatively low ground albedos. This is further justified by the following analysis. When the tilt angle is varied from 50° to 90°, for an array that has a RS of 270 cm and is facing E-W, the POA irradiation reduces by 5.3%, while for an azimuth of 245° the same tilt modification results in a reduction of 12.5%. By doubling the RS and applying identical orientation modifications the POA irradiation reduces by 2.3% and 9.7% respectively; thus, for less dense arrays the differences between E-W vertical and S-N and optimally inclined topologies decay. In addition, the sensitivity to orientation diminishes with wider RS, which was verified previously for S-N topologies as well. Another important observation is that the sensitivity to tilt angle is more apparent for an array that is facing south-west, rather than E-W, since the previous is better oriented for direct light harvesting, which is true regardless of the RS. For vertical installations any deviation in azimuth from E-W facing slightly reduces

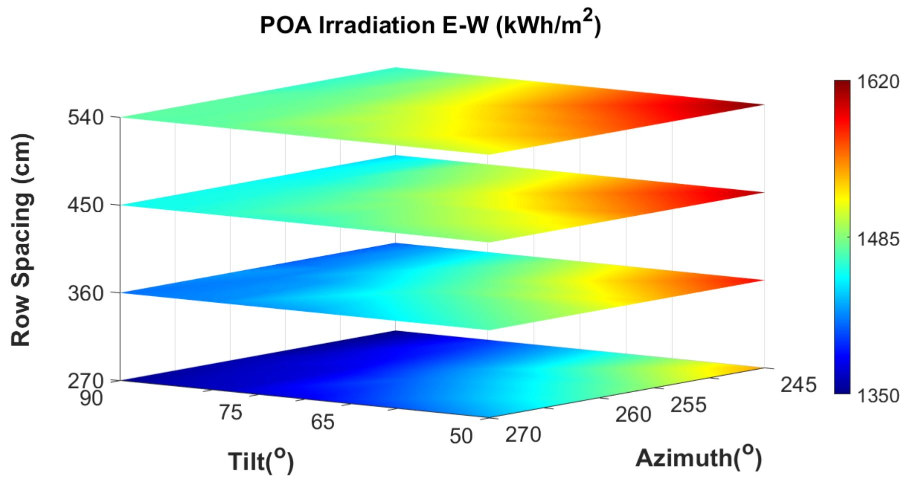

Figure 38 – Annual, average plane of array irradiation sensitivity to tilt and azimuth angle, as well as row spacing for east-west facing topologies. The colour bar on the right displays the intensity of irradiation incident on both sides of the PV module in kWh/m², with a bifaciality factor of 90% as described in [190].

POA irradiation (less than 1%), which was verified for various RS. It is thus intriguing to orient vertical arrays towards south of due west to allow a higher light penetration in the morning for crops, and increased shading in the afternoon without jeopardizing electricity yield. Note that this change in azimuth will shift the peak of power output to afternoon potentially providing a better match to electricity demand, which is maximized around that time as well.

The RS range simulated for both E-W and S-N orientations is quite limited, in order to avoid computational exhaustion as additional simulations would be required to extend the 4D plots. Since the RS is one of the most crucial parameters influencing light availability below the array, and consequently ground reflected irradiance it is examined in detail in the following subsection. Furthermore, it is essential to extend the width of the RS to examine any potential saturation effects with regards to irradiation throughout the APV array.

4.1.3 Row spacing in-depth

The macro-scale sensitivity analysis is continued for two specific deployment configurations; the S-N and E-W facing topologies with a tilt and azimuth angle of 33°, 193° and 90°, 260° respectively. Note that for both topologies the lowest edge height is chosen as 5 m and they are oriented to face south-west to permit optimal growth conditions for the crops below. The tilt angle of the S-N topology is selected based on the maximization of annual POA irradiation, while for the E-W the vertical tilt prioritizes crop growth.

In the previous subsection, the sensitivity analysis for the annual average ground irradiation was examined. However, it is crucial to observe the influence of RS on minimum irradiation, to ensure light homogeneity and subsequently crop growth uniformity. For this reason, both minimum and average irradiation are plotted for a wide range of RS, incremented by 76 cm as shown in Figure 39. At first, any increase in the RS results in an abrupt gain of ground irradiation, especially for the S-N topology, and even more so for its minimum irradiation. Due to the tilt angle of the S-N topology the SVF of the ground is

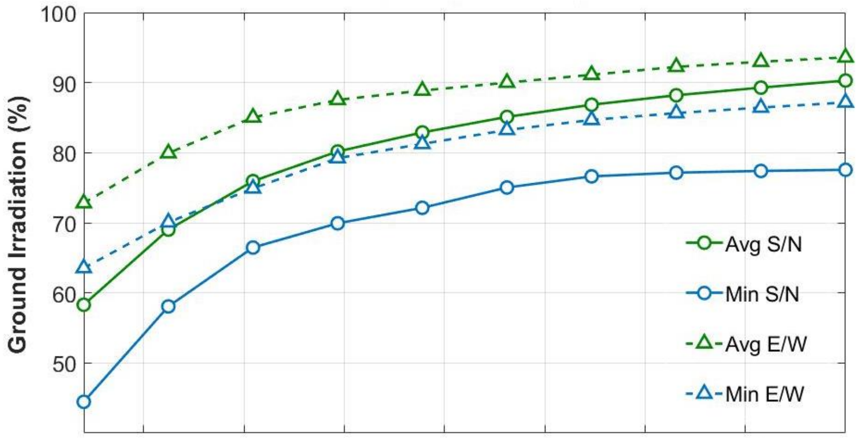

Figure 39 – Annual ground irradiation consisting of both average and minimum values in relation to the row spacing as well as PV array topology. Ground irradiation is expressed as a percentage of full sun conditions.

significantly reduced, which can be partially solved by increasing the RS. Essentially, by installing rows at a wider distance the shading of neighbouring rows on the ground patch below is effectively mitigated; consequently, allowing the SVF of the ground to be increased. However, as the RS is further increased the gain saturates, especially for the minimum ground irradiation of the S-N topology. The saturation occurs at a RS of around 7 m, with a minimum irradiation of 77%, which is based on the minimum SVF reduction of the specified PV topology. The trend can be approximated as logarithmic, which applies to the other curves as well, but to a lesser extent. It is unclear as to why the minimum irradiation does not attain saturation for the E-W topology, although the rate of the increase declines significantly. One explanation could be the vertical tilt, which expands the region of influence by further elongating shadows. Similarly, the rate of increase of the average ground irradiation reduces considerably with wide spacings for both topologies; however, saturation is not accomplished completely. This is a direct result of the shadows casted by neighbouring rows during times when the solar elevation is low, which greatly extends their length. Overall, the E-W topology offers supplementary ground irradiation, especially for dense arrays. The S-N topology is more sensitive to the RS, while as the spacing is increased the difference between the two topologies diminishes to a constant. That constant represents the difference in the ground's SVF reduction between the two topologies. For the crop yield modelling the average ground irradiation is used; however, it is vital to set a constraint on the minimum ground irradiation to ensure a homogeneous light distribution without jeopardizing the marketable value of the crops. This will be examined further in section 4.3 Generic case study.

To conceptualize the underlying trade-offs in the design of an APV system, a comparison between average ground irradiation and overall AC electrical yield is performed as shown in Figure 40. Both topologies follow a similar behaviour, where as the RS is widened

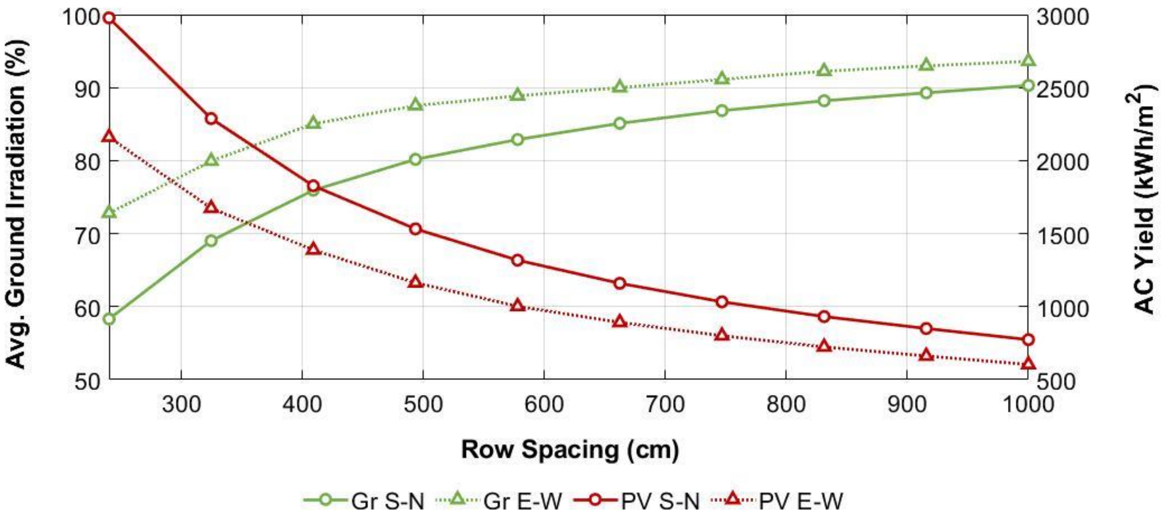

Figure 40 – Sensitivity of the average ground irradiation and total AC electrical yield (both annual) to row spacing and PV topology. Note that the energy yield of the reference GMPV case is around 3 MWh/m^2. Although bifacial modules are used, which result in enhanced yield, they are placed in landscape orientation, thus reducing the GCR and subsequently the overall energy yield.

ground irradiation increases and electrical yield decreases. In fact, energy yield can be represented with a negative exponential trend, thus indicating that a saturation in the reduction can occur at a sufficient RS. This is justified by the plentiful ground reflected irradiance that amplifies POA irradiation, thus compensating for the reduction in electrical yield through increasing specific yield. In other words, a wide RS decreases the overall energy yield of the APV farm, since less rows are present, yet they permit maximum light availability for both PV and crops. Therefore, a trade-off arises between a sustainable or synergistic design where ground irradiation and yield per module is maximized (specific yield), and a design that exploits the land most effectively in terms of overall energy yield. Although the latter offers the highest possible AC electrical yield, it does not necessarily imply that the land's productivity is maximized, since crop yield is greatly impinged under such conditions. Naturally, the latter will greatly depend on crop selection, as shade tolerant species could be cultivated under such conditions. Notice that the energy yield reduction of the S-N topology is more pronounced than that of the E-W, which implies that the latter scales better with RS. To summarize, the ground irradiation of an E-W topology scales worse with RS, while its energy yield benefits considerably more with RS in comparison to the S-N topology analysed. Note that the saturation effect in energy yield would be further intensified if a rigorous thermal model was applied that appropriately considers the influence of PV density on convective cooling and thus PV performance.

Although ground irradiation is a vital parameter in characterizing the productivity of crops, what is of greater interest is crop yield. Once again, to assess the performance of various APV topologies the crop yield ratio is used instead, which subsequently allows the calculation of the LER. To investigate the influence of various shade tolerant species on crop yield Figure

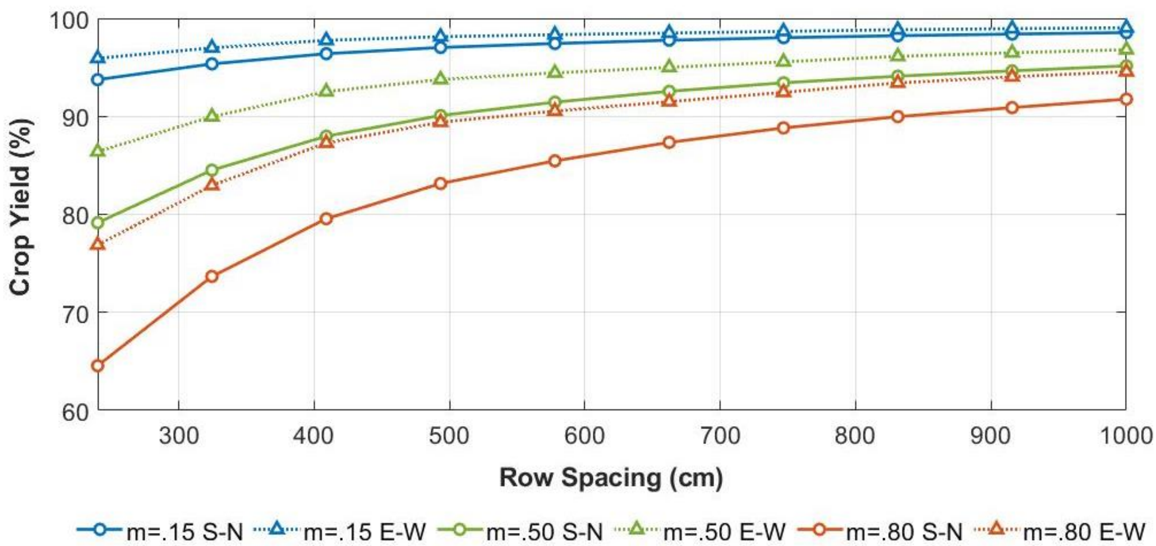

Figure 41 – Crop yield sensitivity to shade tolerance and PV array row spacing. The letter m represents the crop's acclimation to shade with high values representing a shade intolerant crop. For instance, a crop with m = 0.8 could represent the light response of maize, while m = 0.15 could be utilized for blackberries that require low light conditions to be cultivated effectively.

41 is included. It is of no surprise that shade tolerant species receive minimum yield reductions. Furthermore, the E-W topology results in a higher crop yield ratio than the S-N for all shade tolerance levels and RS, which is especially true for dense arrays. This is in accordance with the findings discussed previously for ground irradiation; however, as the RS increases the difference between the two topologies decays, even more so for crops that can tolerate shade. Consequently, it can be claimed that crop yield is less sensitive to the deployment configuration as the RS is widened. As previously discussed, the relationship between ground irradiation and RS closely resembles a logarithmic trend, similarly to what is observed in Figure 41 for the crop yield ratio. Since crop yield is assumed to scale linearly with ground irradiation, this is to be expected. Overall, the E-W topology is better opted for shade intolerant crops, especially when dense arrays are employed. This concludes the macro scale sensitivity analysis with regards to conventional module arrangements.

4.2 Module sensitivity – meso scale

In conventional large-scale PV farms modules are usually placed in portrait orientation, where the lowest edge is the short one, thus maximizing the number of modules per given area. Since APV systems serve more than one function, it is intriguing to examine whether the landscape orientation is more appropriate. Conventional modules are quite large to be suitable for APV applications, since the casted shadows can cover a whole crop, or even multiple. This can heavily interrupt the rate of photosynthesis for the entire crop canopy, leading to non-uniform growth and an increase of the unmarketable yield. Furthermore, prospects for the bifacial PV market include sizing up of modules, which will aggravate the issue. To mitigate the intensified shading caused by such modules, they should at least be placed in landscape orientation; consequently, the length of shadows is reduced considerably and photosynthesis throughout the crop canopy is enhanced. On the other hand, the PV array is less dense, which results in a lower energy yield; however, this is a reasonable compromise to achieve the dual function of APV systems. For all simulation results reported previously as well as those that follow the landscape orientation is adopted, except for the reference case in the LER calculation, which is supposed to represent a conventional GMPV array.

As previously examined, the gain in ground irradiation associated with increasing RS can saturate; consequently, for crops that require plenty of light, CS widening is inevitable. Naturally, the increase of the spacing between modules in the same row is of great interest to arrays that have more than one row per row RPR. To permit the operation of agricultural machinery, APV arrays are highly elevated, which leads to a substantial increase in support structure costs. In fact, as reported by [9], the capital expenditure associated to the mounting structure dominates the overall CAPEX of APV, but this should not be generalized, since the cost associated to the support structure greatly depends on the design; elevation, number of mounting pillars, PV array density. Although not investigated in this thesis, reduction of the materials associated to the construction of the mounting structure is crucial to ensure that the levelized cost of electricity LCOE can compete with that of building integrated PV BIPV or GMPV. Arguably, one way to minimize the size of the support structure, is to increase the RS of the array; however, that would lead to a decreased energy yield and subsequent reduction of the LER. It is thus compelling to mount more than one RPR, and simultaneously increase the RS, thus allowing a reduction in the number of supporting pillars, while maintaining energy yield.

By increasing the number of RPR to two, the ground patch below the array experiences a considerably decrease in SVF, thus reducing light availability to levels that do not sustain growth for most crops. Widening of the RS partially resolves this; however, as it was shown in Figure 39 for the conventional module arrangement (one RPR), the minimum ground irradiation quickly saturates. This effect is further intensified for two RPR, thus this is the main incentive for increasing the CS between modules. The CS was varied from the conventional (equal to module width) to twice the module's width for an array with two RPR, a RS of 9 m, and a S-N topology to examine the impact on the ground's light availability for the 15th of July. As the CS was doubled, average daily ground irradiation increased by 10.4% in a linear fashion, therefore indicating that CS extension is a viable option for enhancing light penetration. More importantly, the number of grid cells NGC that receive low irradiation is decreased considerably. To quantify this, the ratio of the NGC (RNGC) is used, which can be obtained by dividing the NGC that receive irradiation below a certain fraction of FS conditions to the total NGC in the farm sample. The dependency of the RNGC for 70% and 60% of FS conditions is plotted in Figure 42 versus the CS. The RNGC quickly decays with increasing CS, thus mitigating non-uniform crop growth. For instance, when the CS is increased the RNGC with irradiation less than 60%FS reduces abruptly, and when the CS is doubled RNGC (<70%FS) reduces to 2.5%. In other words, 2.5% of the total farm sample simulated receives irradiation less than 70% of FS conditions, ultimately enhancing light distribution. Another parameter required to define the deployment configuration of such topologies is the IRS; however, any extension of this spacing does not influence ground irradiation or RNGC considerably. As a result, a short IRS should be adopted thus permitting efficient material utilization with regards to the support structure.

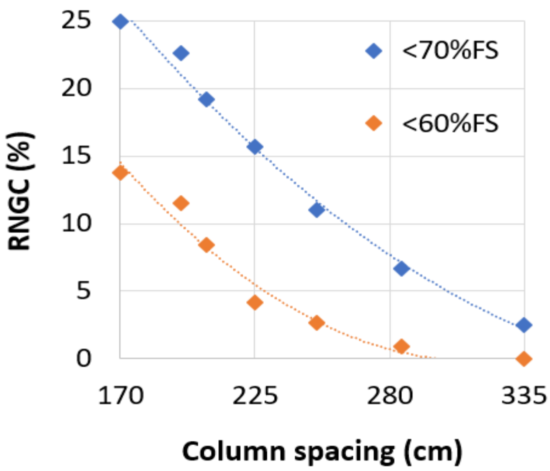

Figure 42 – Ratio of grid cells receiving irradiation below 70% and 60% of FS conditions with respect to the column spacing.

Nonetheless, a large CS does not necessarily lead to an optimal design, since it reduces the density of the array and subsequently the energy yield in total. By introducing the ICS it is possible to modify the previous topology into one that is better suited for APV applications, known as the checkerboard arrangement. As the name suggests, it is comprised of two RPR, with a CS that is two times the conventional, and an ICS that is equal to the module's width. Additional RPR can be included; however, it is important to note that an increasing number of rows per mounting rack can greatly diminish the ground's SVF, which cannot be compensated by widening of the RS or CS. As previously discussed, conventional modules lead to extended shadowing on the ground that can potentially cover multiple crops. It is thus compelling to design modules specifically for APV applications, which is briefly explored here. For a more in-depth examination the reader is referred to section 4.5 Cell sensitivity – micro scale. At first, the size of the module is reduced with the intent of minimizing shading on crops, and thus allowing part of the canopy to photosynthesize even though a portion of it is shaded. Without adjusting the individual size of cells, or their arrangement, minimal adjustments in the design are required, consequently allowing ease in manufacturing. Multiple module sizes, and layouts were analysed, including the checkerboard arrangement; however, the gain in ground irradiation was not insignificant. If a rigorous crop yield model was applied that can account for light penetration throughout the plant's canopy the benefits of such modules could be addressed more appropriately.

4.3 Generic case study

By completing the sensitivity analysis with regards to conventional modules it is possible to examine which topologies can appropriately address the trade-off between crop and electricity yield. All the suggested topologies are deployed at a significantly lower density than what is conventional, thus prioritizing crop productivity and subsequently specific electrical yield, due to the integration of bifacial PV. The latter is of importance for bifacial PV arrays as the optimal design is not necessarily the one that maximizes total energy yield. Dense arrays lead to significant reductions in BG, due to intensified ground shading. Furthermore, certain costs are proportionate to the total peak power of the installation [256], which can be mitigated through maximizing the specific yield. On the other hand, the cost associated to the land, which promotes the maximization of energy yield, is not as dominant for APV due to its dual nature. From the plethora of deployment configurations simulated four topologies are selected, two with a S-N topology that permit cultivation of summer crops (mid-March to mid-October) and two with an E-W that are more appropriate for permanent crops (annual). Note that all the selected topologies are facing west due of south, and south due of west respectively; nonetheless, the previously mentioned description is used to distinguish them. Although E-W topologies can effectively cultivate summer crops as well, S-N facing and close to optimally inclined arrays are better suited, since they lead to a higher specific and total yield (electrical) for the same number of modules. Furthermore, because of the orientation of S-N topologies, light intensity and distribution on the ground is greatly impinged, leading to unfavourable conditions for crop growth during winter – at least with conventional modules – which will become clear by the end of this section.

4.3.1 Summer crop

Deployment configuration

For the growth of summer crops two distinct deployment configurations are selected as shown in Figure 43. Both topologies differ considerably from conventional GMPV arrays, since they are highly elevated, installed at lower densities, and arranged differently. The S1 topology has approximately double the RS of conventional arrays, while S2 is widened even further to mitigate partial shading on modules and overlapping shadows on ground, due to the extended shadows arising from the checkerboard arrangement. Naturally, for crops with high light requirements the design could be adjusted accordingly; however, it is crucial to consider whether the associated gain in ground irradiation with increasing RS compensates for the reduction in energy yield. If not other modifications in the deployment configuration should be explored to mitigate this trade-off.

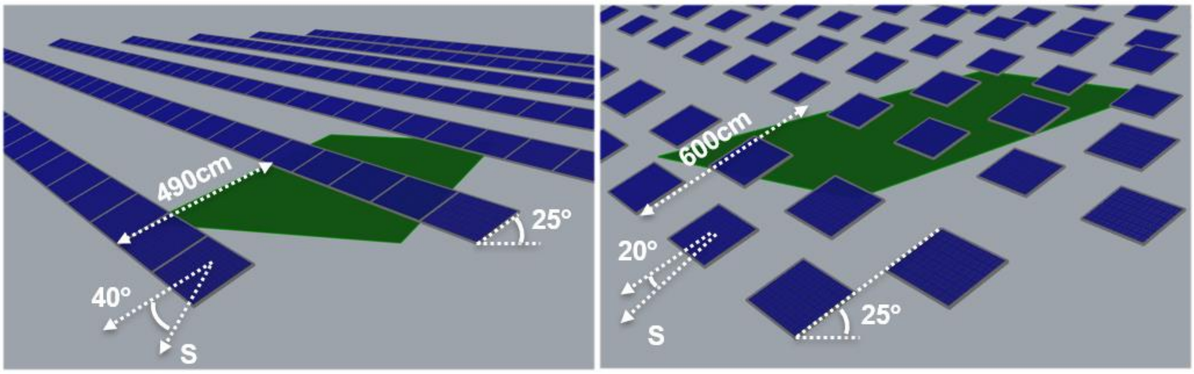

Figure 43 – Main parameters characterizing the deployment configuration of two APV topologies for the cultivation of summer crops; on the left the conventional module arrangement is used (labelled as S1), while on the right the checkerboard arrangement is utilized (labelled as S2).

One such alternative is through the modification of the tilt angle. Although annual ground irradiation can be insensitive to tilt variations, depending on the RS, the daily amount of light incident on crops can be effectively fine-tuned. Consequently, to permit additional light penetration during spring and fall months the tilt is varied from optimal (for POA irradiation). In fact, lower tilts are preferable to avoid wind loads, ultimately reducing support structure costs and because of efficient light absorption when the sun is close to its zenith. The latter is based on the increase of direct light irradiance, and SVF of the bifacial module's front side. Crops are prioritized when selecting the azimuth angle as well, where the array is set to face south-west to enhance the rate of photosynthesis in the morning and afternoon through displacing the accompanied shading pattern and its intensity. Note that this beneficial effect in crop productivity is not incorporated in the current model, potential leading to an under-estimation of the crop yield ratio. Finally, the influence of the IRS of the checkerboard arrangement on ground irradiation is examined in Figure 44. In fact, it was determined that widening of the IRS does not influence daily ground irradiation (not shown in the plot); however, it can considerably reduce the RNGC for 70% of FS conditions, thus enhancing crop growth uniformity. For the selected day in March, RNGC saturates at an IRS of 150 cm, while for July it is attained at 130 cm. RNGC with irradiation values below 60% of FS are relatively reduced as well, from 0.6% for March and 0.7% for July to 0.1% and 0.3% respectively, when the IRS is widened from 115 to 150 cm. Any further increase does not lead to a change; thus, 150 cm is adopted. Note that the influence of the support structure on module or ground shading is not accounted for; however, the previous could be resolved by integrating the support between the two inter-rows, thus enhancing the BG of the array.

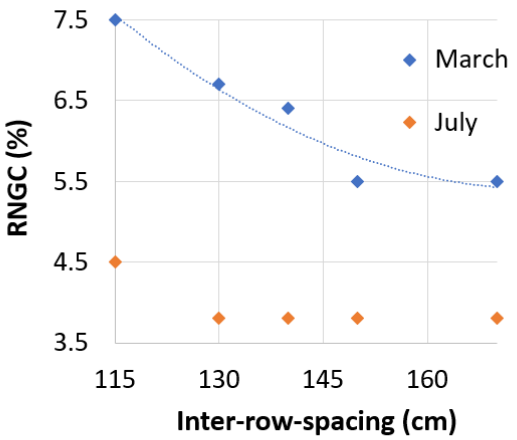

Figure 44 - Ratio of grid cells receiving irradiation below 70% of FS conditions with respect to the inter-row-spacing for two days with clear sky conditions.

Ground irradiation

To gain a better understanding of the light availability below the array for the various topologies analysed, both average and minimum daily ground irradiation are calculated for one day per month. Initially, the average is examined, which lies well above 70% of FS conditions, expect for December as shown in Figure 45 (a). During the winter months, the S-N topologies lead to extended ground shadowing, due to the low solar elevation. The checkerboard arrangement permits increased light penetration below the array for all months simulated, which is justified by the increased RS, and module layout. The gain in ground irradiation when switching to the checkerboard is displayed in orange. Although the reduction in ground illuminances is not too grave, at least when compared to FS conditions, the actual daily irradiation for some of the winter days is considerably below 6 MJ/m^2/day. For example, 5.3 and 5 MJ/m^2/day was found for the simulated days in December and January respectively, indicating that even for an optimized array crop cultivation in the winter is not guaranteed. On the other hand, for summer days like those in June and July, the average daily irradiation was determined to be 21.4 and 23.5 MJ/m^2/day, which is considerably above what is required, thus demonstrating the limitations of a fixed APV array.

Next, the minimum daily ground irradiation is examined as shown in Figure 45 (b), which lies between 60-80% of FS conditions, except for December. Essentially, in winter days where the solar elevation is low, grid cells that are shaded during solar noon result in minimum daily ground irradiation values. As the sun moves over the hemisphere it illuminates previously shaded areas, thus increasing their average daily value, which is not as pronounced in the winter months. Unlike the results found previously for the average irradiation, the conventional arrangement leads to a gain of the minimum ground irradiation as depicted in blue. This could be due to the additional SVF reduction associated with the checkerboard arrangement, as the width per row is increased. On the other hand, the conventional layout is oriented further to the west, which can also have an impact. The differences between the two topologies decay for days with overcast or intermittent sky conditions, as displayed for May and August. Under such conditions the diffuse fraction of the incident light is maximized leading to a more uniform distribution and subsequently higher minimum ground irradiation. In contrast, for the rest of the days which are relatively clear, the conventional arrangement permits more satisfactory results, depending on the clearness index. Ultimately, for the cultivation period of summer crops (March to October) ground irradiation – both minimum and average – is significantly higher that the set constraint. Even though the S2 topology leads to lower minimum values, the RNGC for 70% of FS conditions is less than 1%, apart from March (4.3%). Either way, 70% of FS conditions for the summer period is significantly higher than 6 MJ/m²/day, thus indicating that denser PV arrays can be employed without jeopardizing crop yield.

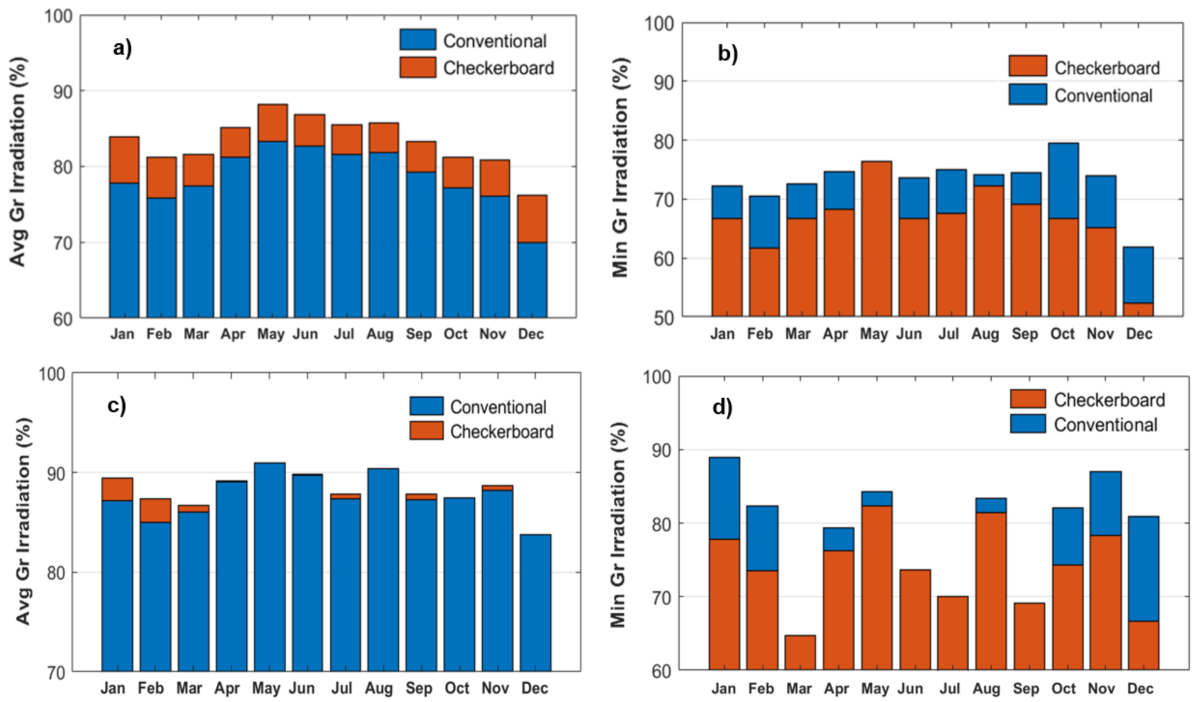

Figure 45 – Daily average and minimum ground irradiation throughout the year for the selected topologies analysed. Graphs (a) and (b) represent a comparison between S1 (conventional) and S2 (checkerboard) for summer crops (S-N), while graphs (c) and (d) display the differences between S3 (conventional) and S4 (checkerboard) for permanent crops (E-W).

4.3.2 Permanent crop

Deployment configuration

Logically, for the growth of permanent crops wider spacings will be necessary to permit sufficient light penetration during the winter months. The selected topologies (S3 and S4) can be seen in Figure 46. Both are oriented south due of west, while maintained at a vertical tilt to prioritize crop productivity. Note that as the array is oriented towards south, lower tilts become desirable from an electricity production point of view; however, the impact on LER due to the reduced ground irradiation is not properly compensated. The front side of the bifacial modules is set to face south-west to allow for enhanced light harvesting. This is arguable, since it will be subjected to higher air and ground temperatures, which reduce the overall module efficiency. To examine this trade-off further, a more rigorous thermal model would be required, that accounts for hourly variations in the module's operating temperature. On the other hand, by orienting the array south-west the peak power better matches electricity demand.

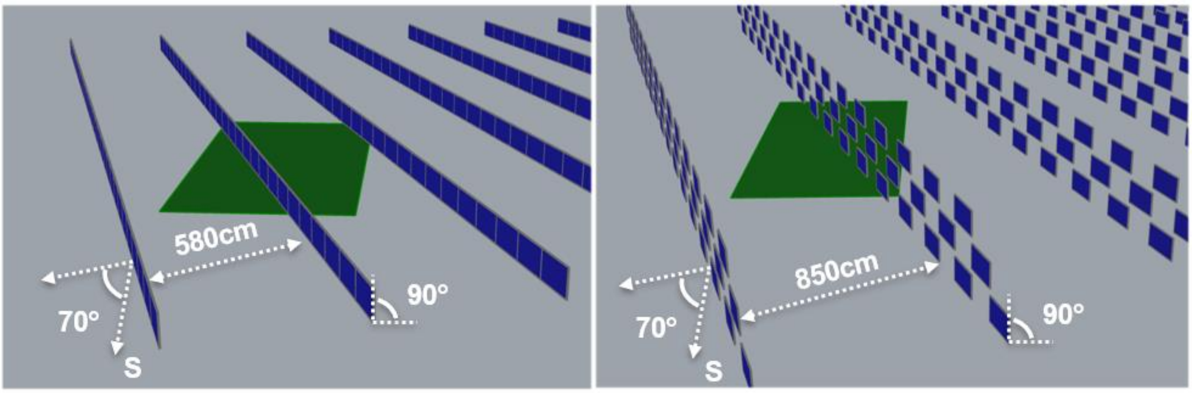

Figure 46 – Main parameters characterizing the deployment configuration of two APV topologies for the cultivation of permanent crops; on the left the conventional module arrangement is used (labelled as S3), while on the right the checkerboard arrangement is utilized (labelled as S4).

For the S4 topology the RS is increased significantly to resolve partial shading or masking between rows, as well as overlapping shadows on the ground, due to the extended width of each row that consists of three RPR. Since a constraint is set of 3.5 m for the maximum width of each row, the IRS is chosen as 125 cm. A distinct advantage of this topology is the option to mount modules at a lower elevation (1.5 m), due to the extended RS and the minimal GCR offered by the vertical tilt. Although machinery operating will not be allowed to pass under the array, farming activities can still proceed due to the wide spacing between each row.

Ground irradiation

As permanent crops are grown annually, ground irradiation must be adequate throughout the year, which is the main incentive for utilizing an E-W orientation. Light availability is significantly amplified, especially during winter days as shown in Figure 45 (c). The latter is of great importance, since during these months solar potential is quite low, thus impinging crop growth. The differences between the two module arrangements are almost negligible, at least for the daily average ground irradiation. This is not the case for the minimum irradiation, where the conventional arrangement leads to a substantial gain, which is depicted in Figure 45 (d), in blue. This amplification in ground irradiation is distinct for winter days, which is justified by the combination of low solar elevation and additional height of the S4 topology. Therefore, leading to extended DNI shadowing and DHI masking. For instance, in December and January, the S4 topology results in intensified shading and subsequent reduction of the minimum ground irradiation below 70% (< 5.3 MJ/m²/day) and 80% (< 5.2 MJ/m²/day) respectively. Consequently, in terms of light availability the S3 topology is preferable, at least for relative shade-intolerant crops. In addition, for both topologies, sunny days in March, July, and September lead to minimum irradiation values below 70% with 11.9, 21.2, and 13.7 MJ/m²/day respectively. Since the solar potential for these days is already plentiful, the reduction is beneficial.

4.3.3 Agrivoltaic performance comparison

After introducing the optimal topologies for each cultivation period and examining the light availability on the ground throughout the year, additional APV performance indicators are compared to the reference case (GMPV). This includes loss in energy yield associated to the lower PV density, increase in specific yield due to the integration of bifacial PV, increase in land productivity related to the dual use of land, and increase in light inhomogeneity arising from the shadows casted by the array. These parameters are summarized in Table 7, which will be further discussed in the following subsections. In addition, to conceptualize the differences in light intensity and distribution throughout the various topologies analysed the shading patterns and schedule is also examined. By considering various timescales ranging from hourly to monthly it is possible to appropriately assess which orientation is optimal in terms of microclimatic control and overall synergy with crop cultivation.

Table 7 – Summary of the agrivoltaic performance for the various topologies analysed.

	AC yield[1]	Specific yield[1]	Land productivity	Number of modules
S1	-54%	36%	32%	3332
S2	-61%	41%	27%	2744
S3	-68%	12%	22%	2842
S4	-67%	10%	23%	2940

[1] loss in electrical AC yield and gain in specific yield in comparison to the GMPV case

Land Equivalent Ratio

Since the S-N topologies, S1 and S2, are more appropriate for summer crops where irradiance is plentiful, higher PV densities are expected; consequently, the overall AC electrical yield obtained is significantly enhanced. In contrast, growth in winter necessitates additional compromises, leading to a non-optimal orientation for direct light harvesting and widening of the RS. The previous is also reflected on the lower specific yield of S3 and S4 deployment configurations. Notice, that even though a wider RS is applied for E-W vertical, the yield produced per module is considerably lower. Although light availability is enhanced, leading to a higher crop yield – depending on the climate and species grown – the associated reduction in electrical yield cannot be compensated, ultimately reducing LER. Regarding the S-N topologies, the S2 is better oriented for front side light absorption; however, the energy yield as well as LER is reduced due to the increased RS. Furthermore, the number of modules for S2 is significantly lower, thus promoting a cost-efficient design, without great compromises in energy yield. As for E-W oriented, S4 results in a slightly lower specific yield, potentially due to the additional masking that is caused by mounting three modules per row. Although the S4 topology has a wider RS, more modules can be mounted per row, thus increasing the overall PV density (number of modules), and subsequently the energy yield and LER. Note that as the RS is increased, the number of pillars required is expected to be reduced along with the number of modules, which can ultimately lead to significantly lower initial capital costs. In specific, for the S4 topology, the array is elevated at a lower height (1.5 m), leading to substantial reductions in costs associated to the support structure, which could permit a higher LCOE in comparison to S3.

Shading pattern and schedule

To appropriately assess which topology is optimal for crop cultivation, it is essential to examine the underlying shading pattern and schedule, ranging from hourly to monthly timescales. Shading intensity throughout the year is already discussed; however, the average or minimum ground irradiation are not sufficient to describe the distribution of light below the array. At first the daily shading patterns are examined for every month, with only May, October, and December being displayed, including the annual shading distribution, as shown in Figure 47 and Figure 48 for topologies S1, S2, and S3, S4 respectively. Then, the hourly shading patterns are examined for the three main topologies; S-N, E-W vertical, and E-W hinged, thus concluding the shading schedule analysis.

When comparing the shading distribution and intensity of the S-N topologies, it is clear that the arrangment of modules can have a significant impact. The conventional arrangment casts striped patterns that result in fluctuating ground irradiation values, whose frequency depends on the RS employed. A compelling alternative that arises due to this repetitive striped shading patterns, is the application of intercropping, which can promote sustainable agriculture through efficient use of resources, mitigation of pests, diseases, and other potential risks such as drought and frost [257]. Essentially, the regions which are usually shaded at solar noon can be utilized to cultivate shade-tolerant species, while the remaining farm can incorporate shade-intolerant. On the other hand, by employing the array in a checkerboard layout shading patterns become patchier and modules that are placed on the second RPR lead to less intense shading, due to their slightly higher elevation. Furthermore, owing to the increased RS and closer to south azimuth of S2 topology, irradiation gradients become sharper, which is easily observed in the 15th of December.

Naturally, for days with overcast or intermittent sky conditions, like the one in May, the minimum irradiation is significantly increased, and subsequently the homogeneity of light. For clearer days, inhomogeneity is enhanced through the intensified shading, leading to a considerably higher CV. Nonetheless, the climate of Boston is frequently intermittent,

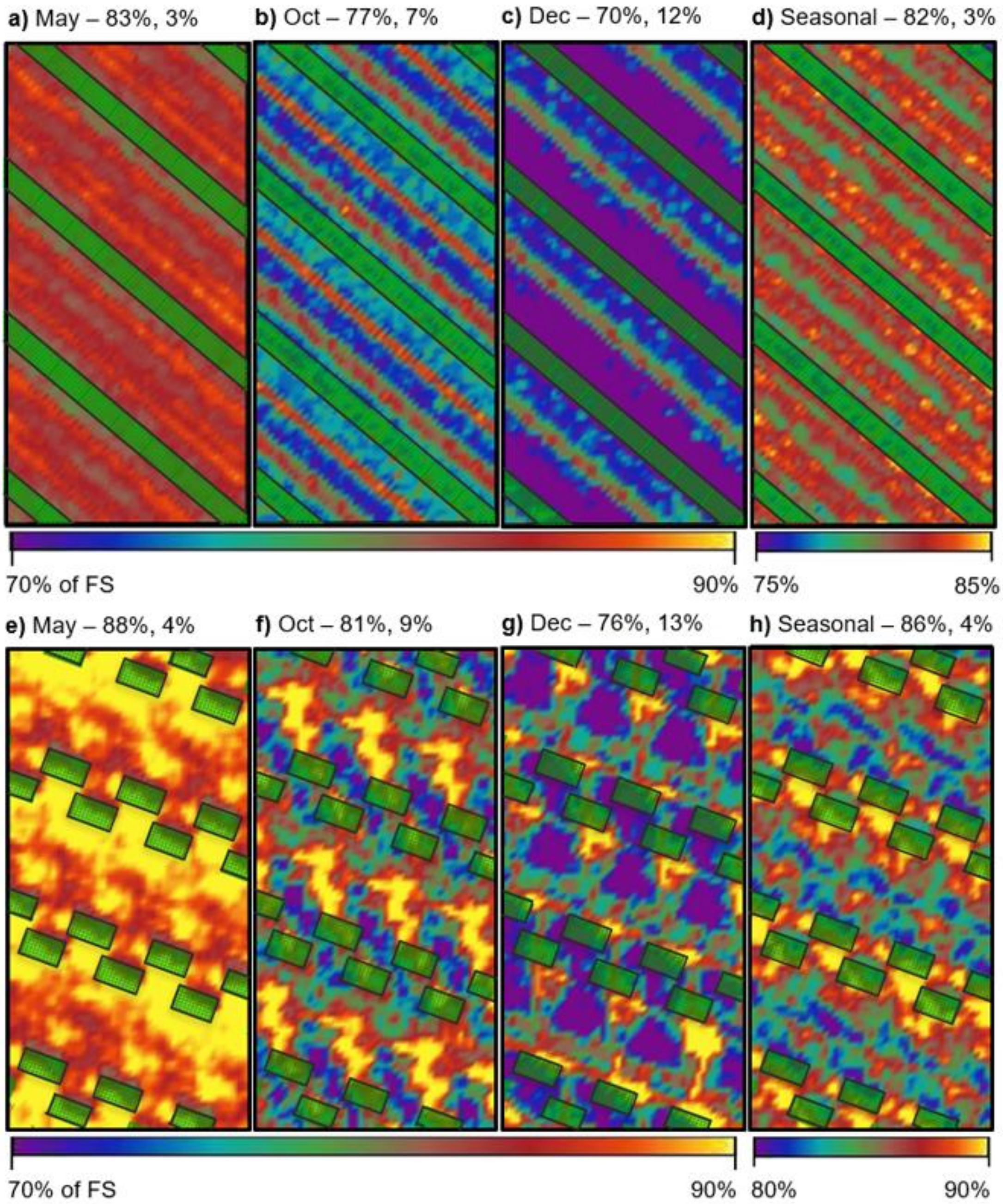

Figure 47 – Shading intensity and distribution for S-N topologies, where S1 has the conventional arrangement as shown from (a) to (d), and S2 the checkerboard from (e) to (h). Three days are selected: one in May with intermittent to overcast, while from October to December the sky conditions are relatively clear. The daily average light availability on ground is expressed as a percentage of FS conditions, along with the coefficient of variation, which are included for each corresponding simulation period. Seasonal patterns are representative of the period between mid-March and mid-October.

resulting in an annual CV from 3-4%. During winter, and for days with clear sky conditions, shading on the ground is extended due to the lower solar elevation, thus increasing the area of potential insufficient crop growth. The area of the casted shadows decreases as the AOI attains zero, which is during the late spring and early fall months.

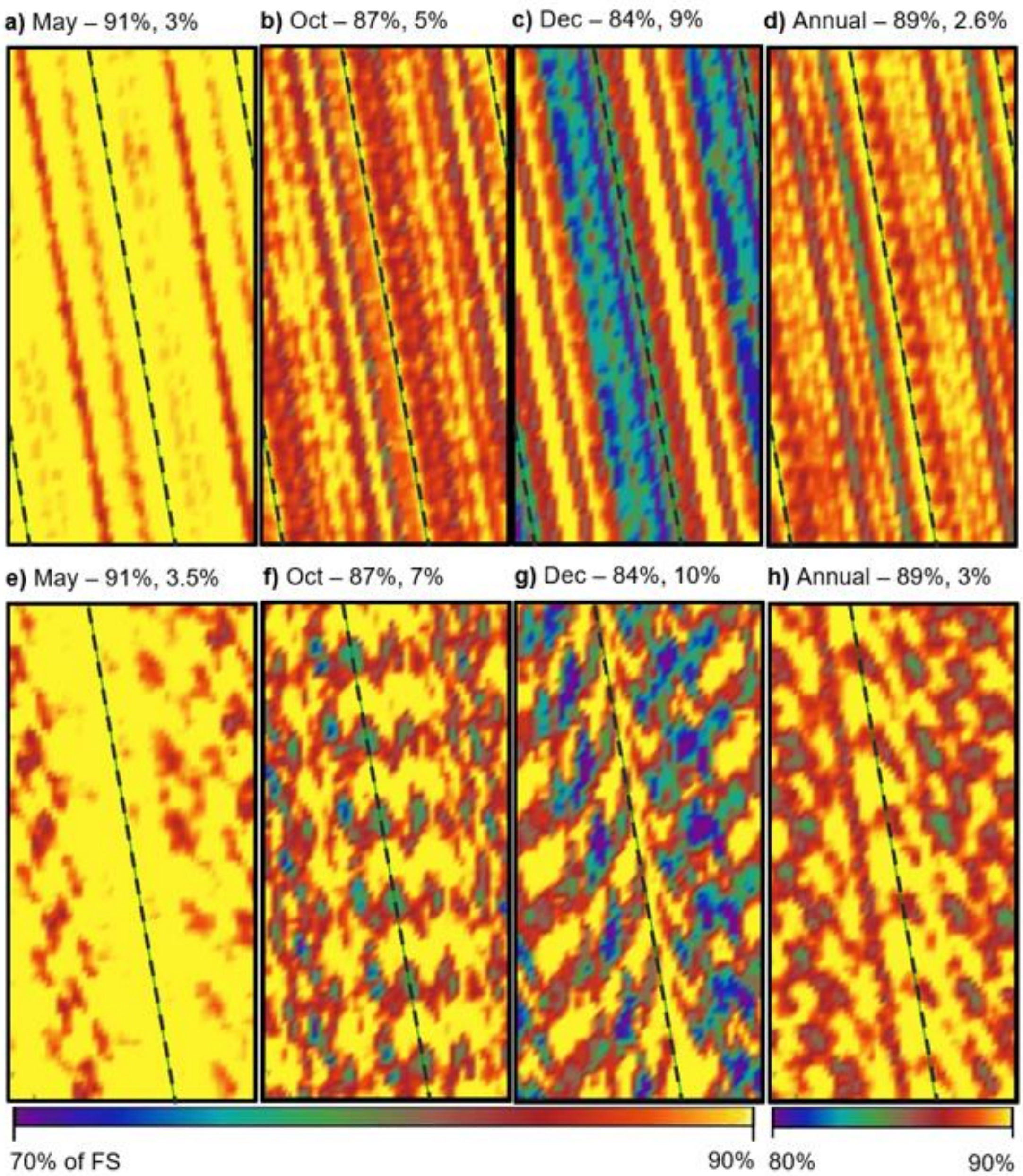

Figure 48 – Shading intensity and distribution for E-W vertical topologies, where S3 has the conventional arrangement as shown from (a) to (d), and S4 the checkerboard from (e) to (h). Three days are selected; one in May with intermittent to overcast, while the ones from October and December have relatively clear sky conditions. The daily average light availability on ground is expressed as a percentage of FS conditions, along with the coefficient of variation, which are included for each corresponding simulation period. Note that the same irradiation range is used for both topologies, which is included at the bottom.

The intensity and distribution of light for the E-W topologies can portray similarities to that of the S-N, which is true for various module arrangement as well. The strips or patches of shadows are just shifted to the E-W direction, depending on the azimuth change between the two topologies. Overall, the daily and annual average irradiation as well as light homogeneity is considerably increased, since vertically tilted modules result in minimal shading during solar noon where the solar potential is usually maximized. This is further amplified during the winter months, where the sun does not diverge as much from south, thus allowing maximum light penetration throughout the day for vertical and E-W facing deployment configurations. When the checkerboard arrangement is employed, displayed from Figure 48 (e) to (h) ground irradiation does not change considerably, yet the distribution is made more inhomogeneous as justified by the increased CV. This is a direct result of the multiple rows per mounting rack (RPR), that lead to additional SVF reduction for the ground, and subsequently intensified irradiation gradients. The latter is also amplified by the wider RS of the S4 topology, which increases light availability between the shaded regions; however, it does not lead to a considerable increase of the minimum irradiation in shade due to the potential saturation effect. Finally, the differences in CV between topologies decays as the timescale is increased, which is direct consequence of Boston's relatively high diffuse fraction. For climates where skies are predominantly clear, the unique characteristics of each topology would be more distinct.

To select the most appropriate topology for a certain crop and climate, it is essential to examine the shading patterns in all timescales including hourly, as displayed in Figure 49. For a south facing array that is optimally inclined the shading patterns are non-homogenous, because they accumulate at a certain region as shown for both the 21st of June and December. During the latter, the area occupied by the shadows is extended due to the lower sun elevation, while the region at the centre is darker, since it is shaded throughout the day. In June, there are regions that receive full-sun exposure, which justifies the application of intercropping with species of varying shade tolerances. For the E-W vertical the patterns become more homogeneous, since there are no overlapping shadows throughout the day, rather they vary in space. The highest light penetration occurs at solar noon, while the lowest

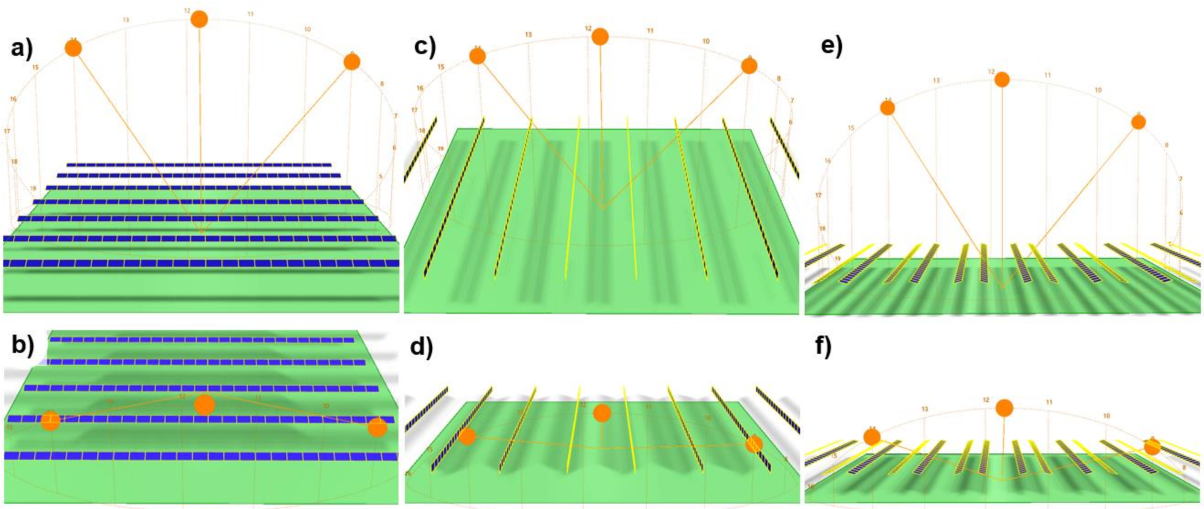

Figure 49 – Hourly shading distribution for the three main topologies analysed: (a, b) south-north facing and latitude inclined, (c, d) east-west facing and vertical, and (e, f) east-west hinged. The shading patterns are accumulated for three time-instants: morning, solar noon, and afternoon. Two days are simulated: 21st of June as depicted in (a, c, and e) and 21st of December (b, d, and f).

during morning and afternoon. This is undesirable, since at noon solar irradiance can be harmful for crop growth, while in the morning it is beneficial. As previously discussed, by maximizing light penetration at solar noon, light availability on the ground is maximized for longer timescales as well. A compelling alternative to the aforementioned topologies is the E-W hinged as shown in Figure 49 (e) and (f), which permits an optimal shading schedule. Because of its low tilt, crops are effectively shaded during solar noon, without accumulating at certain regions due to the E-W orientation. Consequently, homogeneity of shading is ensured, thus combining the best traits of the previous topologies. Note that as longer timescales are considered the distinct characteristics of each topology decay, since the sky conditions in Boston are frequently intermittent.

Overall, the agrivoltaic performance for each of the main APV topologies simulated is qualitatively summarized in Figure 50. At first, they can be divided according to growing season. The EW orientation offers additional light penetration, and even more so during winter, thus permanent or winter crops are preferred. In terms of shading schedule, or spatial homogeneity of light, the hinged is the most optimal, while the S-N leads to intense and non-homogeneous shading. Furthermore, vertical E-W topologies do not shade at noon, which is undesirable. As a result, the S-N orientation necessitates the use of shade-tolerant crops, while vertical E-W is the only one that can maintain shade-intolerant crops. The E-W hinged configuration permits the cultivation of wide variety of shade-tolerant crops, due to its superior shading schedule. When it comes specific yield, the S-N is the most optimal, while the vertical E-W offers the lowest, due to its orientation. Electrical yield and subsequently land productivity are maximized for S-N topologies; however, the hinged E-W configuration optimizes the trade-off between crop and electricity yield. Additional synergies arise for crops that require a support structure. The vertical E-W scales better with wide row spacings, and it is also less prone to soiling. While the hinged E-W, allows semi-indoor farming and thus protection from harmful weather conditions.

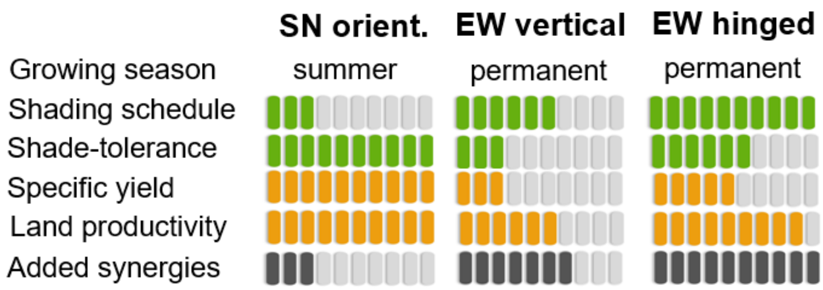

Figure 50 – Agrivoltaic performance comparison for the three main topologies analysed: south-north facing and latitude inclined, east-west facing and vertically inclined, as well as the east-west hinged.

4.5 Cell sensitivity – micro scale

So far, the sensitivity analysis with regards to conventional modules is performed and the associated limitations in APV performance are discussed. These include insufficient ground irradiation for shaded crops, non-homogeneous irradiance distribution (hourly-daily timescales), and decreased PV density. By designing a module for APV applications, it is possible to overcome these limitations and offer more appropriate microclimate control for the crops below. At first, the potential benefits of utilizing a translucent cover are investigated, along with its dimensioning. Then, various cell layouts are examined, as well as cell spacings to determine their influence on the intensity and distribution of shading.

Unlike the previous sensitivity analyses, the micro scale sensitivity applies to a specific deployment configuration and crop. By selecting a crop, it is possible to fine-tune the PV module's transparency according to the crop's LCP and LSP. Furthermore, certain crops, like blueberries, are planted in rows with a considerably crop RS. To ensure that they are shaded during solar noon, the PV array is installed right above it with a certain vertical clearance. As a result, mid-day closure of stomata is mitigated, and the photosynthetic rate of the crop is increased. For this case, the RS of the array is constrained by the crop's RS; consequently, an alternative should be explored that can enhance light penetration other than the RS, which will be elaborated in the following subsections. The topology adopted is the E-W hinged, due to its superior shading schedule and compromise between crop and electricity yield, which is shown in Figure 51. The vertical clearance selected along with the opening at the top should be such that permit free and natural convection between crops and the surrounding air. Note that the lowest edge height is chosen as 3.2 m, which is assumed to be sufficient for the operation of small agricultural machinery. To amplify light penetration on crops, the array's tilt is quite low. Furthermore, it extends the area of the casted shadows during solar noon, while offering protection for other harmful weather conditions, such as hail, heavy rainfall, drought, and frost. This is of equal importance as high value crops, like blueberries, require protection, which could be met by the suggested APV topology. Note that frameless modules are used that permit higher light penetration on crops, while reducing the overall weight of the array and subsequently the cost of the support structure.

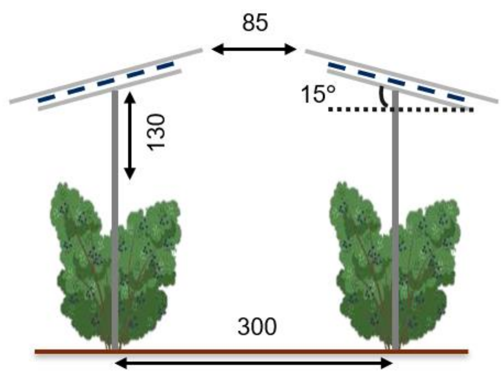

Figure 51 - Front view of E-W hinged configuration (observer is positioned due south). The dimensions are given in cm.

4.5.1 Glass extension

After the deployment configuration of the E-W hinged topology is selected, it is possible to proceed with the cell optimization. Various cell spacings and arrangements were examined; however, although light homogeneity on the ground was enhanced the gain in ground irradiation was not considerable. It can be argued whether the increase in light homogeneity can increase crop growth uniformity and balance the loss of energy yield due to the increased cell spacing. To avoid such a trade-off, other cover materials are examined such as the prismatic glass SG80 whose properties were introduced in subsection 3.1.2 Optical properties. Through the integration of such a translucent cover, the overall fraction of diffuse light incident on crops increases significantly, thus softening the shadows casted by the PV cells. To further increase light availability below the array and mitigate sharp irradiation gradients that can be harmful for crop growth the top cover is extended as shown in Figure 52. If both top and bottom covers were to be extended, the gain in ground irradiance would not be as significant, while the overall material requirements would be doubled. As the length of the cover is extended, the ground's irradiance right below the panel increases linearly. However, after a certain length is achieved it is expected that the gain in PAR would diminish, as most

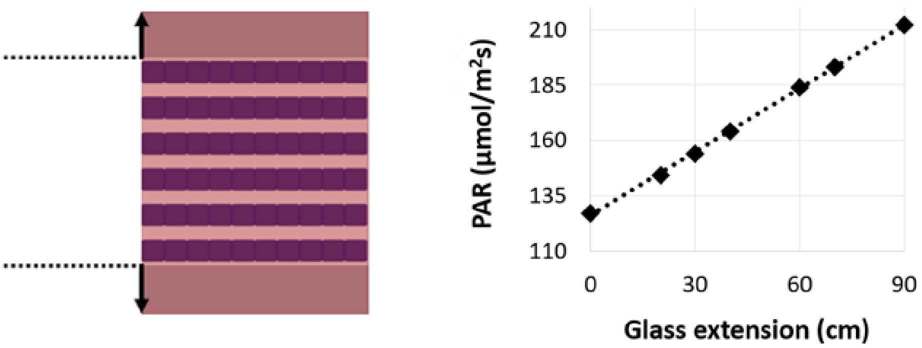

Figure 52 – Top cover extension shown in red for the given cell layout. The plot on the right describes the relationship between total cover extension along both sides and the ground's PAR availability for the 21st of December (clear sky) at solar noon. Note that a maximum of 90 cm is employed as any further increase could lead to inappropriate ventilation for crops.

of the light that is transmitted diffusely from the outer portion of the cover would not be able to reach the central patch. Since the translucent material is treated by Radiance as a Lambertian scatterer, this effect is not observed; nonetheless, it could be investigated through modifying the cover's scatter angle. After performing a trial and error process the necessary extension of the top cover was found to be 35 cm along both directions, leading to 70 cm. Note that this additional glass cover could considerably increase the overall cost of the support structure, by increasing the module's weight. This, along with the elongation of the moment arm could intensify bending stresses in the support, thus requiring additional material to be addressed.

4.5.1 Cell spacing & arrangement

Since the translucent cover simulated has a high HF, a significant fraction of the incoming light is converted into diffuse, thus illuminating regions under shade more appropriately. Consequently, the influence of cell arrangement on ground irradiance uniformity is lessened, which is verified by the simulations performed in Radiance. Nonetheless, the checkerboard cell arrangement provides the highest uniformity; however, this layout could complicate the wire interconnection. Since the issue of light inhomogeneity is already resolved by the diffuse cover, it is sufficient to just increase the spacing between cells, thus permitting more light to be transmitted and ultimately converted into diffuse. Yet again, another trade-off arises, between energy yield, PAR availability on crops, and module transparency as shown in Figure 53. Similarity to the RS, as the transparency increases PAR experiences a considerable gain, with a decreasing rate; consequently, for highly transparent modules PAR gain saturates. A hypothesis was formed, based on what was observed for the RS, that at high transparencies the loss in electricity yield would diminish significantly, resulting in a negative exponential trend as depicted with the dotted line in Figure 39; however, the trend was found to be linear. A rigorous thermal model that accounts for the better heat dissipation associated to high transparencies could show otherwise. Since a wider cell spacing enhances irradiance on the ground, it is natural to expect an increase in the module's BG. Indeed, rear irradiance is increased by 4%, when the transparency is changed from 7% to 73%; however, this is probably optimistic, since the AOI modifier for the PV cover is not modelled leading to an overestimation of the cover's transmittance. Furthermore, for the same module transparency change, the CV decreased from 7.6% to 3.3% during solar noon. The CV is already quite low for both layouts, while the difference between the two is expected to decay as the timescale increases. The recommended transparency for the climate of Boston, given APV configuration, and crop was determined as 38%, while the transparency of the conventional bifacial module is around 7% as it was estimated from the datasheet in [190].

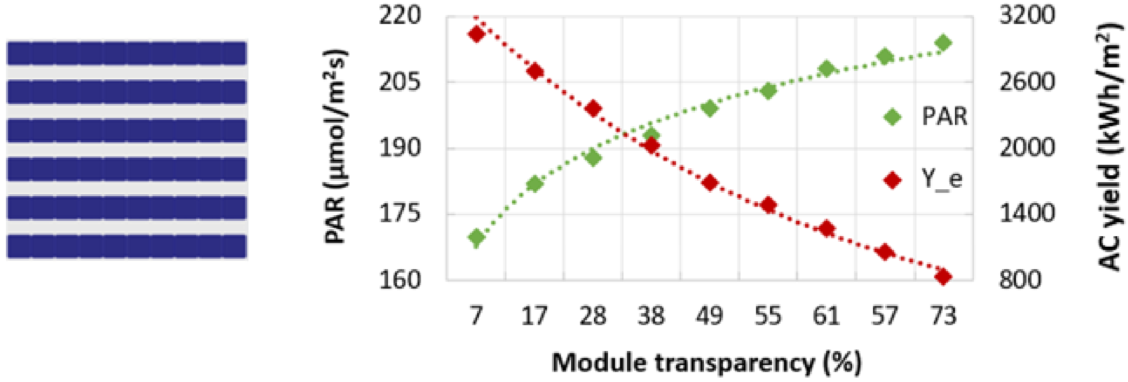

Figure 53 – Sensitivity of the average photosynthetically active radiation (PAR) incident on ground during solar noon and total AC electrical yield (annual) to the module's transparency. Note that the energy yield of the reference GMPV case is around 3 MWh/m². Although bifacial modules are used, which result in enhanced yield, they are placed in landscape orientation, thus reducing the GCR and subsequently the overall energy yield.

4.6 Blueberries case study

For the optimal growth of blueberries an APV module is designed that can transmit enough light for high photosynthetic rates, even under shade. In the following subsections, the performance of the E-W hinged configuration will be examined, which includes ground irradiance at solar noon for two days per month, one with clear and the other with overcast sky conditions, as well as the increase in the land's productivity.

4.6.1 Ground irradiance under shade

To ensure that crops can photosynthesize effectively throughout the year, the incident light must permit a growth rate above 80% of the saturated value. Naturally, there will be days, for instance during overcast conditions in winter, where irradiance over crops is insufficient as the SVF reduction due to the integration of the array can lead to a considerable obstruction of the sky. The irradiance incident on the ground for two days per month, throughout the year, is shown in Figure 54 (a). In orange, one can observe the additional solar irradiance under FS conditions, and in blue the irradiance under the shade of the APV. The difference between the two is highest for clear days, especially during the summer months. In fact, the reduction in

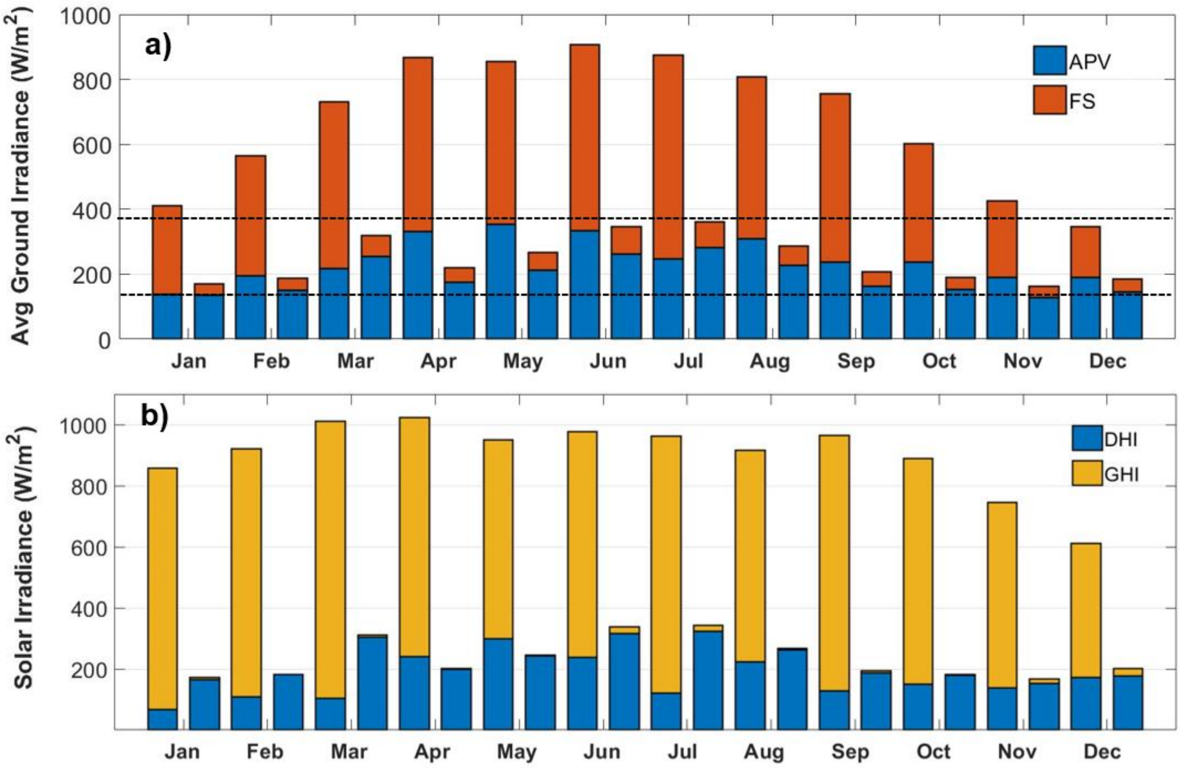

Figure 54 – Graph (a) depicts the light availability under shade casted by the APV array during solar noon, throughout the year. Two days per month are shown, one with clear and the other with overcast sky conditions. The upper horizontal and dotted black line indicates the crop's light saturation point, while the lower one sets the minimum light intensity necessary to attain a photosynthetic rate of at least 80% in comparison to the saturated value. Plot (b) is included to illustrate the solar potential: diffuse horizontal irradiance (DHI) in blue, and the added gain in irradiance due to global horizontal irradiance (GHI) in yellow.

irradiance or the shading rate can vary from 20% in overcast up to 65% in clear sky conditions. This is desirable, as in clear days the solar potential is plentiful to allow saturation to occur, thus a high shading rate is employed. On the other hand, for overcast days shading should be minimized to ensure enough growth. Indeed, the average ground irradiance under shade lies between the two dotted lines that indicate the range for effective photosynthesis. This is not the case for some of the winter days; however, at least for overcast conditions this is inevitable as the solar potential under such conditions would not allow optimum crop growth even in an open field, as verified by the diffuse horizontal irradiance (DHI) in blue. In contrast, for a sunny day in January, although the solar potential in sufficient for crops to attain saturation in an open field, it is not enough to properly illuminate regions under shade. This is an extreme case of a clear day, as observed by its DHI. It is precisely for this reason that researches have been exploring the potential of dynamic panels. The APV system is expected to perform better during cloudy skies, where the diffuse fraction is high. For comparison, observe the difference in DHI between May and July, for a sunny day. Although the total solar potential is approximately the same, the irradiance under the shade of the APV is considerably higher for May. This is a direct consequence of the higher diffuse fraction in May, which permits enhanced light penetration. In general, crops are effectively shaded and protected by harmful irradiance without impinging their growth; however, this boost is not quantified in the crop yield modelling.

4.6.2 Agrivoltaic performance

After examining the variation of irradiance throughout the year, it is essential to discuss some additional APV performance indicators, as depicted in Table 8. In comparison to the generic case studies, where conventional modules are used, the electrical yield is significantly enhanced. By utilizing a shade tolerant crop, like blueberries, higher PV densities can be installed, leading to a reduction of around 33% compared to the reference GMPV case. The difference between the two could be further reduced for southern climates where the solar

Table 8 – APV performance of the E-W hinged topology that incorporates crop specific modules. The values (other than the coefficient of variation) represent the loss or gain in performance compared to the GMPV reference case and separate production of biomass and electricity.

Electrical yield	Specific yield	Land productivity	Number of modules	CV
-33%	18%	59%	5656	1.9%

potential is higher. In addition, an increase in electrical yield would be expected if the effect of the microclimate on the operating temperature of the PV module was considered. This of course would also impact the specific yield, which is already higher due to the use of bifacial modules. Nonetheless, the increase is not significant, since the tilt is quite low to minimize partial shading, and to effectively protect crops from harmful weather conditions. On the other hand, the effect of shading caused by the support structure and the interception of reflected irradiance by the leaves could negatively affect specific yield, and subsequently the overall energy yield. The crop yield ratio was determined as 92%, although a relative high PV density is installed. Since the LER is based on the comparison between APV and under an open field crop yield, the previous has the clear advantage of shading and protecting the crop from damaging weather conditions. This along with maximized electricity yield promotes the overall land productivity to be increased by 59%, which is in the upper range of stationary APV systems found in literature [95, 98, 236]. Note that a more detailed crop yield model could lead to an increase of the overall biomass produced, as the potential benefits of crop cooling on the rate of photosynthesis would be properly addressed. Finally, annual homogeneity of irradiance over the crops is guaranteed with an annual CV of 1.9%, and a daily CV range of 2.5-7.9%, and 1% for relatively clear, and overcast sky conditions respectively. With the introduction of the diffuse cover, the gradients of irradiance are also smoothened.

5

CONCLUSION & RECOMMENDATIONS

5.1 Conclusion

APV systems are proposed as an alternative that can lead to the alleviation of the land-use conflict associated with the installation of GMPV on agricultural land. In this thesis, a series of guidelines and design strategies are provided to promote the medium-to-large-scale deployment of these systems. Furthermore, the integration of bifacial PV is investigated along with any potential synergies that ultimately lead to the maximization of the land's productivity. To address the objectives of this thesis, the modelling approach utilized is robust, yet flexible enough to allow manipulation of the deployment configuration and subsequently efficient optimization. By carrying out a multi-scale sensitivity analysis which includes modifications ranging from cell-to-module-to-array level, the most influential parameters in an optimization process are defined. Essentially, each parameter is isolated to evaluate its impact on the availability of light throughout space, which is then utilized by the crop and electrical yield models to determine the APV performance, and ultimately the LER.

At first, it is crucial to examine which crops can be effectively cultivated in an agrivoltaic system without greatly compromising electricity production. This was addressed through the literature review on the plethora of environmental and genetic factors that govern the photosynthetic rate and cumulative production of biomass. Logically, shade tolerant species (mainly C3 crops) are preferable as they can acclimate to shade effectively and simultaneously allow higher PV densities to be installed. It is therefore crucial to know the type of crop cultivated and its appropriate shading rate, before proceeding with the APV design. The introduction of the PV array is expected to influence the microclimate below depending on the deployment configuration; however, the main parameters affected are light intensity and homogeneity, which are subsequently used to model crop yield.

Since the amount of irradiance incident on the ground must be sufficient for crop growth, the integration of bifacial PV in agrivoltaic systems becomes desirable. In addition, APV arrays are highly elevated to allow the operation of agricultural machinery and employed at lower densities to maximize crop yield; consequently, rear irradiance homogeneity and BG are enhanced, thereby providing additional synergies. Because of this synergy between rear PV side and ground irradiance, the reduction in the total electrical yield is partially mitigated for wide RS, which is characterized by a negative exponential trend. Due to their unique topology, irradiance modelling is performed with Radiance's RT algorithm in combination with the daylight coefficient approach of Daysim and the Perez All Weather sky model. To couple irradiance modelling with geometric, a plug-in of Rhinoceros is utilized, DIVA. By applying material properties to each object of the parameterized scene, and selecting the samples where irradiance is calculated – front and rear PV sides, as well as ground – the sky model can be chosen and finally, RT can be initiated. The resulting irradiance is then linked to the crop and electricity yield models, which are coupled through the LER.

Next, it is essential to examine how the deployment configuration of the PV array affects the performance of the system, and which parameters lead to the highest sensitivity. To meet crop-specific needs, the APV topology can vary significantly from the one found in GMPV arrays. The row spacing and tilt angle are chosen according to the crop's light requirements, while the orientation is towards southwest for increased light penetration in the morning and afternoon shading. For all topologies analysed the sensitivity of ground irradiation to tilt and azimuth angle rises with increasing PV density, while the opposite is true for the sensitivity of POA. Even though POA irradiation of the E-W topology scales better with RS, its ground irradiation is not as sensitive. Nonetheless, to achieve a comparable POA irradiation to a S-N topology, a wide RS is necessary. Both minimum and average ground irradiation portrayed a saturating behaviour with increasing RS, with the previous being more pronounced, especially for S-N oriented topologies; consequently, to further enhance light intensity and homogeneity other modifications should be explored.

To address the limits in light intensity and distribution that are imposed by the conventional design, as well as reduce support structure costs additional module arrangements were explored. Due to its superior shading schedule the E-W hinged topology is adopted for the micro-scale sensitivity, where the PV glass cover and layout of cells are modified to investigate whether blueberries can photosynthesize effectively under shade. A great variety of cell spacings and arrangements were analysed; however, the increase in ground irradiation was not considerable. This was resolved by the adoption of a translucent cover, whose front side was extended to increase the fraction of transmitted diffuse light, which can penetrate deeper into the crop canopy. By extending the front cover, the PAR availability under the shade of the module increased linearly. Similar to the RS, as the module's transparency increased a gain in transmitted PAR was observed; however, at high transparencies the gain saturates leading to a logarithmic trend. On the other hand, unlike the RS, the influence of transparency on energy yield was found to be linear.

Finally, the unique characteristics of each APV topology are discussed, along with the conditions under which one is adopted. By examining the impact of shade tolerance on crop yield for various RS, it can be concluded that the E-W topology is better suited for shade intolerant crops, especially when the array is deployed at a high density. On the other hand, as the RS increases, the sensitivity of crop yield ratio to deployment configuration decreases, which is further amplified for shaded tolerant crops. In general, E-W facing, and vertical topologies offer additional light penetration, especially during winter months; consequently, such deployment configurations are better opted for permanent crops. On the other hand, S-N topologies lead to unfavourable conditions for growth during winter as the magnitude and distribution of irradiance is greatly impinged, thus they are preferred for cultivation during summer. The statistical measure used to define homogeneity of incident light is the CV, which was found to vary based on PV deployment configuration, and sky conditions. Naturally, for days with intermittent or overcast sky conditions ground homogeneity is enhanced, thus the sensitivity to deployment configuration decreases, while the opposite is true for clear days. By adopting an E-W topology, light availability is amplified leading to a higher crop yield; however, the associated reduction in electrical yield is not compensated, ultimately reducing the LER. In contrast, S-N topologies are characterized by significantly higher specific yields, and subsequently AC electrical yields; therefore, maximizing the land's productivity which is dominated by the impact of energy yield.

In addition, the shading patterns and sequence in an hourly timescale were examined to determine the most appropriate for crop cultivation. Shading was intensified and distributed non-homogeneously for the S-N topologies, while E-W and vertical arrays partly resolved these issues, especially during solar noon. Since shading during noon is beneficial, the E-W hinged topology was introduced, which combines the best traits in terms of shading schedule. This along with the integration of a bifacial PV module with a customised transparency and glass cover, resulted in effective crop shading from harmful irradiance without jeopardizing crop yield. Therefore, higher PV densities can be installed, which is partly due to the cultivation of a shade tolerant crop (blueberries). Compared to the refence GMPV case the reduction in electrical yield is a third, while the land's productivity is increased by 59%.

The above illustrated the potential benefits and challenges of modelling bifacial PV that are integrated in agrivoltaic systems. An individual assessment per selected deployment configuration should be performed based on the shading patterns and sequence, as well as electrical performance. However, when addressed properly, an APV system can provide a plethora of functions; generate electricity, act as a shading element, offer protection against harmful weather conditions, partially control the microclimate, and could be used as a support structure for certain crops. These functions, along with the simultaneous and synergistic production of food and renewable energy promote its adoption as a valuable alternative to a sustainable agriculture, therefore alleviating the land-use conflict.

5.2 Recommendations

Research on agrivoltaic systems is still ongoing, and this report serves as an introduction to their design. For the successful implementation of APV systems and future optimization the following research pathways are listed.

- Formulate a rigorous thermal model that can account for the unique deployment configuration of APV systems as well as the influence of the microclimate and the potential cooling effect on PV modules.
- Assess the influence of agricultural activity on the soiling rate of the APV array.
- Design the support structure and assess the impact on ground shading as well as partial shading on the bifacial PV rear side.
- Account for border effects and examine
- Investigate the influence of the translucent cover on the electrical performance of the PV array and account for the corresponding scatter angle.
- Perform a cell sensitivity analysis for the S-N facing and latitude inclined topologies, as well as E-W and vertically inclined. Then, these customized APV modules can be compared to the one obtained for the E-W hinged topology.
- Calculate the LCOE of the APV system and compare it to BIPV and GMPV.
- Investigate the application of intercropping for S-N facing and latitude inclined arrays, due to its underlying striped shading patterns.
- Examine whether the cultivation of shade intolerant species is feasible, which would require lower PV densities, consequently permitting high specific electrical yields for bifacial APV systems.
- Examine the influence of various climates on the optimal APV topology and agrivoltaic performance.

Note that a great amount of work should be performed to ensure the accuracy of crop yield modelling in APV systems, which would necessitate verification through experimentally obtained results.

APPENDIX

Table 9 – Bifacial PV module performance under standard test conditions (STC) obtained from the data sheet in [190].

Module efficiency	η	18.5%
Maximum power	P_{mpp}	270 Wp
Open circuit voltage	V_{oc}	39.0 V
Short circuit current	I_{sc}	9.28 A
Maximum power point voltage	V_{mpp}	31.3 V
Maximum power point current	I_{mpp}	8.68 A

Table 10 – Bifacial PV module temperature characteristics and dimensions obtained from the data sheet in [190].

Thermal characteristics	
NOCT	48 °C
Thermal coefficient κ_P	-0.43 %/K
Dimensions	
Length	1675 mm
Width	1001 mm
Height	33 mm
Cell	156x156 mm^2
Cells per module	60

Abstract uploaded in AgriVoltaics conference 2021:

The recent expansion of solar photovoltaic (PV) technologies coupled with rapid cost reductions and advances in conversion efficiency have resulted in a remarkable decrease of the levelized cost of electricity (LCOE) of ground mounted PV (GMPV) [1]. This is desirable as the global energy consumption is projected to increase by 50% from 2018 to 2050 [2]; however, due to the diffuse nature of light a significant land-coverage is anticipated. This can intensify the land-use conflict associated with the installation of GMPV on agricultural land [3]. One promising solution is the simultaneous cultivation of crops and production of electricity through the concept of agrivoltaics [4] or agrophotovoltaics (APV) [5]. In specific, the aim of this study is to investigate the optimal topology for a medium-to-large-scale and fixed bifacial APV array, which is simulated for the climate of Boston, USA (42.37˚N, 71.01˚W). Previous studies explored the potential of utilizing tracking – either solar or controlled tracking for optimal crop growth – nonetheless, it is compelling to explore the limitations of static configurations, ultimately benefiting all its derivatives. Bifacial PV, which are already part of the standard technologies for GMPV applications, are examined as they are associated with various synergistic effects when integrated in agrivoltaics. By carrying out a multi-scale sensitivity analysis that includes adjustments ranging from cell-to-module-to-array the most influential parameters in an optimization process can be defined. Therefore, the unique features of each APV topology and the conditions under which one is adopted can be properly addressed. To model irradiance incident on both sides of the bifacial PV module and ground, the raytracing algorithm of Radiance was combined with the daylight coefficient approach of Daysim along with the Perez All Weather sky model. The resulting data were then coupled to the crop and electrical yield models to determine the overall land productivity increase and ultimately assess which topology optimizes the trade-off between crop and electricity yield. For the effective cultivation of crops irradiance incident on the ground must adequate for growth; consequently, it is desirable to integrate bifacial PV as their rear side power output scales with ground reflected irradiance. As APV arrays are highly elevated – depending on crop and farming practice – to ensure the operation of agricultural machinery, rear side irradiance homogeneity and consequently bifacial gain (BG) were enhanced. The latter was further amplified through the decrease in PV density that was necessary for sufficient light penetration over the crops. In fact, the row spacing (RS) and tilt angle of the array were selected according to the crop's light requirements, while the orientation was set towards south-west to enhance light penetration in the morning and shade in the afternoon. For the deployment configurations analyzed as the PV density increased the sensitivity of ground irradiation to azimuth and tilt angle was augmented, as displayed in Fig. 56. In contrast, the opposite occurred for the sensitivity of plane of array (POA) irradiation. Due to the significance of the RS, it was examined in more detail as shown in Fig. 55. Widening of the RS led to a logarithmic increase of ground irradiation, whereas the total energy yield reduced in a negative exponential fashion underlying the synergistic behavior with bifacial rear side. Essentially, scarce arrays permit a higher BG, thus mitigating the overall reduction in energy yield with increased RS. This effect was more apparent for vertical and E-W facing topologies; nonetheless, to achieve the same POA irradiation with latitude inclined and S-N facing topologies a wider RS was obligatory. To address the limitations of conventional modules, a customized one was investigated to assess whether blueberries can photosynthesize under shade. By integrating such a module in an E-W hinged PV topology, that permitted the most

optimal shading patterns and sequence, the performance was optimized. Relative to the reference case, energy yield reduced by a third, while the land's productivity increased by 59%. Through this holistic approach that encompasses a multi-scale sensitivity analysis, a spherical understanding of the limitations and synergies related to the dual use of land can be attained, ultimately reassuring a sustainable future for agriculture.

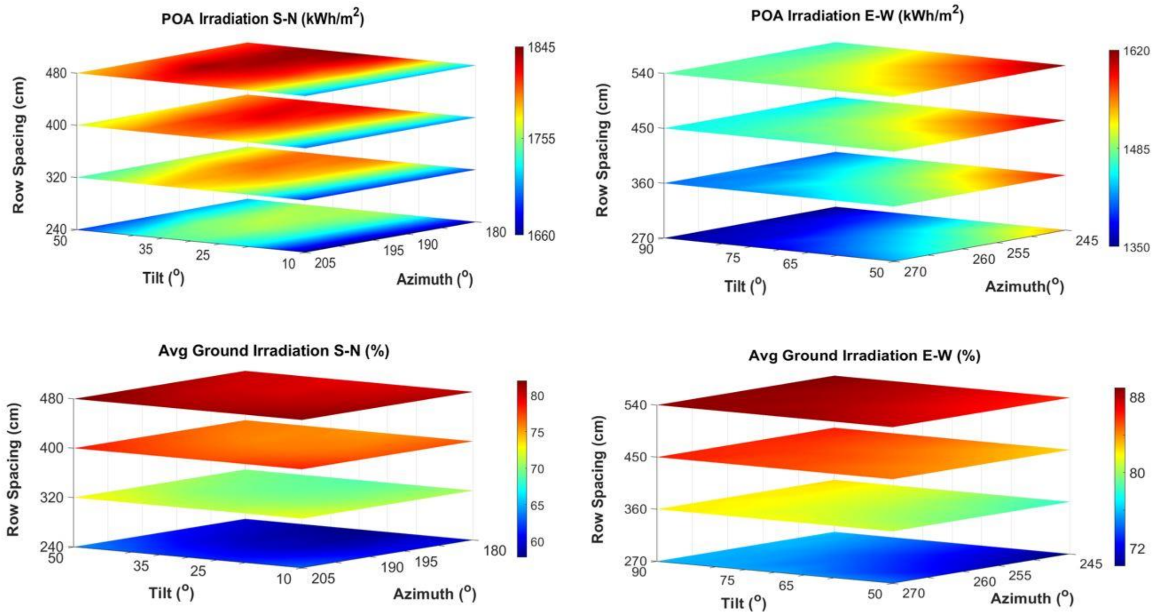

Fig. 56: Annual POA irradiation and average ground irradiation sensitivity to deployment configuration for S-N and E-W facing PV topologies. The color bar displays the intensity of POA on both sides of the module and ground irradiation with respect to full sun conditions respectively.

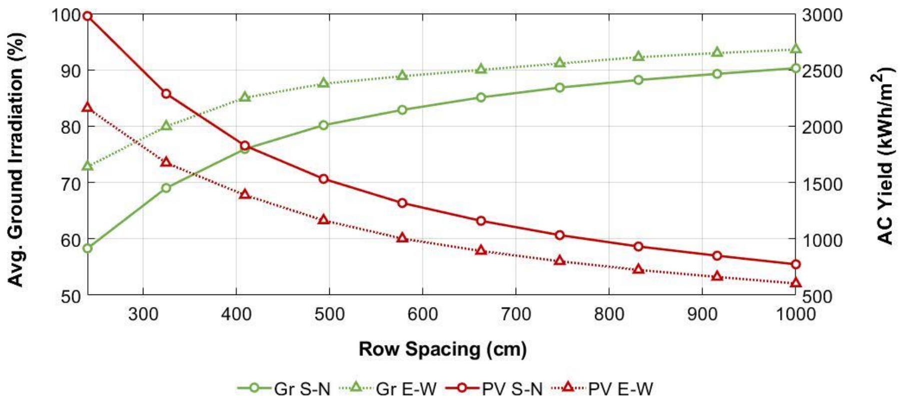

Fig. 55: Sensitivity of annual average ground irradiation and overall AC electrical yield to row spacing and PV topology.

BIBLIOGRAPHY

[1] IRENA. (2020). Renewable Power Generation Costs in 2019. International Renewable Energy Agency. Abu Dhabi, UAE.

[2] Branker K, Pathak M JM, Pearce JM.A Review of Solar Photovoltaic Levelized Cost of Electricity. *Renewable & Sustainable Energy Reviews*. 2011;15:4470-4482.

[3] Capuano L. U.S. Energy Information Administration (EIA). (2020). U.S. EIA International Energy Outlook 2020. *Independent Statistics & Analysis.*

[4] Weselek A, Ehmann A, Zikeli S, Lewandowski I, Schindele S, Hogy P. Agrophotovoltaic systems: applications, challenges, and opportunities. A review. *Agronomy for Sustainable Development*. 2019:6-12. https://doi.org/10.1007/s13593-019-0581-3.

[5] Pimentel D, Marklein A, Toth M, Karpoff M, Paul G, Mccormack R, Kyriazis J, Krueger T. Food versus biofuels: environmental and economic costs. *Human Ecology*. 2009;37:1–12.

[6] Tilman D, Socolow R, Foley JA, Hill J, Larson E, Lynd L, Pacala S, Reilly J, Searchinger T, Somerville C, Williams R. Beneficial biofuels: the food, energy, and environment trilemma. *Science*. 2009;325:270–271.

[7] IPCC. Climate change and land: an IPCC special report on climate change, desertification, land degradation, sustainable land management, food security, and greenhouse gas fluxes in terrestrial ecosystems. 2019;2:16-37.

[8] Goetzberger A, Zastrow A. On the coexistence of solar-energy conversion and plant cultivation. *International Journal of Solar Energy*. 1982;1:55-69

[9] Schindele S, Trommsdorff M, Schlaak A, Obergfell T, Bopp G, Reise C, Braun C, Weselek A, Bauerle A, Högy P, Goetzberger A, Weber E. Implementation of agrophotovoltaics: Techno-economic analysis of the price-performance ratio and its policy implications. *Applied Energy.* 2020;265. doi:https://doi.org/10.1016/j.apenergy.2020.114737.

[10] Hong SJ. Overview of Korean PV Market, Policies and Industry: Key note speech 2 (04.04.2019). Green Energy Expo. Session 2: Market Trend and Technology (Host: Prof. Jung Jae Hak), Daegue, Korea; 2019. Retrieved from: http://greenconference.kr/eng/doc/program02.php.

[11] Xue J. Photovoltaic agriculture – new opportunity for photovoltaic applications in China. *Renew Sustain Energy Rev*. 2017;73:1–9. https://doi.org/10.1016/j.rser.2017.01.098.

[12] Bellini E. (2020). Giant agrivoltaic project in China. *PV magazine*. URL: https://www.pv-magazine.com/2020/09/03/giant-agrivoltaic-project-in-china/#:~:text=The%20Baofeng%20Group%20is%20building,so%20far%20been%20grid%2Dconnected.

[13] Bouchard Q. Adapting Mounting Systems and Geometries of a Photovoltaic Power Plant for an Agrivoltaic Application. Poster presented at: AgriVoltaics 2020 – Launching Agrivoltaics World-wide; 2020 October 14-16; Online.

[14] Nagashima A. Sunlight Power Generation System. Japan Patent No. 2005-277038, 6 October 2005.

[15] MA, USA. Department of Energy Resources, Department of Agricultural Resources. (2018). Guideline Regarding the Definition of Agricultural Solar Tariff Generation Units.

[16] Yang F, Zhang Y, Hao Y, Cui Y, Wang W, Ji T. Visibly transparent organic photovoltaic with improved transparency and absorption based on tandem photonic crystal for greenhouse application. *Appl Opt*. (34), 10232. doi:https://doi.org/10.1364/AO.54.010232.

[17] Li Z, Yano A, Cossu M, Yoshioka H, Kita I, Ibaraki Y. Shading and electric performance of a prototype greenhouse blind system based on semi-transparent photovoltaic technology. *Journal of Agricultural Meteorology*. 2018;74(3):114-122. doi:10.2480/agrmet.d-17-00047.

[18] Croce R, Van Amerongen H. Natural strategies for photosynthetic light harvesting. *Nat Chem Biol*. 2014;(7):492–501.doi:https://doi.org/10.1038/nchembio.1555.

[19] Massa GD, Kim HH, Wheeler RM, Mitchell CA. Plant productivity in response to LED lighting. *HortScience*. 2008;43(7):1951–6.

[20] Marucci A, Cappuccini A. Dynamic photovoltaic greenhouse: Energy efficiency in clear sky conditions. *Applied Energy*. 2016; 170:362-376. doi: 10.1016/j.apenergy.2016.02.138.

[21] Hopkins WG, Hüner Norman P. A. Carbon Assimilation and Productivity. In: *Introduction to Plant Physiology*. 2nd ed. Hoboken: John Wiley & Sons; 2009:257-262.

[22] Lambers, H. 1985. Respiration in intact plants and tissues. Its regulation and dependence on environmental factors, metabolism and invaded organisms. In: R. Dource, D. A. Day (eds.), *Higher Plant Cell Respiration. Encyclopedia of Plant Physiology*, *New Series*. 18-418-473.

[23] Pearcy, R. W., J. Ehlenger, H. A. Mooney, P. W. Rundel. 1989. *Plant Physiological Ecolology: Field Methods and Instrumentation*. London, New York: Chapman and Hall.

[24] Biology Online. *Plant Metabolism*. URL: https://www.biologyonline.com/tutorials/plant-metabolism

[25] Ziegler, H. 1987. The evolution of stomata. In: E. Zeiger, G. D. Farquhar, I. R. Cohen (eds.), *Stomatal Function*. Stanford, CA: Stanford University Press, pp. 29-55.

[26] Matthaeus WJ, Zechmann B. Novel perspectives on stomatal impressions: Rapid and non-invasive surface characterization of plant leaves by scanning electron microscopy. *PubMed*. May 2020.

[27] Dieleman, A., Meinen, E., Warmenhoven, M., Steenhuizen, J., Uenk, D., Chizhmak, S. and Visser, P. de. 2007. Efficiëntie van groeilicht gedurende het etmaal Nota 490, Wageningen UR Glastuinbouw.

[28] Tenhunen, J. D., O. L. Lange, M. Braun, A. Meyer, R. Losch, J. S. Pereira. 1980. Midday stomatal closure in *Arbutus unedo* leaves in a natural macchia and under simulated habitat conditions in an environmental chamber. *Oecologia*. 47:365-367.

[29] Mansfield, T. A., C. J. Atkinson. 1990. Stomatal behaviour in water stressed plants. In: R. G. Alscher, J. r. Cumming (eds.), *Stress Responses in Plants: Adaptation and Acclimation Mechanisms*. New York: Wiley-Liss, pp. 241-264.

[30] Kortschack, H. P., C. C. E. Hartt, G. O. Burr. 1965. Carbon dioxide fixation in sugarcane leaves. *Plant Physiology.* 40:209-213.

[31] Raghavedra, A. S., V. S. R. Das. 1978. The occurrence of C4-photosynthesis: A supplementary list of C4 plants reported during late 1974–mid-1977. *Photosynthetica.* 12:200-208.

[32] Yin X, Struik PC. C3 and C4 photosynthesis models: An overview from the perspective of crop modelling. *Elsevier*. 2009;57(27).

[33] Hovi, T., Nakkila, J. and Tahvonen, R. 2004. Interlighting improves production of year-round cucumber. Scientia Horticulturae 102 (3): 283-294.

[34] Farquhar, G.D. and Roderick, M.L. 2003. Pinatubo, diffuse light and the carbon cycle. Science 299: 1997-1998.

[35] Lakso, A.N. and Musselman, R.C. 1976. Effects of Cloudiness on Interior Diffuse Light in Apple Trees. J. Amer. Soc. Hort. Sci. 101 (6): 642-644.

[36] Sheehy, J.E. and Chapas, L.C. 1976. The Measurement and Distribution of Irradiance in Clear and Overcast Conditions in Four Temperature Forage Grass Canopies. J. Appl. Ecol. 13(3): 831-840.

[37] Gu, L., Baldocchi, D.D., Wofsy, S.C., Munger, J.W., Michalsky, J.J., Urbanski, S.P. and Boden, T.A. 2003. Response of a Deciduous Forest to the Mount Pinatubo Eruption: Enhanced Photosythesis. Science 299: 2035-2038.

[38] Brodersen, C.R., Vogelmann, T.C., Williams, W.E. and Gorton, H.L. 2008. New paradigm in leaf-level photosynthesis: direct and diffuse lights are not equal. Plant Cell Environ. 31:159-164.

[39] Markvart, J., Rosenqvist, E., Aaslyng, J.M. and Ottosen, C.-O. 2010. How is canopy photosynthesis and growth of Chrysanthemums affected by diffuse and direct light? Eur. J. Hort. Sci. 75:253-258.

[40] DeLucia, E.H., Nelson, K., Vogelmann, T.C. and Smith, W.K. 1996. Contribution of intercellular reflectance to photosynthesis in shade leaves. Plan, Cell and Environment 19: 159-170.

[41] Vogelmann, T.C., Bornman, J.F. and Yates, D.J. 1996. Physiologia Plantarum 98, 43-56.

[42] Hemming S, Mohammadkhani V, Dueck T. Diffuse Greenhouse Covering Materials - Material Technology, Measurements And Evaluation Of Optical Properties. Acta Horticulturae. 2008;(797):469-475. doi:10.17660/actahortic.2008.797.68.

[43] Hemming, S. (2016, Oct). Light Transmission and Distribution in Vegetable Greenhouses. Presentation at the Canadian Greenhouse Conference, Niagara Falls, Canada.

[44] Al-Mahdouri A, Baneshi M, Gonome H, Okajima J, Maruyama S. Evaluation of optical properties and thermal performances of different greenhouse covering materials. Solar Energy. 2013;96:21-32. doi:10.1016/j.solener.2013.06.029.

[45] Hemming, S., van der Braak, N., Dueck, T., Elings, A. and Marissen, N. 2005. Filtering natural light by the greenhouse covering – More production and better plant quality by diffuse light? Acta Hort. 711: 105-110.

[46] Hemming S, Dueck T, Janse J, Noort FV. The Effect Of Diffuse Light On Crops. Acta Horticulturae. 2008;(801):1293-1300. doi:10.17660/actahortic.2008.801.158.

[47] Victoria NG, Kempkes F, Weel PV, Stanghellini C, Dueck T, Bruins M. Effect Of A Diffuse Glass Greenhouse Cover On Rose Production And Quality. Acta Horticulturae. 2012;(952):241-248. doi:10.17660/actahortic.2012.952.29.

[48] Dueck T, Janse J, Li T, Kempkes F, Eveleens B. Influence Of Diffuse Glass On The Growth And Production Of Tomato. Acta Horticulturae. 2012;(956):75-82. doi:10.17660/actahortic.2012.956.6.

[49] Johnson, D.M. and Smith, W.K. 2006. Low clouds and cloud immersion enhance photosynthesis in understory species of a southern Appalacian spruce-fir forest (USA). Amer. J. Bot. 93:1625-1632.

[50] Bjorkman, O. 1968. Carboxydismutase activity in shade-adapted and sun-adapted species of higher plants. Physiol. Plant. 21: 1-10

[51] Boardman N.K.: Comparative photosynthesis of sun and shade plants. – Annu. Rev. Plant Physio. 28: 355-377, 1977.

[52] Bohning, R. H., Burnside, C. A. 1956. The effect of light intensity on rate of apparent photosynthesis in leaves of sun and shade plants. Am. J. Bot. 43:557-61

[53] Rabinowitch, E. I. 1951. Photosynthesis and Related Processes, Vol. 2, part I . New York: Interscience. 1 208 pp.

[54] Ojanguren C.T., Goulden M.L.: Photosynthetic acclimation within individual Typha latifolia leaf segments. – Aquat. Bot. 111: 54-61, 2013.

[55] Bjorkman, O., Boardman, N. K., Anderson, J. M., Thorne, S. W., Goodchild, D. J., Pyliotis, N. A. 1972. Effect of light intensity during growth of Atriplex patula on the capacity of photosynthetic reactions, chloroplast components and structure. Carnegie Inst.Washington Yearb. 7 1 : 1 1 5-35

[56] Bjorkman, O., Holmgren, P. 1963. Adaptability of the photosynthetic apparatus to light intensity in ecotypes from exposed and shaded habitats. Physiol. Plant. 16:889-9 14

[57] Bjorkman, O., Holmgren, P. 1966. Photosynthetic adaptation to light intensity in plants native to shaded and exposed habitats. PhysioL Plant. 19:854-89

[58] Burnside, C. A., Bohning, R. H. 1957. The effect of prolonged shading on the light saturation curves of apparent photosynthesis in sun plants. Plant Physiol. 32:61-63

[59] Singh, M., Ogren, W. L., Widholm, J. M. 1974. Photosynthetic characteristics of several C3 and C4 plant species grown under different light intensities. Crop Sci. 14:563-66

[60] Wassink, E. C., Richardson, S. D., Pieters, G. A. 1956. Photosynthetic adaptation to light intensity in leaves of Acer pseudop latanus. Acta Bot. Need. 5:247-56

[61] Woledge, J. 1971 . The effect of light intensity during growth on the subsequent rate of photosynthesis of leaves of tall fescue (Festuca arundinacea Schreb.) Ann. Bot. 35:31 1-22

[62] Ludlow, M. M., Wilson, G. L. 1971. Photosynthesis and illuminance history. Aust. J. Biol Sci. 24:1065-75

[63] McCree, K. J., Troughton, J. H. 1 966. Prediction of growth rate at different light levels from measured photosynthesis and respiration rates. Plant Physiol. 4 1 :559-66

[64] Osipova, O. P., Khein. Kh. Ya., Nichiporovich, A. A. 1971. Activity of the photosynthetic apparatus of plants grown under different light intensities. Fiziol. Rast. 1 8:257-63

[65] Crookston, R. K., Treharne, K. J., Ludford, P., Ozbun, J. 1. 1 975. Response of beans to shading. Crop Sci. 1 5:41 2-16

[66] Esau, K. 1965. Plant Anatomy. pp. 429-30. New York: Wiley. 767 pp. 2nd ed.

[67] Nobel, P. S., Zaragoza, L. J., Smith, W. K. 1975. Relation between mesophyll surface area, photosynthetic rate and illumination level during development of leaves of Plectranthus parviflorus Henckel. Plant Physiol. 55:1067-70

[68] Turrell, F. M. 1936. The area of the internal exposed surface of dicotyledon leaves. Am. J. Bot. 23:255-64

[69] Wylie, R. B. 1951. Principles of foliar organization shown by sun-shade leaves from ten species of deciduous dicotyledonous trees. Am. J. Bot. 38:355-61

[70] Pearce, R. B., Lee, D. R. 1969. Photosynthetic and morphological adaptation of alfalfa leaves to light intensity at different stages of maturity. Crop Sci. 9:791-94

[71] Atanasova L., Stefanov D., Yordanov I. et al.: Comparative characteristics of growth and photosynthesis of sun and shade leaves from normal and pendulum walnut (Juglans regia L.) trees. – Photosynthetica 41: 289-292, 2003.

[72] Mishra Y., Jänkänpää J.H., Kiss A.Z. et al.: Arabidopsis plants grown in the field and climate chambers significantly differ in leaf morphology and photosystem components. – BMC Plant Biol. 12: 6, 2012.

[73] Martins S.C.V., Galmés J., Cavatte P.C. et al.: Understanding the low photosynthetic rates of sun and shade coffee leaves: bridging the gap on the relative roles of hydraulic, diffusive and biochemical constraints to photosynthesis. – PLoS ONE 9: e95571, 2014.

[74] Jiang C.D., Wang X., Gao H.Y. et al.: Systemic regulation of leaf anatomical structure, photosynthetic performance, and highlight tolerance in sorghum. – Plant Physiol. 155: 1416-1424, 2011.

[75] Way D.A., Pearcy R.W.: Sunflecks in trees and forests: from photosynthetic physiology to global change biology. – Tree Physiol. 32: 1066-1081, 2012.

[76] Sage RF, Mckown AD. Is C4 photosynthesis less phenotypically plastic than C3 photosynthesis?*. *Journal of Experimental Botany*. 2005;57(2):303-317. doi:10.1093/jxb/erj040.

[77] Jurik TW, Chabot JF, Chabot BF. 1982. Effects of light and nutrients on leaf size, CO2 exchange, and anatomy in wild strawberry (Fragaria virginiana). Plant Physiology 70, 1044–1048.

[78] Wylie RB. 1939. Relations between tissue organization and vein distribution in dicotyledon leaves. American Journal of Botany 26, 219–225.

[79] Wylie RB. 1951. Principles of foliar organization shown by sun–shade leaves from ten species of deciduous dicotyledonous trees. American Journal of Botany 38, 355–361.

[80] Zhao C, Liu B, Xiao L, Hoogenboom G, Boote KJ. A SIMPLE crop model. *European Journal of Agronomy*. 2019;104:97-106. doi:https://doi.org/10.1016/j.eja.2019.01.009.

[81] Monteith, J.L., 1965. Light distribution and photosynthesis in field crops. Ann. Bot. 29 (113), 17–37.

[82] Williams, J., Jones, C., Kiniry, J., Spanel, D., 1989. The EPIC crop growth-model. Trans. ASAE 32 (2), 497–511.

[83] R.S. Loomis, J.S. Amthor. Yield potential, plant assimilatory capacity, and metabolic efficiencies. Crop Sci., 39 (1999), pp. 1584-1596. https://doi-org.tudelft.idm.oclc.org/10.2135/cropsci1999.3961584x

[84] M.P. Bange, G.L. Hammer, K.G. Rickert. Effect of radiation environment on radiation use efficiency and growth of sunflower. Crop Sci., 37 (1997), pp. 1208-1214

[85] T.R. Sinclair, T. Shiraiwa, G.L. Hammer. Variation in crop radiation-use efficiency with increased diffuse radiation. Crop Sci., 32 (1992), pp. 1281-1284

[86] Amir, J., Sinclair, T.R., 1991. A model of water limitation on spring wheat growth and yield. Field Crops Res. 28, 59–69.

[87] T.M. Monsi, T. Saeki. Über den Lichtfaktor in den Pflanzengesellschaften und seine Bedeutung für die Stoffproduktion. Jap. J. Bot., 14 (1953), pp. 22-52

[88] Hirose T. Development of the Monsi–Saeki Theory on Canopy Structure and Function. Annals of Botany. 2005;95:493-494. doi:doi:10.1093/aob/mci047.

[89] Saeki T. 1960. Interrelationships between leaf amount, light distribution and total photosynthesis in a plant community. Botanical Magazine, Tokyo 73: 55–63.

[90] Tamiya H. 1951. Some theoretical notes on the kinetics of algal growth. Botanical Magazine, Tokyo 64: 167–173.

[91] Boysen Jensen P. 1932. Die Stoffproduktion der Pflanzen. Jena: Gustav Fischer.

[92] J. Warren Wilson. Stand structure and light penetration. I. Analysis by point quadrats.
J. Appl. Ecol., 2 (1965), pp. 383-390.

[93] J. Warren Wilson. Stand structure and light penetration. III. Sunlit foliage area
J. Appl. Ecol., 4 (1967), pp. 159-165.

[94] Praderio S, Perego A (2017) Photovoltaics and the agricultural landscape: the agrovoltaico concept. http://www.remtec.energy/en/2017/08/28/photovoltaics-form-landscapes/. Accessed 6 April 2020.

[95] Dupraz C, Marrou H, Talbot G, Dufour L, Nogier A, Ferard Y (2011) Combining solar photovoltaic panels and food crops for optimising land use: towards new agrivoltaic schemes. *Renewable Energy* 36:2725–2732. https://doi.org/10.1016/j.renene.2011.03.005

[96] Marrou H, Guilioni L, Dufour L, Dupraz C, Wery J (2013) Microclimate under agrivoltaic systems: is crop growth rate affected in the partial shade of solar panels? *Agric for Meteorol.* 177:117–132. https://doi.org/10.1016/j.agrformet.2013.04.012

[97] Reher T, Willochx B, Cappelle J, Van de Poel B. Measurable Indicators of Agrivoltaic Crop Growth Potential. Poster presented at: AgriVoltaics 2020 – Launching Agrivoltaics World-wide; 2020 October 14-16; Online.

[98] Amaducci S, Yin X, Colauzzi M (2018) Agrivoltaic systems to optimise land use for electric energy production. *Appl. Energy* 220:545-561. https://doi.org/10.1016/j.apenergy.2018.03.081

[99] Marrou H, Wery J, Dufour L, Dupraz C (2013) Productivity and radiation use efficiency of lettuces grown in the partial shade of photovoltaic panels. Eur J Agron 44:54–66. https://doi.org/10.1016/j.eja.2012.08.003

[100] Ofir Y. (2018). Increased use of Shading Nets to Overcome Global Warming Damages. *IsrealAgri*. URL: http://www.israelagri.com/?CategoryID=402&ArticleID=1604

[101] Obergfell T, Schindele S. Combining PV and Food Crops to Agrophotovoltaic? Optimization of Orientation and Harvest. ResearchGate. 2012. https://doi.org/10.4229/27thEUPVSEC2012-5AV.2.25.

[102] Obergfell T, Bopp G, Reise C, Schindele S (Eds.), (2017) Landwirtschaft unter Photovoltaik – die weltweit erste APV-Forschungsanlage im Reallabor, 15 pp.

[103] (2018). 'High PPFD Cultivation Guide' [PowerPoint presentation]. FLUENCE Bioengineering. Available at: https://overgrow.com/uploads/default/original/3X/2/3/23aa20345f49333322d00364bf1df89205218fa5.pdf (Accessed: 10 Mar 2020).

[104] Li F, Meng P, Fu D, Wang B. Light distribution, photosynthetic rate and yield in a Paulownia-wheat intercropping system in China. *Agroforest Syst*. 2008;74:163-172. doi:10.1007/s10457-008-9122-9.

[105] Fischer RA (1985) Number of kernels in wheat crops and the influence of solar radiation and temperature. J Agric Sci 105:447. https://doi.org/10.1017/S0021859600056495

[106] (2015). 'Solar Radiation in Corn Production' [PowerPoint poster]. Du Pont Pioneer Agronomy Sciences. Available at: https://www.pioneer.com/CMRoot/Pioneer/US/Non_Searchable/agronomy/cropfocus_pdf/solar-radiation-corn-2015.pdf

[107] Liu, W. M. Tollenaar, 2009. Physiological mechanisms underlying heterosis for shade tolerance in maize. Crop Sci. 49:1817-1826.

[108] Reed, A.J., Singletary, G., Schussler, J., R. Williamson, D., Christy, A.L., 1988. Shading effects on dry matter and nitrogen partitioning, kernel number, and yield of maize. CROP science - CROP SCI 28. https://doi.org/10.2135/cropsci1988.0011183X002800050020x

[109] Mbewe DMN, Hunter RB (1986) The effect of shade stress on the performance of corn for silage versus grain. Can J Plant Sci 66:53–60

[110] Cantagallo JE, Medan D, Hall AJ. Grain number in sunflower as affected by shading during floret growth, anthesis and grain setting. Field Crops Research. 2004;85:191-202. https://doi.org/10.1016/S0378-4290(03)00160-6.

[111] Villalobos FJ, Soriano A, Fereres E. 1992. Effects of shading on dry matter partitioning and yield of field-grown sunflower. Eur. J. Agron. 1, 109-115.

[112] Stein JS, Riley D, Lave M, Hansen C, Deline C, Toor F. Outdoor Field Performance from Bifacial Photovoltaic Modules and Systems. 2017 IEEE 44th Photovoltaic Specialist Conference (PVSC). 2017. https://doi.org/ 10.1109/PVSC.2017.8366042d

[113] Castillo-Aguilella, J. (2016) "Multi-Year Study of Bifacial Energy Gains Under Various Field Conditions", 6th PVPMC Workshop, Freiburg, Germany: http://www.slideshare.net/sandiaecis/44castilloaguilellamultiyearstudyofbifacialenergygains (Accessed Feb 2020).

[114] Reise C, (2016) "Realistic Yield Expectations for Bifacial PV Systems – an Assessment of Announced, Predicted and Observed Benefits", 6th PVPMC Workshop, Freiburg, Germany: http://www.slideshare.net/sandiaecis/42reiserealisticyieldexpectationsforbifacialpvsystems-56350717 (Accessed Mar 2020).

[115] Asgharzadeh A, Marion B, Deline C, Hansen C, Stein JS, Toor F. A sensitivity study of the impact of installation parameters and system configuration on the performance of bifacial PV arrays. IEEE J Photovoltaics. 2018;8(3):798-805.

[116] T. Dullweber, C. Kranz, R. Peibst, U. Baumann, H. Hannebauer, A. Fulle, S. Steckemetz, T. Weber, M. Kutzer, M. Muller, G. Fischer, P. Palinginis and D. H. Neuhaus, Proceedings of the 31st European Photovoltaic Solar Energy Conference, 2015, pp. 341–350.

[117] E. Lohmu¨ller, S.Werner, M. H. Norouzi, S. Mack, M. Demant, S. Gutscher, P. Saint-Cast, M. Hermle, A. Wolf, B. Bitnar, P. Palinginis, H. Neuhaus and M. Konig, Proceedings of the 33rd European PV Solar Energy Conference, Amsterdam, 2017.

[118] N. Ishikawa, Presented at the Bifi PV Workshop, Konstanz, Germany, 2012.

[119] I. G. Romijn, B. B. Van Aken, J. Anker, P. Barton, A. Gutjahr, Y. Komatsu, M. Koppes, E. J. Kossen, M. W. P. E. Lamers, D. S. Saynova, K. C. J. J. Tool, Y. Zhang Steenwinkel, P. R. Venema, A. H. G. Vlooswijk, C. Schmitt, H. Kuhnlein, N. Bay, M. Konig and A. Stassen, Proceedings of the 28th European Photovoltaic Solar Energy Conference, 2013, pp. 736–740.

[120] V. D. Mihailetchi, A. Halm, C. Comparotto, S. Aulehla and R. Kopecek, Presented at the 2nd Bifi PV Workshop, Chambery, France, 2014.

[121] I. G. Romijn, Presented at the 4th Bifi PV Workshop, Konstanz, Germany, 2017.

[122] Sun X, Khan MR, Deline C, Alam MA. Optimization and performance of bifacial solar modules: A global perspective. Applied Energy. 2018;212. doi:10.1016/j.apenergy.2017.12.041.

[123] Kreinin L, Bordin N, Karsenty A, Drori A, Grobgeld D, Eisenberg N. PV module power gain due to bifacial design: preliminary experimental and simulation data. In: Proceedings of the 35th IEEE PVSC, Hawaii, USA; 2010. p.2171–2175.

[124] Egido MA, Lorenzo E. Bifacial photovoltaic panels with sun tracking. Int. J. Sol. Ener. 1986; 4:97–107.

[125] Berrian D, Libal J, Peter C, Klenk M, Marco M, Nussbaumer H. Rear irradiance inhomogeneity of bifacial PV modules: Modelling and quantification by MoBiDiG. In: 6th Bifacial Workshop ISC, Konstanz, Germany; 2019.

[126] U. A. Yusufoglu, T. M. Pletzer, L. J. Koduvelikulathu, C. Comparotto, R. Kopecek, and H. Kurz, “Analysis of the Annual Performance of Bifacial Modules and Optimization Methods,” IEEE J. Photovoltaics, vol. 5, no. 1, pp. 320–328, Jan. 2015.

[127] Deline C, MacAlpine S, Toor F, Shishavan AA. Assessment of Bifacial Photovoltaic Module Power Rating Methodologies - Inside and Out. IEEE Journal of Photovoltaics. January 2017. doi:DOI: 10.1109/JPHOTOV.2017.2650565.

[128] Yusufoglu UA, Lee TH, Pletzer T, Halm A. Simulation of Energy Production by Bifacial Modules with Revision of Ground Reflection. Energy Procedia. 2014;55. doi:10.1016/j.egypro.2014.08.111.

[129] Calculating the Additional Energy Yield of Bifacial Solar Modules. SOLARWORLD White Paper. 2016. doi:Corpus ID: 174775800.

[130] D. Faiman and A. Dolev, “Optimum orientation of bi-facial PV modules,” in Proc. 19th Eur. Photovoltaics Sol. Energy Conf, Paris, France, 2004, pp. 2470–2473.

[131] Shoukry I, Libal J, Kopecek R, Wefringhaus E, Werner J. Modelling of bifacial gain for stand-alone and in-field installed bifacial PV modules. Energy Procedia. 2016;92:600-608. doi:doi: 10.1016/j.egypro.2016.07.025.

[132] Guerrero-Lemus R, Vega R, Kim T, Kimm A, Shephard LE. Bifacial solar photovoltaics - A technology review. Renewable and Sustainable Energy Reviews. 2016;60:1533-1549. doi:http://dx.doi.org/10.1016/j.rser.2016.03.041.

[133] Appelbaum J. Bifacial photovoltaic panels field. *Renewable Energy*. 2016;85:338-343. doi:http://dx.doi.org/10.1016/j.renene.2015.06.050.

[134] Khan R, Hanna A, Sun X, Alam M. Vertical Bifacial Solar Farms: Physics, Design, and Global Optimization. Applied Physics. November 2017. doi:1704.08630v2.

[135] Ooshaksaraei P, Sopian K, Zulkifli R, Alghoul MA, Zaidi SH. Characterization of a Bifacial Photovoltaic Panel Integrated with External Diffuse and Semimirror Type Reflectors. *International Journal of Photoenergy*. 2013;2013:1-7.doi:10.1155/2013/465837.

[136] Hezel R. Novel applications of bifacial solar cells. *Progress in Photovoltaics: Research and Applications*. 2003;11(8):549-556. doi:10.1002/pip.510.

[137] K. Sugibuchi, N. Ishikswa, S. Obara, Bifacial-PV power output gain in the field test using “EarthON” high bifaciality solar cells, in: 28th European Photovoltaic Solar Energy Conference ,Paris, 2013.

[138] A. Huber, A.G. Aberle, R. Hezel, Temperature behavior of monofacial and bifacial silicon solar cells, in: 26th PVSC, Sept.30-Oct.3, 1997 (Anaheim, CA,USA).

[139] Zheng L, Zhao G, Dong J, Ge Q, Tao J, Zhang X. Spatial, temporal, and spectral variations in albedo due to vegetation changes in China’s grasslands. ISPRS Journal of Photogrammetry and Remote Sensing. 2019;152:1-12. https://doi.org/10.1016/j.isprsjprs.2019.03.020.

[140] Ziar H, Sonmez FF, Isabella O, Zeman M. A comprehensive albedo model for solar energy applications: Geometric spectral albedo. *Applied Energy*. 2019;255. https://doi.org/10.1016/j.apenergy.2019.113867.

[141] Wang S. Pavement albedo assessment: methods, aspects, and implication. Iowa State University; 2015.

[142] Lewis P, Barnsley M. Influence of the sky radiance distribution on various formulations of the earth surface albedo. In: 6th International symposium on physical measurements and signatures in remote sensing. ISPRS. CNES Val d'Isere, France; 1994. p. 707–15.

[143] R.W. Andrews, J.M. Pearce, The effect of spectral albedo on amorphous silicon and crystalline silicon solar photovoltaic device performance, Sol. Energy 91 (2013) 233–241.

[144] N. Kasahara, K. Yoshioka, T. Saitoh, Performance evaluation of bifacial photo-voltaic modules for urban application, in:Proceedings of the Third World Conference on Photovoltaic Energy Conversion, 3(2) (2003) 2455–2458.

[145] R. Rther, J. Livingstone, Seasonal variations in amorphous silicon solar module outputs and thin film characteristics, Sol. Energy Mater. Sol. Cells 36 (1995) 29–43.

[146] R. Gottschalg, T.R. Betts, D.G. Infield, M.J. Kearney, On the importance of considering the incident spectrum when measuring the outdoor performance of amorphous silicon photovoltaic devices, Meas. Sci. Technol. 15 (2004) 460–466.

[147] Roy PS. Spectral reflectance characteristics of vegetation and their use in estimating productive potential. Proc Indian Acad Sci (Plant Sci). 1989;99:59-81.

[148] R.W. Andrews, J.M. Pearce, The Effect of Spectral Albedo on Amorphous Silicon and Crystalline Silicon Solar Photovoltaic Device Performance, Sol. Energy 91 (2013) 233-241.

[149] Brennan, M., Abramase, A., Andrews, R., & Pearce, J. (2014). Effects of spectral albedo on solar photovoltaic devices. Solar Energy Materials and Solar Cells, 124, 111-116. doi:10.1016/j.solmat.2014.01.046

[150] Gausman HW, Allen WA. Optical Parameters of Leaves of 30 Plant Species. Plant Physiol. 1973; 52:57-62.

[151] H. W. Gausman, W. A. Allen, C. L. Wiegand, D. E. Escobar, R. R. Rodriguez, A. J. Richardson. 1970. Reflectance, transmittance, and absorptance of light of leaves for 11 plant genera with different leaf mesophyll arrangements. Texas A&M Univ. Tech. Monograph No. 7.

[152] H. W. Gausman, W. A. Allen, M. L. Schupp, C. L. Wiegand, D. E. Escobar, R. R. Rodriguez. 1973. The Leaf Mesophylls of Twenty Crops, their Light Spectra, and Optical and Geometrical Parameters.

[153] 'Spectral Reflectance of Vegetation, Soil, and Water' [PowerPoint presentation]. LWR314.

[154] Woolley JT. Reflectance and Transmittance of Light by Leaves. Plant Physiol. 1971;47:656-662.

[155] Gausman HW, Allen WA, Cardenas R. Reflectance of Cotton Leaves and Their Structure. Remote Sensing of Environment. 1969:19-22.

[156] Jacobsen A, Broge NH, Hansen BU. Monitoring Wheat Fields and Grasslands Using Spectral Reflectance Data. In: International Symposium on Spectral Sensing Research (ISSSR), Melbourne, Victoria, Australia, 26 Nov – 1 Dec, 1995.

[157] Kuester T, Spengler D, Segl K, Guanter L, Kaufmann H. 2009. On the Spectral Resolution Requirements for the Derivation of Leaf Area Index from Hyperspectral Remote Sensing Data. EARSeL Workshop on Imaging Spectrospopy. Tel-Aviv, Isral.

[158] Nicolai BM, Beullens K, Bobelyn E, Peirs A, Saeys W. Nondestructive measurement of fruit and vegetable quality by means of NIR spectroscopy: A review. *ScienceDirect*. 2007; 46:99-118. doi:doi:10.1016/j.postharvbio.2007.06.024.

[159] Blanke MM. Alternatives to reflective mulch cloth (Extenday) for apple under hail net? *Scientia Horticulturae*. 2008;116:223-226. doi:doi:10.1016/j.scienta.2007.12.004.

[160] Overbeck V, Schimtz-Eiberger MA, Blanke MM. Reflective mulch enhances ripening and health compounds in apple fruit. *J Sci Food Agric*. 2013;93:2575-2579. doi:DOI 10.1002/jsfa.6079.

[161] Y. S. Khoo, A. Nobre, R. Malhotra, D. Yang, R. Ruther, T. Reindl and A. G. Aberle, IEEE J. Photovolt., 2014, 4, 647–653

[162] Nussbaumer H, Janssen G, Berrian D, Wittmer B. Accuracy of simulated data for bifacial system with varying tilt angles and share of diffuse radiaton. *Solar Energy*. 2020;197(6):6-21. https://doi.org/10.1016/j.solener.2019.12.071.

[163] Berrian, D., Libal, J., Glunz, S., 2017. MoBiDiG simulations and LCOE. Presented at the 4th bifi PV workshop, Konstanz, Germany.

[164] Janssen, G.J.M., Burgers, A.R., Binani, A., Carr, A.J., Van Aken, B.B., Romijn, I.G., Klenk, M., Nussbaumer, H., Baumann, T., 2018. How to Maximize the kWh/kWp Ratio: Simulations of Single-Axis Tracking in Bifacial Systems. In: 35th European Photovoltaic Solar Energy Conference and Exhibition, pp. 1573–1577. https://doi.org/10.4229/35theupvsec20182018-6bo.7.5.

[165] A. Mermoud and B. Wittmer, "PVsysts new framework to simulate bifacial systems PVPMC Workshop," in Proc. PVPMC Workshop, 2016. [Online]. Available: https://fr.slideshare.net/sandiaecis/pvsystsnew-framework-to-simulate-bifacial-systems

[166] Berrian D, Libal J. A comparison of ray tracing and view factor simulations of locally resolved rear irradiance with the experimental values. *Progress in Photovoltaics: Research and Applications*. 2020;28(6):609-620. doi:10.1002/pip.3261.

[167] Marion W, Deline C, Silvana A. Bifacial_Radiance, 17 Dec. 2017. Web. https://doi.org/10.11578/dc.20180530.16 https://www.osti.gov/doecode/biblio/6869

[168] Ward G.J. The Radiance lighting simulation and rendering system. In: Proceedings of the 21st annual conference on computer graphics and interactive techniques; 1994:459-472.

[169] Berrian D. Performance of Bifacial PV Arrays with Fixed Tilt and Horizontal Single-Axis Tracking: Comparison of Simulated and Measured Data. *IEEE Journal of Photovoltaics*. 2019.

[170] F. Bizzarri, G. Leotta, and A. Di Stefano, “La Silla PV plant as a utilityscale side-by-side test for innovative modules technologies,” in Proc. 33rd Eur. Photovolt. Sol. Energy Conf. Exhib., Nov. 2017, pp. 1978–1982. [Online]. Available: http://www.eupvsec-proceedings.com/proceedings?paper=44211

[171] Kang J, Reise C. Practical Comparison Between View Factor Method and Ray-tracing Method for Bifacial PV System Yield Prediction. *36th European PV Solar Energy Conference and Exhibition*. September 2019.

[172] M. Chiodetti, J. Kang, C. Reise, A. Lindsay, Predicting Yields of Bifacial PV Power Plants – What Accuracy Is Possible?, EU PVSEC, 2018. doi:10.4229/35thEUPVSEC20182018-6CO.3.4

[173] M. Chiodetti, A. Lindsay, Enhancing Bifacial Modelling with Ray-Tracing, PVPMC Workshop, 2016.

[174] Hansen CW, Stein JS, Deline C, Macalpine S, Marion B, Asgharzadeh A, Toor F. Analysis of Irradiance Models for Bifacial PV Modules. *2016 IEEE 43rd Photovoltaic Specialists Conference (PVSC)*. 2016. doi:10.1109/pvsc.2016.7749564.

[175] C. Lo, Y. Lim, and F. Rahman, New integrated simulation tool for the optimum design of bifacial solar panel with reflectors on a specific site. Renewable Energy, 2015. 81: p. 293-307.

[176] Santbergen R, Meguro T, Suezaki T, Koizumi G, Yamamoto K, Zeman M. GenPro4 Optical Model for Solar Cell Simulation and Its Application to Multijunction Solar Cells. *IEEE Journal of Photovoltaics*. 2017:2156-3381. doi:10.1109/JPHOTOV.2017.2669640.

[177] Kajiya, James T., "The Rendering Equation," Computer Graphics, Vol. 20, No. 4, August 1986.

[178] G. Ward, R. Shakespeare, in: Rendering with RADIANCE, The Art and Science of Lighting Visualization, Morgan Kaufmann Publishers, 1998, p. 9.

[179] C.F. Reinhart, S. Herkel, The simulation of annual daylight illuminance distributions—A state of the art comparison of six RADIANCE-based methods, Energy & Buildings 32 (2) (2000) 167–187.

[180] R. Perez, R. Seals, J. Michalsky, All-weather model for sky luminance distribution—preliminary configuration and validation, Solar Energy 50 (3) (1993) 235–245.

[181] Reinhart CF, Andersen M. Development and validation of a Radiance model for a translucent panel. *Energy and Buildings*. 2006;38:890-904. doi:10.1016/j.enbuild.2006.03.006.

[182] D. Bourgeois, C. F. Reinhart & G. Ward (2008) Standard daylight coefficient model for dynamic daylighting simulations, Building Research & Information, 36:1, 68-82, DOI: 10.1080/09613210701446325

[183] C.F. Reinhart, O. Walkenhorst, Dynamic RADIANCE-based daylight simulations for a full-scale test office with outer Venetian blinds, Energy & Buildings 33 (7) (2001) 683–697.

[184] Reinhart C, Breton PF. EXPERIMENTAL VALIDATION OF 3DS MAX® DESIGN 2009 AND DAYSIM 3.0. *LEUKOS the J of the Illuminating Eng Society of North America*. 2009. doi:10.1582/LEUKOS.2009.06.01001.

[185] *Foundations the Grasshopper Primer Third Edition*. (2014). Retrieved Mar 4, 2020, from https://www.modelab.is/grasshopper-primer/

[186] Reinhart, C.F., Lagios, K., Niemasz, J., Jakubiec, A. 2011. DIVA for Rhino Version 4.0. https://solemma.com/Diva.html/ (accessed on March 2020).

[187] Jakubiec JA, Reinhart CF. DIVA 2.0: INTEGRATING DAYLIGHT AND THERMAL SIMULATIONS USING RHINOCEROS 3D, DAYSIM AND ENERGYPLUS. Proceedings of Building Simulation 2011: 12th Conference of International building Performance Simulation Association, Syndey, 14-16 November. 2011.

[189] Wang et al., 2017. Y. Wang, Q. Song, D. Jaiswal, A.P. de Souza, S.P. Long, X. Zhu. Development of a three-dimensional ray-tracing model of sugarcane canopy photosynthesis and its application in assessing impacts of varied row spacing. Bioenergy Res., 10 (2017), pp. 626-634. https://doi-org.tudelft.idm.oclc.org/10.1007/s12155-017-9823-x

[190] Sunmodule Bisun SW 270 DUO Data sheet. SolarWorld AG. 2016. https://www.solaricashop.com/download/solarworld/sw_bisun_270_en.pdf

[191] Holsteens K, Moerkens R, Poel BVD, Vanlommel W. The Effect of Low-Haze Diffuse Glass on Greenhouse Tomato and Bell Pepper Production and Light Distribution Properties. *Plants*. 2020;9(7):806. doi:10.3390/plants9070806.

[192] Mead, D. (2010). "Trans" Materials – Modelling and Specifying a Next Generation. Presentation at the Sustainable Building Advisor Workshop, Freiburg, Germany. https://www.radiance-online.org/community/workshops/2010-freiburg/PDF/DavidMead.pdf

[193] Mischler G. 2012. Rayfront 1.0 User Manual. Schorsch. https://www.schorsch.com/en/software/rayfront/manual/transdef.html

[194] ASTMD1003, Standard test method for haze and luminous transmittance of transparent plastics, ASTM International, West Conshohocken, PA, USA, 2015.

[195] Stoner ER, Baumgardner MF. Characteristic Variations in Reflectance of Surface Soils. *Soil Science Society of America Journal*. 1981;45(6):1161-1165. doi:10.2136/sssaj1981.03615995004500060031x.

[196] Baumgardner MF, Silva LRF, Biehl LL, Stoner ER. Reflectance Properties of Soils. *Advances in Agronomi*. 1986;38:1-44. doi:https://doi.org/10.1016/S0065-2113(08)60672-0.

[197] Lillesand, T. M., Kiefer, R. W., & Chipman, J. W. (2004). Remote sensing and image interpretation (p. 763). Wiley

[198] Santbergen R, Zolingen RV. The absorption factor of crystalline silicon PV cells: A numerical and experimental study. *Solar Energy Materials and Solar Cells*. 2008;92(4):432-444. doi:10.1016/j.solmat.2007.10.005.

[199] Riverola A, Mellor A, Alvarez DA, Llin LF, Guarracino I. Mid-infrared emissivity of crystalline silicon solar cells. *Solar Energy Materials and Solar Cells*. 2018;174:607-615. doi:http://dx.doi.org/10.1016/j.solmat.2017.10.002.

[200] Montero S, Pedro J, Nofuentes G, Diez JV, Spectral Reflectance Patterns of Photovoltaic Modules and Their Thermal Effects. *Journal of Solar Energy Engineering*. 2010;132. http://doi.org/10.1115/1.4002246

[201] Taveres-Cachat E, Bøe K, Lobaccaro G, Goia F, Grynning S. Balancing competing parameters in search of optimal configurations for a fix louvre blade system with integrated PV. *Energy Procedia*. 2017;122:607-612. doi:10.1016/j.egypro.2017.07.357.

[202] Reflectance of Solar Innova PV Modules. SOLAR INNOVA. http://www.importsunpv.com/marcas/solarinnova/Reflectance.of.Solar.Innova.PV.panels.pd f

[203] Dow NC. Aluminum Surfaces. Anomet. https://anomet.com/reflective-aluminum. Accessed April 2020.

[204] Tetlow K. Anodized Aluminum for Architectural Applications. Continuing Education Center. https://continuingeducation.bnpmedia.com/courses/lorin-industries-inc/anodized-aluminum-for-architectural-applications/5/. Published November 2013. Accessed April 2020.

[205] Rubin M. Optical Properties of Soda Lime Silica Glasses. Solar Energy Materials. 1985;12:275-288.

[206] Chudinzow D, Haas J, Díaz-Ferrán G, Moreno-Leiva S, Eltrop L. Simulating the energy yield of a bifacial photovoltaic power plant. *Solar Energy*. 2019;183:812-822. doi:10.1016/j.solener.2019.03.071.

[207] Mardaljevic J. Daylight simulation: validation, sky models and daylight coefficients. 2000:166-170.

[208] Jacobs, A. (2012). Radiance Tutorial. URL: http://www.jaloxa.eu/resources/radiance/documentation/docs/radiance_tutorial.pdf

[209] Mardaljevic, J. (2014). Ambient Calculation Crash Course. Presentation in: 13th International Radiance Workshop 2014, September 1-3, London, UK.

[210] Mardaljevic, J. (2003). Radiance Course Day 1 Daylight Simulation. Workshop presentation, Berkeley, CA. URL: https://www.radiance-online.org/community/workshops/2003-berkeley/presentations/Mardaljevic/rc_day1.pdf

[211] Ladybug Tools. n.d. Comparison of simulation parameters for Radiance. https://www.ladybug.tools/radiance/image-parameters#sidebyside

[212] Cano J, John JJ, Tatapudi S, Samy G, Mani T. "Photovoltaic modules: Effect of tilt angle on soiling. Master's thesis. Arizona State Univ., Tempe, AZ, USA, 2011.

[213] Bhaduri S, Kottantharayil A. Mitigation of Soiling by Vertical Mounting of Bifacial Modules. *IEEE Journal of Photovoltaics*. 2019; 9(1):240-244. doi:10.1109/jphotov.2018.2872555.

[214] M. Mani and R. Pillai, "Impact of dust on solar photovoltaic (PV) performance: Research status, challenges and recommendations," *Renew. Sustain. Energy Rev.*, 2010; vol. 14, no. 9, pp. 3124–3131.

[215] Nepal P, Korevaar M, Ziar H, Isabella O, Zeman M. Accurate Soiling Ratio Determination with Incident Angle Modifier for PV Modules. *IEEE Journal of Photovoltaics*. 2019;9(1):295-301. doi:10.1109/jphotov.2018.2882468.

[216] M. R. Maghami, H. Hizam, C. Gomes, M. A. Radzi, M. I. Rezadad, and S. Hajighorbani, "Power loss due to soiling on solar panel: A review," Renewable Sustain. Energy Rev. 2016; vol. 59, pp. 1307–1316.

[217] Ravi S, Macknick J, Lobell D, Field C, Ganesan K, Jain R, Elchinger M, Stoltenberg B (2016) Colocation opportunities for large solar infrastructures and agriculture in drylands. Appl Energy 165:383–392. https://doi.org/10.1016/j.apenergy.2015.12.078.

[218] H. Hottel, B. Woertz. Performance of flat-plate solar-heat collectors. Trans. ASME. 1942; 64.

[219] Ross, R.G.Jr., 1980. Flat-plate photovoltaic array design optimization. In: Photovolt Spec Conf 14th, San Diego, Calif, January (1980) 7-10, Conf Rec (A81-27076 11-44). Inst Electr Electron Eng Inc., New York, pp. 1126–1132, 1980, 1126–1132.

[220] Mattei M, Notton G, Cristofari C, Muselli M, Poggi P. 2006. Calculation of the Polycrystalline PV Module Temperature using a Simple Method of Energy Balance. Vol. 31. http://dx.doi.org/10.1016/j.renene.2005.03.010.

[221] D.L. King , W.E. Boyson , J.A. Kratochvill , Photovoltaic Array Performance Model, Sandia National Laboratories, 2004.

[222] M. D'Orazio, C. Di Perna, E. Di Giuseppe, Experimental operating cell tempera- ture assessment of BIPV with different installation configurations on roofs un- der Mediterranean climate, Renew. Energy 68 (2014) 378–396 10.1016/j.renene. 2014.02.009

[223] P. Trinuruk, C. Sorapipatana, D. Chenvidhya, Estimating operating cell temperature of BIPV modules in Thailand, Renew. Energy 34 (2009) 2515–2523 10.1016/j.renene.2009.02.027.

[224] Zouine M, Akhassi M, Erraissi N, Aarich N, Bennouna A, Mustapha R, Outzourhit A. Mathematical Models Calculating PV Module Temperature Using Weather Data: Experimental Study. Lecture Notes in Electrical Engineering. 2018; 519, 630–639. DOI: 10.1007/978-981-13-1405-6_72

[225] Fuentes, M.K., 1987. A simplified thermal model for Flat-Plate photovoltaic arrays. Albuquerque, NM (USA).

[226] E. Lorenz, T. Scheidsteger, J. Hurka, D. Heinemann, and C. Kurz. 2011. Prog. Photovolt: Res. Appl. 19, 757.

[227] Deline C, Pelaez S-A, MacAlpine S, Olalla C. Bifacial PV System Mismatch Loss Estimation and Parametrization. *Presented at the 2019 European Photovoltaic Solar Energy Conference:* Marseille, France, 2019; September 9-13, NREL/CP-5K00-73541.

[228] M., S. A., Jäger, K., Isabella, O., Van, S. R., & Zeman, M. (2016). Designing grid-connected PV-system. In *Solar Energy: The physics and engineering of photovoltaic conversion, technologies and systems*. Cambridge, England: UIT Cambridge.

[229] W. Bower, M. Behnke, W. Erdman, and C. Whitaker, "Performance test protocol for evaluating inverters used in grid-connected photovoltaic systems," (2004), www.gosolarcalifornia.org/equipment/documents/2004-11-22_Test_Protocol.pdf.

[230] M88H high efficiency three phase solar inverters for the European market - Data sheet. DELTA. 2017. https://krannich-solar.com/fileadmin/content/pdf/International/Delta_M88H.pdf

[231] Durisch, W., Leutenegger, S., Tille, D., 1998. Comparison of small inverters for grid-independent photovoltaic systems. Renew. Energy 15, 585–589 (Renewable Energy Energy Efficiency, Policy and the Environment).

[232] Isabella O, Nair GG, Tozzi A, Barreto JHC, Mouli GRC, Lantsheer F, Berkel SV, Zeman M. Comprehensive modelling and sizing of PV systems from location to load. *MRS Proceedings*. 2015;1771:17-23. doi:10.1557/opl.2015.347.

[233] Almonacid, F., Rus, C., Prez-Higueras, P., Hontoria, L., 2011. Calculation of the energy provided by a {PV} generator. Comparative study: conventional methods vs. artificial neural networks. Energy 36, 375–384.

[234] R. Mead, R.W. Willey. The concept of a "land equivalent ratio" and advantages in yields from intercropping. Exp. Agric., 16 (3) (1980), pp. 217-228

[235] Riley J. A general-form of the land equivalent ratio. Experimental Agriculture 1984; 20:19-29.

[236] Riaz MH, Younas R, Imran H, Alam M, Butt N. Module Technology for Agrivoltaics: Vertical Bifacial vs. Tilted Monofacial Farms. *IEEE Journal of Photovoltaics*. 2020. doi:arXiv:1910.01076v2.

[237] Wang Q, Sun D, Hao H, Zhao X, Hao W, Liu Q. Photosynthetically active radiation determining yields for an intercrop of maize with cabbage. *European Journal of Agronomy*. 2015; 69:32-40. doi:10.1016/j.eja.2015.05.004.

[238] Younas R, Imran H, Riaz MH, Butt N. Agrivoltaic Farm Design: Vertical Bifacial vs. Tilted Monofacial Photovoltaic Panels. *App Ph.* 2019. Doi:arXiv:1910.01076v1.

[239] Kelley K. Sample size planning for the coefficient of variation from the accuracy in parameter estimation approach. *Behavior Research Methods*. 2007; 39:755–766. doi: 10.3758/BF03192966.

[240] Panichkitkosolkul W. Confidence Intervals for the Coefficient of Variation in a Normal Distribution with a Known Population Mean. *Journal of Probability and Statistics*. 2013. doi:10.1155/2013/324940.

[241] Gruber S, Högy P, Trommsdorff M. Crop Selection for APV Systems: Overview of Performances, Potentials, and Perspectives for Germany. Poster presented at: AgriVoltaics 2020 – Launching Agrivoltaics World-wide; 2020 October 14-16; Online.

[242] Spaargaren Ir JJ. Supplemental lighting for greenhouse crop. Netherlands: Hortilux Schreder B.V. and P.L. Light System Inc; 2001.

[243] Blacquiere T, Spaargaren JJ. Necessity of supplemental lighting for year-round production of greenhouse vegetables. Acta Hortic 2003;611:75–8.

[244] Moretti S, Marucci A. A Photovoltaic Greenhouse with Variable Shading for the Optimization of Agricultural and Energy Production. *Energies*. July 2019:3-4.

[245] Cossu M, Murgia L, Ledda L, Deligios PA, Sirigu A, Chessa F, et al. Solar radiation distribution inside a greenhouse with south-oriented photovoltaic roofs and effects on crop productivity. Appl Energy 2014;133:89–100.

[246] Castilla N. Greenhouse technology and management. 2nd ed. CABI; 2013.

[247] Dorais M. The use of supplemental lighting for vegetable crop production:light intensity, crop response, nutrition, crop management, cultural practices. In: Canadian greenhouse conference. Toronto (Ontario), Canada; 2003.

[248] Rho H, Yu DJ, Lee HJ. Limitation Factors for Photosynthesis in 'Bluecrop' Highbush Blueberry (Vaccinium corymbosum) Leaves in Response to Modeterate Water Stress. *Plant Biol*. 2012;55(450).

[249] Li X, Chen W, Li Y. Study on Photosynthetic Characteristics of Blueberry in Greenhouse. *Acta Horticulturae*. 2012;(926):315-319. doi:10.17660/actahortic.2012.926.43.

[250] Retamales JB, Montecino JM, Lobos GA, Rojas LA. Colored shading nets increase yields and profitability of highbush blueberries. *Acta Horticulturae.* 2008; 193–197. DOI: 10.17660/ActaHortic.2008.770.22

[251] Kim SJ, Yu DJ, Kim T-C, Lee HJ. Growth and photosynthetic characteristics of blueberry (Vaccinium corymbosum cv. Bluecrop) under various shade levels. *Scientia Horticulturae*. 2011; 129:486-492. doi:10.1016/j.scienta.2011.04.022.

[252] Lobos GA, Retamales JB, Hancock JF, Flore JA, Romero-Bravo S, del Pozo A. Productivity and fruit quality of Vaccinium corymbosum cv. Elliott under photo-selective shading nets. *Scientia Horticulturae*. 2013; 153:143–149. doi:10.1016/j.scienta.2011.04.022

[253] Retamales JB, Hancock JF. Blueberries. *CABI Publishing*. Wallingford, UK. 2012

[254] Eck P, Gough RE, Hall IV, Spiers JM. Blueberry management. In: G.J. Galletta and D.G. Himelrick (eds.). Small fruit crop management. Prentice Hall, Englewood Cliffs, N.J. 1990; 273-333.

[255] Eck P, Stretch AW. Nitrogen and plant spacing effects on growth and fruiting of potted highbush blueberry. *HortScience*. 1986;21:249–250.

[256] Lindsay A, Chiodetti M, Dupeyrat P, Binesti D, Lutun E, Radouane K. Key Elements in the Design of Bifacial PV Power Plants. 31st European Photovoltaic Solar Energy Conference and Exhibition. 2015; 1764–1769. doi:10.4229/EUPVSEC20152015-5CO.14.4.

[257] Lithourgidis AS, Dordas CA, Damalas CA, Vlachostergios DN. Annual intercrops: an alternative pathway for sustainable agriculture. *Aust. J. Crop Sci*. 2011;5:396–410.